

RECYCLING OF SLAG IN SUBMERGED ARC WELDING

Submitted by:

Deepanjali Nimker

(Roll No. : 2K13/PhD/ME/04)

Mechanical Engineering Department

**In partial fulfillment of the requirement of the degree of
DOCTOR OF PHILOSOPHY**

Under the guidance of:

Professor Reeta Wattal

Department of Mechanical Engineering



**Delhi Technological University
(Formerly Delhi College of Engineering)**

Bawana Road, New Delhi

August 2022

DECLARATION OF ORIGINALITY

I hereby declare that the research work presented in this thesis titled “ **Recycling of Slag in Submerged Arc Welding**” is an original and authentic work carried out by me under the supervision of Dr. Reeta Wattal, Professor, Department of Mechanical Engineering, Delhi Technological University, Delhi. This Thesis has been prepared in conformity with the rules and regulations of the Delhi Technological University, Delhi. The research work reported and the results presented in the thesis have not been submitted either in part or full to any other university or institute for the award of any other degree or diploma. As per my understanding, this thesis is free from any plagiarized contents.

DEEPANJALI NIMKER

2K13/PhD/ME/04

Research Scholar

Department of Mechanical Engineering

Delhi Technological University

CERTIFICATE

This is to certify that the Ph.D. thesis entitled “*Recycling of Slag in Submerged Arc Welding*” being submitted by Ms. Deepanjali Nimker for the award of the degree of Doctor of Philosophy in Mechanical Engineering, to Delhi Technological University, Delhi, India, is a bonafide record of original research work carried out by her under my guidance and supervision. The work presented in this thesis has not been submitted to any other university or institution for the award of any degree or diploma.

Dr. Reeta Wattal

Professor

Department of Mechanical Engineering,

Delhi Technological University,

Delhi

ACKNOWLEDGEMENTS

The work presented here would not have been possible without the help of a few experienced and talented people.

I wish to express my deep sense of gratitude to Professor (Dr.) Reeta Wattal, my supervisor from the Department of Mechanical Engineering at Delhi Technological University, for her encouragement, inspiring guidance, personal attention, constructive criticism, and valuable suggestions throughout the course of this research work. I am grateful for her unwavering support, motivation, and creative freedom. I had the privilege of working under her guidance, and I have not only experienced the lessons for my research work but also lessons for life. I am very thankful to her for helping me to get access to all the necessary facilities at Delhi Technological University. I would also like to thank her husband, Dr Chand Wattal, and their children, Dr Sushant and Ms. Shweta, for their hospitality whenever I visited them at home.

I would like to convey my sincere gratitude to Professor S.K. Garg, HOD, Department of Mechanical Engineering, DTU Delhi, for his valuable suggestions and motivation during this research work.

I would also like to sincerely acknowledge my gratitude to the team of experts, the members of SRC for my research work at DTU, Delhi, Professor S.K. Garg, Department of Mechanical Engineering, Prof R.S. Mishra, Department of Mechanical

Engineering, Prof. D.S. Nagesh, Department of Mechanical Engineering and Professor S. Indu, Department of Electronics and Communications for their guidance and encouragement. I am also thankful to Professor Vijay Gautam, Department of Mechanical Engineering, DTU Delhi, for his wholehearted cooperation in my research work.

My appreciation and deep sense of gratitude to Professor Sunil Pandey, Professor Mechanical Engineering, JNU Delhi, for his constant encouragement, timely advice, and necessary technical suggestions throughout my research work. I am thankful to him for helping me to procure the slag material from Cheema Boilers, Kurali Punjab.

I am also indebted to Professor Sachin Maheshwari, Professor, Department of MPAAE, Netaji Subhas University of Technology Delhi for help and support during the literature survey for research by providing useful and hard-to-find research papers, which helped me a lot during my research.

I sincerely thank the technical staff of the welding laboratory, Mr. Vinay and Mr. Sanjay, for all the help received during experimentation.

I would also like to thank technical staff of central workshop, Mr. Manjeet Singh, Mr. Darshan, as well as the technical staff of Metallurgy Laboratory, Metal Forming Laboratory, and Sand Testing Laboratory, Mr. Tek Chand, and Mr. Om Prakash.

I am also thankful to the non-teaching staff of the Department of Mechanical Engineering, Central Library, Administration Department, and Academic Department for their timely help and cooperation.

I am also thankful to my fellow researchers, Mr. Bharat Sangha, Mrs. Uma Gautam, Mr. Anmol Bhatia, Dr Harwinder Singh, and Dr Amrik Singh, for boosting my enthusiasm and extending help whenever I required.

Above all, I am deeply thankful and blessed to have such a wonderful family for their appreciation, patience, and motivation during this research work. My parents, Mr. Kishore Kumar and Mrs. Sheela Nimker, were always there for me with their unconditional support. I would like to express my special thanks to my sister, Dr Shwetanjali, and brother, Mr. Kumar Rahul, for their immense love and constructive criticism during research work. And finally, I want to thank my truly amazing husband, Dr Naveen Kumar. He supported me at every step of the way, with patience, great insight, support and love.

Deepanjali Nimker

ABSTRACT

Flux used in submerged arc welding converts into slag during welding, which is considered as waste. Such a large quantity of slag has to be disposed of in a land fill space. Since it is non-bio-degradable in nature, it will not decay with time. It cannot be used as a filling material in building construction because it is brittle and glassy. Due to this reason, cost will increase, apart from environmental pollution. Non-renewable resources may be exhausted due to continuous mining. Thus, slag generated during submerged arc welding is a waste and imposes a number of problems. The higher the amount of slag generated, the higher the wastivity. It is not possible to stop the generation of slag because it is a by-product of the process, but slag can be reused as a flux in the same submerged arc welding process. Wastivity can be decreased by recycling the slag, thus resulting in higher productivity. Furthermore, the slag can be processed according to one's requirements and applications. Therefore, an attempt has been made to develop technology for the recycling of slag so as to use it for commercial purposes. The process of recycling has been performed in various stages so as to confirm the overall soundness of the slag developed.

In the first stage, pure slag has been collected from the industry, then washed, crushed and sieved to the same grain size as that of fresh flux, and then a weld pad has been obtained using pure slag. After performing spectro analysis, it was found that the weld metal composition was not in accordance with ASME SFA 5.17. Therefore, it was decided that slag should be recycled.

In order to replenish the slag, pulverised form (100 mesh size) slag was added with deoxidisers, i.e., CaCO_3 ; Al powder; Mn powder with K_2TiO_3 , which acts as an arc

stabiliser. K_2SiO_3 was added as a binder to bind the mixture. They were then mixed and agglomerated. After which this mixture was air dried and baked at 850°C . This baked mass, after crushing and sieving, is known as recycled slag. After performing spectro analysis of the weld pad prepared using recycled slag, it was found that, the weld metal composition of recycled slag was in accordance with ASME SFA 5.17. The weld pad obtained using recycled slag was then investigated to evaluate its mechanical properties by performing visual inspection, dye penetrant and radiographic tests. Later, the specimen was removed from the middle of the weld pad to perform mechanical testing. It was found that, the tensile test and impact strength were in accordance with ASME SFA 5.17.

To study the effect of welding parameters on weld quality, it is necessary to consider the transfer of elements such as C, Mn, Si, S, and P into the weld metal using recycled slag. A design matrix was developed using two-level half factorial Design. Empirical models were developed for the responses obtained. These models were then checked for adequacy and significance of model using the 'F' test and 't' test respectively. It was observed that the transfer of C, Mn, and P was directly related to arc voltage, whereas it was inversely related to the wire feed rate. Moreover, the transfer of Si decreased with an increase in wire feed rate but remained the same with varying arc voltage, welding speed, and contact tube to plate distance. Furthermore, it was noticed that welding speed and contact tube to plate distance have insignificant effect on weld metal chemistry. It was concluded that recycled slag gives satisfactory results and can be used as a fresh flux.

Apart from element transfer behaviour, weld bead geometry and shape relationships were also studied using recycled slag. Here, empirical models were developed to relate the input parameters viz. wire feed rate, arc voltage, travel speed, and contact tube to plate distance with response parameters (such as bead width, bead height, bead penetration, weld penetration shape factor, and weld reinforcement form factor). These models were then checked for adequacy and significance of model using 'F' test and 't' test, respectively. It was observed that responses such as bead width, bead penetration and weld reinforcement form factor increased with the increase in wire feed rate. In addition, bead height decreased with the increase in travel speed whereas weld reinforcement form factor increased with the increase in travel speed. Adequacy test revealed that newly designed slag proves beneficial in indicating the weld bead quality.

Another stage of this research presented a comparative study of the microstructure and micro hardness of weld pads prepared using pure slag, recycled slag, and fresh flux. Results revealed that recycled slag gives a microstructure like that of flux, whereas pure slag was unable to achieve the standards. Micro hardness tests performed show that recycled slag had a high hardness as compared to fresh flux. On the other hand, pure slag failed to reach the prescribed limit of micro hardness.

In the final stage, a cost analysis was performed for recycled slag and then compared with fresh flux. It evaluates the processing cost by adding all the costs involved in producing suitable recycled slag. This cost analysis was helpful in predicting the efficiency of recycled slag over fresh flux.

INDEX

<i>Title</i>	<i>Page No</i>
<i>Declaration of Originality</i>	<i>i</i>
<i>Certificate</i>	<i>ii</i>
<i>Acknowledgements</i>	<i>iii-v</i>
<i>Abstract</i>	<i>vi-viii</i>
<i>List of Figures</i>	
<i>List of Tables</i>	
<i>Nomenclature</i>	
 CHAPTER 1: INTRODUCTION	 1-28
1.1 Overview of Submerged Arc Welding	1
1.2 SAW Process	3
1.3 SAW Components	4
1.3.1 Wire Electrodes	4
1.3.2 Multi Wire and Variants	4
1.4 SAW Fluxes	5
1.4.1 Role of Flux	6
1.4.2 Classification of SAW Fluxes	7
1.4.2.1 According to the Method of Manufacturing	8
1.4.2.2 According to the Chemical Nature	9
1.4.2.3 According to the Mineral Flux Composition	10
1.4.3 Characteristics of Flux	11
1.4.4 Properties of Flux	11
1.4.4.1 Technological Properties	11
1.4.4.2 Physical Properties at Room Temperature	13
1.4.4.3 Physical Properties at Elevated Temperature	15
1.5 Process Parameters	16
1.5.1 Welding Current	17

<i>Title</i>	<i>Page No</i>
1.5.2 Arc Voltage	18
1.5.3 Travel Speed	18
1.5.4 Size of Electrode	19
1.5.5 Electrode Extension	19
1.5.6 Linear Heat Input	19
1.5.7 Electrode Polarity	20
1.5.8 Flux Depth	21
1.5.9 Electrode Angle	22
1.6 Advantages of SAW Process	23
1.7 Limitations of SAW Process	23
1.8 Applications of SAW Process	24
1.9 Organisation of Thesis	25
CHAPTER 2: LITERATURE REVIEW	29-57
2.1 Introduction	29
2.2 Recycling of Slag and Weldability	29
2.3 Weld Bead Geometry and Shape Relationships	35
2.4 Element Transfer Behaviour	42
2.5 Metallurgical Studies	45
2.6 Need of this Research Work	54
2.7 Motivation	55
2.8 Research Gaps in Literature Review	56
2.9 Research Objectives	56
2.10 Statement of Problem	57
CHAPTER 3: EXPERIMENTAL SET UP AND METHODOLOGY	58-70
3.1 Introduction	58
3.2 Material Selection	59
3.2.1 Base Metal	59

<i>Title</i>	<i>Page No</i>
3.2.2 Filler Wire	59
3.2.3 Flux Type	59
3.2.4 Slag Composition	60
3.3 Welding equipment and Process Parameters	60
3.3.1 Submerged arc Welding Machine	60
3.3.2 Process Parameters	62
3.3.2.1 Indirect Parameters	62
3.3.2.2 Direct Parameters	62
3.3.2.3 Response Parameters	63
3.4 Methodology	63
3.5 Design of Experiments	65
3.5.1 Selection of the Design	65
3.5.2 Selection of Levels	66
3.5.3 Selection of the Model	67
3.5.4 Development of Design Matrix	68
3.5.5 Evaluating the Coefficients of Polynomials	69
3.5.6 Analysing the Adequacy of Empirical Models	70
CHAPTER 4: RECYCLING OF SLAG AND WELDABILITY	71-88
4.1 Introduction	71
4.2 Plan of Investigation	72
4.2.1 Welding with Fresh Flux	73
4.2.2 Welding with Pure Slag	74
4.2.3 Comparison of Chemical Composition of Weld Pad Prepared using Fresh Flux and Pure Slag	75
4.2.4 Recycling of slag	75
4.2.5 Weld Pad Prepared using Different Compositions of Slag	77

<i>Title</i>	<i>Page No</i>
4.2.6 Comparison of Chemical Composition Obtained using Fresh Flux, Pure Slag and Different Compositions of Slag	79
4.2.7 Selection of One of the Composition as Recycled Slag	80
4.2.8 Weld Qualification Tests with Recycled Slag	80
4.3 Results and Discussions	80
4.3.1 Weld Metal Chemistry	80
4.3.2 Visual Inspection of the Weld Bead	81
4.3.3 Slag Detachability and arc Stability	82
4.3.4 Dye Penetrant Test	84
4.3.5 Tensile Test	84
4.3.6 Impact Test	86
4.3.7 Radiography	87
4.4 Summary	88
CHAPTER 5: ELEMENT TRANSFER BEHAVIOUR	89-113
5.1 Introduction	89
5.2 Alloying Elements	90
5.2.1 Carbon	90
5.2.2 Manganese	91
5.2.3 Silicon	92
5.2.4 Sulphur	93
5.2.5 Phosphorus	94
5.3 Plan of Investigation	94
5.3.1 Identifying the Input Factors and Determining their Upper and Lower Limits	95
5.3.2 Developing the Design Matrix	96
5.3.3 Conducting the Experiments as Per Design Matrix using Recycled Slag	96
5.3.4 Recording the Response Parameters	97

<i>Title</i>	<i>Page No</i>
5.3.5 Formulating the Empirical Models	99
5.3.6 Evaluating the Coefficients of Polynomials	99
5.3.7 Evaluating the significance of Coefficients and Obtaining the final Model	101
5.3.8 Analysing Adequacy of the Empirical Models	101
5.4 Results and Discussions	103
5.4.1 Effect of Welding Input Parameters on Carbon	106
5.4.2 Effect of Welding Input Parameters on Manganese	108
5.4.3 Effect of Welding Input Parameters on Silicon	109
5.4.4 Effect of Welding Input parameters on Sulphur	110
5.4.5 Effect of Welding Input Parameters on Phosphorus	111
5.5 Summary	113
CHAPTER 6: WELD BEAD GEOMETRY AND SHAPE RELATIONSHIPS	114-147
6.1 Introduction	114
6.2 Elements of Weld Bead Geometry	116
6.2.1 Bead Width	118
6.2.2 Bead Height	119
6.2.3 Bead Penetration	119
6.2.4 Weld Penetration Shape Factor	122
6.2.5 Weld Reinforcement form Factor	123
6.2.6 Dilution	123
6.3 Plan of Investigation	124
6.3.1 Identifying the Important Welding Parameters and Determining their Upper and Lower Limits	125
6.3.2 Developing the Design Matrix	126
6.3.3 Conducting the Experiments as Per Design Matrix using Recycled Slag	126

<i>Title</i>	<i>Page No</i>
6.3.4 Recording of the Response Parameters	127
6.3.5 Developing the Empirical Models	129
6.3.6 Evaluating the Coefficients of the Polynomials	130
6.3.7 Evaluating the Significance of Coefficients and Obtaining the Final Model	131
6.3.8 Checking the Adequacy of Empirical Models	131
6.4 Results and Discussions	132
6.4.1 Effect of Welding Parameters on Bead Width	136
6.4.2 Effect of Welding Parameters on Bead Height	137
6.4.3 Effect of Welding Parameters on Bead Penetration	139
6.4.4 Effect of Welding Parameters on Weld Penetration Shape Factor	141
6.4.5 Effect of Welding Parameters on Weld Reinforcement Form Factor	143
6.5 Summary	146
CHAPTER 7: METALLURGICAL STUDIES	148-164
7.1 Introduction	148
7.2 Microstructure of Mild Steel	148
7.3 Weld Pool Solidification	153
7.4 Welding Zones	155
7.4.1 Composite Zone	156
7.4.2 Unimixed Zone	156
7.4.3 Partially Melted Zone	156
7.4.4 True Heat Affected Zone	157
7.4.5 Unaffected Base Metal	157
7.5 Experimental Procedure	157
7.6 Results and Discussions	158

<i>Title</i>	<i>Page No</i>
7.6.1 Microstructure Investigations	158
7.6.2 Micro-Hardness Survey	162
7.7 Summary	163
CHAPTER 8: COST ANALYSIS	165-169
8.1 Introduction	165
8.2 Type of Cost	165
8.2.1 Material Cost	166
8.2.2 Processing Cost	166
8.2.3 Overhead Cost	167
8.3 Results and Discussions	168
8.4 Summary	169
CHAPTER 9: CONCLUSIONS AND FUTURE SCOPE	170-173
9.1 Introduction	170
9.2 Conclusions from Chapter 4 Recycling of slag and Weldability	170
9.3 Conclusions from Chapter 5 Element Transfer Behaviour	171
9.4 Conclusions from Chapter 6 Weld Bead Geometry and Shape Relationships	172
9.5 Conclusions from Chapter 7 Metallurgical Studies	172
9.6 Conclusions from Chapter 8 Cost Analysis	173
9.7 Scope for future work	173
REFERENCES	174-197
CURRICULUM VITAE	198-200

LIST OF FIGURES

<i>Figures</i>	<i>Page No.</i>
Figure 1.1 : Submerged arc welding for circumferential joint in large fabrication	2
Figure 1.2 : Submerged Arc Welding	3
Figure 1.3 : Effect of Arc Voltage on bead shape	18
Figure 1.4 : Cross sections of weld bead profile for (a) DCEP polarity (b) DCEN polarity	21
Figure 1.5 : Effect of electrode angle on butt weld	22
Figure 1.6 : Effect of electrode angle on fillet weld	22
Figure 2.1 : (a) Slag as collected from the factory and (b) after crushing to particle size of original flux	32
Figure 2.2 : Micro hardness of single layer claddings prepared using flux and reclaimed slag	33
Figure 2.3 : Bar chart showing variation of weld metal manganese, silicon, nickel, sulphur, carbon, phosphorus and oxygen content in electrode positive (EP) and electrode negative (EN) polarities	39
Figure 2.4 : A schematic diagram of typical SAW welded butt joints with no bevel or gap	40
Figure 2.5 : Direct effect of welding current on (a) form factor and dilution and (b) width, height, A_r and A_p	45
Figure 2.6 : Direct effect of arc voltage on (a) form factor and dilution and (b) width, height, A_r and A_p	45
Figure 2.7 : Plot of acicular ferrite volume fraction of weld metal vs. titanium content of the flux	47
Figure 2.8 : Plot of acicular ferrite length vs. titanium content of the flux	47
Figure 2.9 : Influence of heat input on (a) tensile strength and (b) % elongation	50
Figure 2.10 : Optical micrographs showing the microstructures in different regions of the welded joint	53

<i>Figures</i>	<i>Page No.</i>
Figure 3.1 : Flow chart diagram of Slag recycling process	58
Figure 3.2 : Submerged arc welding machine	61
Figure 3.3 : Methodology for submerged arc welding process	65
Figure 4.1 : Weld pad for spectro analysis (ASME SFA 5.17)	74
Figure 4.2 : Weld pad prepared using fresh flux	74
Figure 4.3 : Weld pad prepared using pure slag	75
Figure 4.4 : Small pellets of recycled slag	76
Figure 4.5 : Steps involved in recycling slag	77
Figure 4.6 : Weld pad prepared using different compositions of slag	78
Figure 4.7 : Transverse section view of specimen cut from different weld pads	78
Figure 4.8 : Comparison of chemical composition of weld pads prepared using pure slag, fresh flux, and different compositions of slag	80
Figure 4.9 : Comparison chart between fresh flux and recycled slag	81
Figure 4.10 : Slag obtained from weld pad prepared using pure slag	83
Figure 4.11 : Slag obtained from weld pad prepared using fresh flux	83
Figure 4.12 : Slag obtained from weld pad prepared using recycled slag	84
Figure 4.13 : Dimensions of tensile test and Impact test assembly in mm as per ASME SFA 5.17	85
Figure 4.14 : Universal Tensile Testing Machine	86
Figure 4.15 : Impact specimen of recycled slag	87
Figure 5.1 : Eight sets of submerged arc welding specimen	97
Figure 5.2 : Scatter diagram between predicted and actual values of Carbon	104
Figure 5.3 : Scatter diagram between predicted and actual values of Manganese	104
Figure 5.4 : Scatter diagram between predicted and actual values of Silicon	105

<i>Figures</i>	<i>Page No.</i>
Figure 5.5 : Scatter diagram between predicted and actual values of Sulphur	105
Figure 5.6 : Scatter diagram between predicted and actual values of Phosphorus	106
Figure 5.7 : Effect of arc voltage on Carbon	107
Figure 5.8 : Effect of wire feed rate on Carbon	107
Figure 5.9 : Effect of arc voltage on Manganese	108
Figure 5.10 : Effect of wire feed rate on Manganese	109
Figure 5.11 : Effect of wire feed rate on Silicon	110
Figure 5.12 : Effect of wire feed rate on Sulphur	111
Figure 5.13 : Effect of arc voltage on Phosphorus	112
Figure 5.14 : Effect of wire feed rate on Phosphorus	112
Figure 6.1 : Weld bead geometry	116
Figure 6.2 : Eight sets of bead geometry welded specimen	126
Figure 6.3 : Specimen removed for observing responses	127
Figure 6.4 : Scatter diagram between predicted and actual values of bead width	133
Figure 6.5 : Scatter diagram between predicted and actual values of bead height	134
Figure 6.6 : Scatter diagram between predicted and actual values of Bead penetration	134
Figure 6.7 : Scatter diagram between predicted and actual values of WPSF	135
Figure 6.8 : Scatter diagram between predicted and actual values of WRFF	135
Figure 6.9 : Effect of wire feed rate on bead width	136
Figure 6.10 : Effect of arc voltage on bead height	138
Figure 6.11 : Effect of travel speed on bead height	138
Figure 6.12 : Effect of contact tube to plate distance on bead height	139
Figure 6.13 : Effect of wire feed rate on bead penetration	140

<i>Figures</i>	<i>Page No.</i>
Figure 6.14 : Effect of contact tube to plate distance on bead penetration	140
Figure 6.15 : Effect of arc voltage on WPSF	142
Figure 6.16 : Effect of wire feed rate on WPSF	142
Figure 6.17 : Effect of contact tube to plate distance on WPSF	143
Figure 6.18 : Effect of arc voltage on WRFF	144
Figure 6.19 : Effect of wire feed rate on WRFF	145
Figure 6.20 : Effect of travel speed on WRFF	145
Figure 6.21 : Effect of contact tube to plate distance on WRFF	146
Figure 7.1 : Iron Carbon phase diagram	150
Figure 7.2 : Microstructural changes during cooling of mild steel	151
Figure 7.3 : Optical micrograph of (a) base metal, (b) grain refined HAZ, (c) grain coarsened HAZ, (d) weld metal	152
Figure 7.4 : Effect of temperature gradient, grain growth rate and cooling rate on solidification	154
Figure 7.5 : Different subzones of a fusion zone	155
Figure 7.6 : Microstructure of base metal	159
Figure 7.7 : Microstructure of weld metal deposited with pure slag	159
Figure 7.8 : Microstructure of weld metal deposited with recycled slag	160
Figure 7.9 : Microstructure of weld metal deposited with fresh flux	161
Figure 7.10 : Microstructure at the fusion boundary of weld deposited with pure slag	161
Figure 7.11 : Microstructure at the fusion boundary of weld deposited with recycled slag	162
Figure 7.12 : Micro-hardness survey across the weld bead	163

LIST OF TABLES

<i>Tables</i>	<i>Page No.</i>
Table 1.1 : Classification of SAW flux according to the chemical nature	10
Table 1.2 : Harmful effects of various alloying elements	13
Table 3.1 : Chemical composition of base metal and filler wire (wt. %)	59
Table 3.2 : Chemical composition of fresh flux (wt. %)	60
Table 3.3 : Chemical composition of pure slag (wt. %)	60
Table 3.4 : Welding conditions for SAW set up	62
Table 3.5 : Welding parameters with their upper and lower limit for element transfer behaviour	67
Table 3.6 : Welding parameters with their upper and lower limit for weld bead geometry and shape relationships	67
Table 3.7 : Design matrix for two level half factorial design	68
Table 3.8 : Design matrix for calculating coefficients after confounding	69
Table 4.1 : Welding parameters to prepare weld pad	73
Table 4.2 : Chemical composition (wt. %) of weld pad prepared using pure slag and fresh flux	75
Table 4.3 : Different compositions (wt. %) of slag	79
Table 4.4 : Chemical composition (wt. %) of weld pads prepared using fresh flux, pure slag and different compositions of slag compared with AWS 5.17 standard	79
Table 4.5 : Results of weld qualification tests	86
Table 5.1 : Welding parameters with their upper and lower limit	96
Table 5.2 : Observed values of weld metal composition (wt. %)	98
Table 5.3 : Observed mean values weld metal composition (wt. %)	98
Table 5.4 : Predicted and actual values of weld metal composition (wt. %)	98
Table 5.5 : Coefficients of the model and their significance	100
Table 5.6 : Final developed model for weld metal composition (wt. %)	101

<i>Tables</i>	<i>Page No.</i>
Table 5.7 : Model adequacy test for weld metal composition (wt. %)	102
Table 6.1 : Welding parameters with their upper and lower limit	125
Table 6.2 : Observed values of weld bead geometry and shape relationships	128
Table 6.3 : Observed mean values of weld bead geometry and shape relationships	128
Table 6.4 : Predicted and actual values of weld bead geometry and shape relationships	129
Table 6.5 : Coefficients of the model and their significance	130
Table 6.6 : Final developed models for weld bead geometry and shape relationships	131
Table 6.7 : Model adequacy test for weld bead geometry and shape relationships	132
Table 8.1 : Cost analysis of recycled slag and fresh flux per 50 kg	168

NOMENCLATURE

α	:	Angle of convexity, degrees
β	:	Angle of entry, degrees
A_t	:	Total weld bead area, mm ²
AWS	:	American welding society
BG & SR	:	Bead geometry and shape relationships
BM	:	Base metal
DCEN	:	Direct current electrode negative
DCEP	:	Direct current electrode positive
HAZ	:	Heat affected zone
h		Bead height, mm
N	:	Contact tube to plate distance, mm
p	:	Bead Penetration, mm
SAW	:	Submerged arc welding
S	:	Travel speed, cm/min
V	:	Arc voltage, volts
W	:	Wire feed rate, cm/min
w	:	Bead width, mm
WM	:	Weld metal
WPSF	:	Weld penetration shape factor, w/p
WRFF	:	Weld Reinforcement form factor, w/h

INTRODUCTION

1.1 Overview of Submerged Arc Welding

Submerged arc welding (SAW) is a popular arc welding process for joining thick and heavy sections. The Linde-Union Carbide Company was the first to develop it. This process, originally known as union melt, began in Pennsylvania in 1930 and was used to create longitudinal seams in pipes. Jones, Kennedy, and Rothermund later patented it in 1935. It is the most widely used process for manufacturing thick plates, marine vessels, heat exchangers, and boilers. Main characteristics of this process include a high deposition rate, a smooth surface appearance, high weld penetration, and a low operating skill requirement. It can weld thin sheets of steel up to 5 mm thick with minimal spatter, making it preferable over MIG process (Houldcroft, 1989). Submerged arc welding for circumferential joints in large fabrication is depicted in Fig. 1.1. This process, in addition to welding, can be utilised in cladding to improve surface wear resistance, resulting in a sound weld with a high impact value (Wilson, 1996).

This process can be operated at a travel speed of up to 5 m/min, resulting in a deposition rate of 27 to 45 kg/hr (Weisman, 1976). This process was designed in many ways (such as the use of three wires, long stick out electrode, narrow gap welding, pulsed arc welding, twin arc welding etc.) to increase the overall efficiency and weld metal properties. This process can produce welds with welding currents of 2000 amps, either AC or DC, using single or multiple wires, and the current can reach 5000 amps with multiple wires (Kalpakjian & Schmid, 2006). It was discovered that

as the number of wires increased, the rate of weld metal deposition increased exponentially (Tusek, 1996). Another study discovered that in the submerged arc welding technique, using metal powder and steady heat input, the deposition rate may be increased by 50% for single arc and 20% for triple arc. Moreover, the deposition rate increased up to 80% with the addition of metal powder (Chandel et al., 1998).



Figure-1.1: Submerged arc welding for circumferential joint in large fabrication (Houldcroft, 1989)

This process is a unique method of joining metals since it involves the electrode completely submerged under the layer of granular flux. This process necessitates the use of a continuously fed consumable solid electrode in order to generate an arc shielded by a layer of flux composed of silica, calcium fluoride, and other compounds. This layer of flux serves as a path of conductance between the electrode and the workpiece. It prevents spatter and spark by inhibiting the harmful UV rays and fumes. The flux layer is transformed into slag during welding and then discarded. Submerged arc welding is depicted schematically in Figure 1.2 (Cary & Helzer, 2005). To perform welding, the solid or flux cored electrode wire is continuously supplied into the flux covered weld metal, as shown in the Figure 1.2. Metallic wires

or a combination of metallic and non-metallic wires are preferred for submerged arc welding. Coated electrodes are obsolete as compared to continuously fed electrodes due to difficulty in its storage and electrical conductivity (Lincoln Electric, 1994).

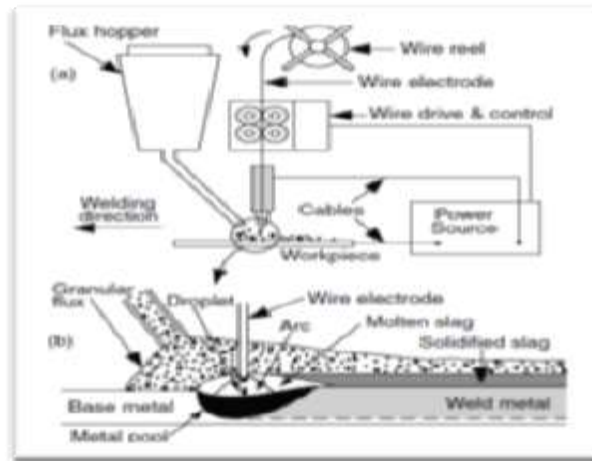


Figure-1.2: Submerged Arc Welding (Kou, 2003)

1.2 SAW Process

A flux delivery tube transfers flux from the container to the flux hopper. It is possible to install a flux recovery system to pick up excess flux depending on the level of automation. Submerged arc welding can be performed with either an alternating current or direct current power source. This process is accomplished with the help of a submerged arc welding machine. The layer of granular flux is thick enough to prevent spatter and pollution while also protecting the weld pool from contamination by harmful gases. As a result, a high-quality weld is produced. When flux comes into contact with hot metal, it forms a protective layer of slag on the weld bead surface. The unmelted flux acts as an insulator and is reused. The slag that deposits on the weld bead usually peels off on its own or can be detached using chipping hammer and can be reused in place of fresh flux or in combination with fresh flux.

1.3 SAW Components

The main components of the machine include a wire electrode, a flux hopper, a wire feed motor attached with wire feed rolls suitable for desired wire diameters, a wire straightener roller, and a power source for current transmission.

1.3.1 Wire Electrodes

Welding electrodes are used for welding stainless steels, low and special alloy steels and some nonferrous metals like copper and nickel. In general, electrodes are coated with copper to prevent rusting and to improve their electrical conductivity. Electrodes are available in both straight and coiled lengths. Their diameters may be 1.6, 2.0, 2.4, 3.2, 4.0, 4.8, and, 6.4 mm. The estimated value of current to weld with 1.6, 3.2 and 6.4 mm diameter electrodes are 150–350, 250–800 and 650–1350 Amperes respectively. Addition of alloying elements in electrodes helps in improving its properties.

1.3.2 Multi Wire and Variants

SAW is normally operated with a single wire on either AC or DC current.

Common type of SAW wires are:

- Twin wire
- Multiple wire (tandem or triple)
- Single wire with addition of hot wire

These different types of wires contribute to increase productivity by significantly increasing weld metal deposition rates. Other considerations to improve overall efficiency of the process are:

- Flux depth/width;
- Flux and electrode classification and type;
- Electrode wire diameter;
- Multiple electrode configurations.

1.4 SAW Fluxes

These fluxes are classified as acidic, basic, and neutral. The flux is chosen based on its ability to meet metallurgical requirements. Most weld metals get oxidised due to the absorption of atmospheric oxygen during welding. Fluxes are used to ensure that oxidation is kept to a minimum by floating off the oxides that form in the weld pool (Bailey, 1991). The selection of an appropriate flux composition is critical for improving the mechanical properties, microstructure, and weld chemistry of weld metal (Paniagua-Mercado & Lopez-Hirata, 2011). Flux is typically composed of metallic oxides such as CaO, MgO, and FeO, as well as fluorides such as CaF₂. It is precisely prepared to be compatible with the given electrode wire, such that the combination of flux and wire results in the desired mechanical properties. It was found that flux composition has significant effect on tensile strength, elongation and impact strength of weld metal (Jindal et al., 2013; Kumar et al., 2020).

SAW flux can incorporate alloying elements just like coating of the coated electrode. Flux's insulating characteristics allow it to provide ideal conditions for very high current densities, concentrating heat in a narrow welding zone. Increased welding speed gives a deeper penetrating arc, narrow grooves with less metal deposition. Flux properties can be operated on a wide range of currents, arc voltages, and travel

speeds, however, all of which can be regulated smoothly independent of one another. As a result, by employing the proper welding procedure, it is possible to achieve welded joints with the desired shapes, geometry, chemistry, and mechanical properties. SAW flux should be formulated in such a way that it does not produce a large amount of gases when exposed to the high temperatures of the welding zone. It should be granular in texture and capable of freely flowing through standard welding equipment's flux feeding tubes, valves, and nozzles. The flux is a non-conductor of electricity in its solid state, but when molten, it becomes a highly conducting medium. Hence, the arc must be initiated using special means. When the arc initiates the surrounding flux melts and the current starts flowing across the arc, this happens because arc acts as a conducting path for the flux. The flux consists of elements which helps in striking of an arc as well as stabilising it after it has been initiated. These elements decrease with the increase in the values of arc voltage and welding current. It was discovered that adding TiO_2 to the flux increases the percentage of acicular ferrite and thus improves weld metal toughness and ductility (Paniagua-Mercado et al., 2009). Similarly, Dowling et al. (1986) discovered that addition of Ti, Mo, and Cr nucleates acicular ferrite by operating as an inert substrate.

1.4.1 Role of Flux

Various functions performed by submerged arc welding flux are as follows:

- Throughout the submerged arc welding process, flux maintains a stable arc. The addition of certain alloying elements that acts as an arc stabiliser, to the flux, improves the maintenance of the arc.

- The flux basicity has a significant impact on the weld bead profile. A flux with higher basicity results in a higher penetration bead (Gupta & Arora, 1991).
- Flux shields the weld pool from oxidation by converting it into slag after welding. This slag increases the time for weld bead solidification, resulting in a smooth bead finish.
- Flux helps in improving the toughness of the weld metal by controlling oxidation and impurities in molten weld pool. It is possible to remove elements such as sulphur and phosphorus by transferring them to slag using calcium oxide. Slag metal reactions at temperatures lower than 2000°C result in improving FeO and reducing SiO₂ content. It is therefore necessary to increase the silica content in order to raise the weld pool temperature (Belton et al., 1963).
- Flux aids in the prevention of undesirable elements from being transferred to the weld pool. Certain alloying elements, such as CrO₃ and NiO, have been added to flux for this purpose.
- Flux regulates the cooling rate of the molten pool by forming a shield known as slag on the weld metal. This slag extends the time required for weld pool solidification.

1.4.2 Classification of SAW Fluxes

SAW fluxes can be categorised into different types using different criteria:

- According to the method of manufacturing.
- According to the chemical nature.
- According to the mineral flux composition

1.4.2.1 According to the Method of Manufacturing

SAW fluxes classified according to the method of manufacturing are as follows:

- **Fused Flux:** To make fused flux, quartz, limestone, and manganese dioxide (MnO_2) are mixed with small amounts of fluorspar and aluminium oxide (Al_2O_3) and then heated in an electric arc furnace to reduce manganese dioxide (MnO_2) to manganese oxide (MnO). This flux is then cooled by streaming cold water on it. After cooling, it is crushed and sieved to obtain grain with a diameter of about 0.2–1.6 mm, and then packed. This process includes drying from 250°C to 300°C for an extended period of time; this process can reduce moisture by up to 0.06 percent (Visvanath, 1983). This flux is homogeneous in nature. The fused welding fluxes have low moisture sensitivity, better storing capacities, and high abrasion resistance. Flux can be recycled without losing particle size using a flux recovery system.
- **Agglomerated Flux:** In the agglomeration process, the ingredients are fed into a rotating disc to dry mix. The powdered mixture is then combined with water glass (a concentrated solution of sodium and potassium silicate) to form pellets. These pellets are baked at 800°C, crushed, sieved to grain size, and packed. Because it is manufactured at a lower temperature than fused flux, it is simpler to produce. During storage, this flux is more susceptible to moisture. It is the most preferred flux in hard-facing operations. During submerged arc welding, it is easy to transfer desired alloying elements from agglomerated flux to the weld pool. Furthermore, using flux dust, agglomerated acidic flux was developed and found to be useful without affecting weld metal quality.

(Kumar et al., 2010) found that weld metal prepared using agglomerated flux have acceptable yield strength, tensile strength and fracture energy.

- **Bonded Flux:** In bonded flux, the dry mixed raw material was bonded with either potassium silicate or sodium silicate solution, or both. The wet bonded mixture is pelletized and baked at a low temperature (450-760°C). After drying, the pellets are broken and screened for particle size. It is easy to add alloying materials and deoxidisers, and it allows for a thicker layer of flux to be used in welding.

1.4.2.2 According to the chemical nature

Basicity Index (BI) clearly express the chemical nature of welding flux (Tulani et al., 1972) and can be defined as follows:

$$BI = \frac{CaO + MgO + CaF_2 + Na_2O + K_2O + Li_2O + 1/2(MnO + FeO)}{SiO_2 + 1/2(Al_2O_3 + TiO_2 + ZrO_2)}$$

Table-1.1 describes the classification of SAW flux according to the chemical nature. As mentioned in this table, it is evident that the flux is acidic when basicity index is less than 1, neutral when it is between 1 to 1.5 and basic when it is greater than 1.2. Higher basicity results in higher impact values but reduces features like welding speed and fine rippling of the weld bead. As a result, it is advantageous to select the lowest possible flux basicity at the specified toughness. In general, neutral flux performs well. While basic fluxes produce the best metallurgical results, they have poor welding properties. Higher basicity fluxes produce narrower heat affected zones than lower basicity fluxes (Gupta & Arora, 1991).

Table-1.1: Classification of SAW flux according to the chemical nature (Weman, 2003)

Welding Flux	Basicity	Melting point	Typical Oxygen level
Acidic	<0.9	1100-1300°C	>750 ppm
Neutral	1.0-1.5	1300-1500°C	550-750 ppm
Basic	>1.2-2.00	>1500°C	300-550 ppm
High Basic	>2	>1500°C	<300 ppm

1.4.2.3 According to the Mineral Flux Composition

SAW fluxes classified according to the mineral flux composition are as follows

- **Calcium Silicate flux:** This flux is characterized by its efficient silicon pickup, which results in high current carrying capacity of 2500 A and higher penetration. It contains more than 45% silica content. It is rust resistant, but due to the high silica content, it is not suitable for multi-pass welds. It may be preferred in applications where toughness is not a major factor.
- **Aluminate-basic flux:** They have a higher Mn pickup, resulting in good mechanical property. A low cracking tendency can be obtained using wire electrodes. They are assumed to be more productive due to their high rust resistance and toughness.
- **Fluoride-basic flux:** They have high cracking insensitivity and good weld metal impact values.
- **Manganese-silicate:** This type of flux is acidic in nature and is suitable for high travel speeds. It is capable of producing welds with high strength and toughness.
- **Rutile:** Because of its low silica content, this flux has good strength and toughness but poor slag detachability. It is also known as acidic flux.

1.4.3 Characteristics of Flux

In the SAW, flux should possess the following characteristics in order to meet the chemical as well as metallurgical requirements:

- Flux should maintain the arc stability throughout the submerged arc welding process particularly in AC welding.
- Flux should absorb less moisture and have a long shelf life.
- Flux should produce slag that is easily detachable from the weld metal.
- Flux should keep the weld deposit free of defects such as inclusions and porosity.

1.4.4 Properties of Flux

The properties of flux are described as below:

- Technological properties
- Physical properties at room temperature
- Physical properties at elevated temperature

1.4.4.1 Technological Properties

- **Slag detachability:** It is defined as the property that allows the solidified slag to be easily separated from the weld metal (Murugan & Parmar, 1997). This property depends upon the thermal coefficients of slag and molten metal (Singh and Singh, 2010). As the thermal coefficient of slag and molten metal increases, slag detachability improves (Wittung, 1980). Multi-pass welding and narrow gap welding are two of its applications. Alumina and slag are

considered self-lifting, carbonate-based slag has poor slag detachability (Renwick & Patchett, 1976).

- **Bead Geometry:** Welding factors such as welding current, arc voltage, travel speed, flux type etc. have a significant impact on this property (Srivyas et al., 2014). It is recommended to use alumina rutile or alumina basic flux slag to control bead shape because slag viscosity is significantly responsible for the bead shape. The depth of penetration increases as the welding current increases. It was observed that arc voltage and welding speed have no effect on penetration and bead height, but current has a significant effect on penetration depth (Karaoglu & Secgin, 2008).
- **Flux consumption rate:** It refers to the amount of flux consumed during the welding process. It is the primary influencing factor in the transfer of various alloying elements from flux to weld metal or from weld metal to slag. It is therefore necessary to maintain the weld quality with low flux consumption. Tensile strength is significantly affected by the addition of CaF_2 and NiO to the flux. Furthermore, the percentage elongation is affected by the basicity index of the flux and the carbon equivalent of the weld. The higher the flux consumed, the greater the transfer of alloying elements, which ultimately affects weld quality (Singh et al., 2014). Various welding parameters, such as flux chemical composition, melting temperature, flux density, and basicity index, were discovered as the most dominant parameters influencing flux consumption. As the voltage rises, so does the flux consumption (Gupta & Arora, 1991). It was discovered that using 1 kg of flux while welding produces equivalent amount of slag (Singh et al., 2006).

- **Toxicity and fumes:** During welding a thick layer of flux shields the molten metal, thus prevents spatter and sparks while also suppressing ultraviolet radiation and fumes. The quantity of gas released differs according to the type of flux used. Fumes are produced in smaller quantities in case of fused flux, whereas fumes are produced in greater quantities in the case of agglomerated flux. These fumes are hazardous to the skin, eyes, and respiratory system. Flux is made up of silica, Mn oxide, CaF_2 , Cr and Ni compounds, and other substances. Fumes produced by the melting of flux during welding causes a variety of health problems. The harmful effects of various alloying elements are shown in Table 1.2.

Table-1.2: Harmful effects of various alloying elements (Singh, 2007)

S. No.	Various alloying elements	Harmful effects
1.	Chromium or Nickel compounds	Irritates skin, respiratory tract causes metal fume fever
2.	Fluorine or Hydrogen compound	Irritation to skin, eyes and throat
3.	Manganese oxides	Affects central nervous system

1.4.4.2 Physical Properties at Room Temperature

Flux is extremely important in submerged arc welding. The properties such as colour, flow ability, friability, particle size, and bulk density, all impart specific characteristics to the flux that affect the weld metal quality. These characteristics are explained below:

- **Colour:** Flux has a distinct colour because of its raw material composition, which remains same prior to welding. The temperature and time of heating during welding have the greatest influence on colour change. The colour of

flux changes as the temperature or duration of welding changes. This change is sometimes caused by the oxidation of a specific alloying element present in the flux composition.

- **Flowability:** It is defined as the ability of a flux to flow through the feeding tube from the flux hopper. The flux hopper's flow ability can be calculated by dividing the amount of flux entered through the feeding tube by the time required. The larger the flow rate, the larger the particle size will be.
- **Friability:** It is defined as the ability of flux to break up into fragments. The angle of repose and the coefficients of external and internal friction are used to calculate this property. This property makes the processing, transport, and the storage of the flux easier.
- **Particle size:** Flux particle size is important in flux composition because it affects current carrying capacity, weld bead profile, surface finish, and rust resistance. The coarser the particle size, the rougher the weld surface, and the finer the particle size, the smoother the weld surface with higher current carrying capacity. Furthermore, finer grains result in higher penetration. On the other hand, very fine particles can cause weld bead irregularities and an unsatisfactory weld bead.
- **Bulk Density:** Bulk density is defined as a parameter that is proportional to the amount of flux used while maintaining constant flux consumption. It has a direct impact on the arc cavity formed during welding. The bulk density of the fused flux was discovered to be greater than that of agglomerated flux. As a result, the flux consumption in agglomerated flux is lower.

1.4.4.3 Physical Properties at Elevated Temperature

Physical properties of flux at elevated temperature (approximately 1100°C) and above (approximately 1350°C) are as follows:

Thermo-Gravimetric Properties: It is defined as the property that indicates the change in weight as the temperature is changed below the melting point over time. To assess this property, 1 gm of alumina crucible was heated at the rate of 50°C per minute to see if the weight increased or decreased as the temperature increased (Davis & Bailey, 1982). This procedure was repeated six times for six different fused fluxes. It was observed that low silica calcium silicate flux has low weight at the decomposition temperature of calcium carbonate, whereas manganese silica initially shows weight loss due to fluorine compound, then weight increases.

Moisture Control: The presence or absence of moisture in the flux has the greatest impact on weld quality. Moisture in the weld metal can cause hydrogen embrittlement. Agglomerated fluxes are hygroscopic in nature, whereas fused fluxes are not. It is defined as the amount of diffusible hydrogen (in millimetres) present per 100g of weld metal deposited during welding. It was discovered that approximately 15ml of hydrogen is present in 100g of deposited weld, where fused flux has a moisture content of 0.03 to 0.06 percent and agglomerated flux has a moisture content of 2%. (Visvanath, 1983).

Viscosity: It is defined as the material property that expresses the relationship between viscous stress and the rate of change of deformation. The slag viscosity is measured in the submerged arc welding process by the chemical composition and the melting temperature of the flux. The depth of penetration increases as slag viscosity

and surface tension between the flux and the weld metal increase (Indacochea et al., 1985; Schwemmer et al., 1979). The presence of silicon dioxide in the flux improves viscosity, whereas the presence of CaO, MnO, Fe₂O₃, and CaF₂ in the flux reduces viscosity (Singh et al., 2013). The addition of CaF₂ to the flux helps in the formation of fluoride gas compounds that protect the weld pool from oxygen, nitrogen, and hydrogen pickup (Cotsee, 2020). The viscosity of the flux aids in the proper shielding of the weld pool as well as the dissolution of gases trapped amidst the melted flux and the weld pool (Butler & Jackson, 1967).

Surface Tension: It is defined as the ability of liquid weld metal to reduce to the minimum surface area. Since, molten slag has a lower surface tension than molten steel; it rises to the surface and coalesces quickly. Increased surface tension between weld metal and flux leads to increased weld penetration, which improves weld quality (Indacochea et al., 1985; Schwemmer et al., 1979).

Melting Point: The melting point of submerged arc welding flux is typically defined as the temperature at which the flux remains molten until the weld metal solidifies. This feature produces a smooth surface appearance with improved weld quality. The melting point of submerged arc welding flux is approximately 1350°C. At melting temperature, increase in thermal conductivity causes an increase in the weld pool length on the plate surface (Debarata et al., 2014).

1.5 Process Parameters

If defect free joints i.e. without cracking, porosity, and undercut are to be obtained, it is critical to select the appropriate welding parameters for the given plate thickness

and joint preparation. Because responses such as bead geometry, deposition rate, weld material, and element transfer are affected by the process parameters. It is important to set the variables to the defined range before initiating SAW in order to achieve high quality welds. The following process variables must be considered:

- Welding current
- Arc voltage
- Travel speed
- Electrode diameter
- Electrode stick out
- Linear heat Input
- Electrode polarity
- Flux depth
- Electrode angle

1.5.1 Welding Current

It regulates the rate at which the electrode melts and, as a result, the rate of weld deposition. It also regulates the depth of penetration. Due to higher welding current in thinner plates and improperly fitted joints, there is excessive weld reinforcement with burn through (Pandey, 2004). Excessive current also results in a too narrow bead and undercutting, whereas excessively low current results in an unstable arc and overlapping. An ammeter is generally included in a SAW control panel to monitor and control the welding current. Current range and polarity influence the percentage difference in melting rate, bead height, bead width, and bead penetration (Chandel et al., 1987).

1.5.2 Arc Voltage

The arc voltage changes directly as the arc length differs. As the arc length increases, so does the arc voltage and thus more heat is available to melt the metal and the flux. However, increasing the arc length causes the arc column to spread wider, resulting in an increase in weld width and volume of reinforcement, while the depth of penetration decreases. The welding current and wire diameter affect the arc voltage. Figure 1.3 shows the effect of arc voltage on bead shape.

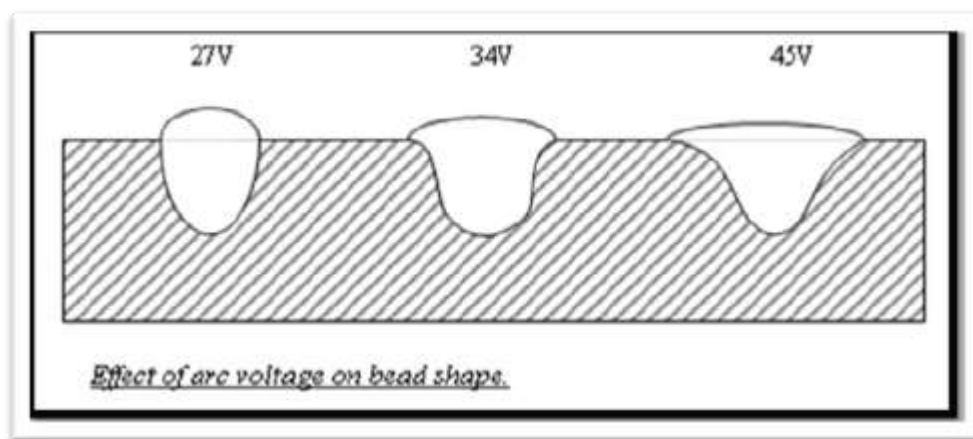


Figure-1.3: Effect of arc voltage on bead shape (Courtesy: TWI Ltd.)

1.5.3 Travel Speed

Welding speed results is inversely proportional to penetration, and weld reinforcement. In addition, increased welding speed lowers the linear heat input for a given combination of welding current and voltage. Very high travel speed reduces fusion between the weld deposit and the parent metal, increasing the likelihood of undercut, arc blow, porosity, and irregular bead shape. Penetration and reinforcement increase as speed decreases, but if the speed is too slow it gives poor penetration. Excessive welding speed reduces wetting action and increases the chances of

undercutting, arc blow, weld porosity, and uneven bead shapes. Excessively low speed results in convex hat-shaped beads that crack and cause excessive melting, ultimately leading to a large weld puddle that flows around the arc, resulting in rough beads, spatter, and slag inclusions.

1.5.4 Size of Electrode

For a given welding current, if the wire diameter decreases then there is increase in current density. This produces a weld that has greater penetration but a slightly decreased width. Since the submerged arc welding process typically uses wires with diameters ranging from 2 to 5 mm, for deeper penetration at low currents 2-3 mm diameter wire is best suited. A smaller diameter electrode results in increased melting rate of submerged arc weld (Chandel et al., 1987).

1.5.5 Electrode Extension

It is also termed as "electrode-stick out." At the high current densities used in the process, the length of the electrode from the end of the contact tube to the arc is subjected to the resistance heating. Longer the stick out, higher the deposition rate, but lower penetration. As a result, when deep penetration is desired, a longer stick-out is avoided. Increased electrode extension raises the melting rate of the weld metal (Chandel et al., 1987).

1.5.6 Linear Heat Input

The linear heat input is directly proportional to the current and voltage and inversely proportional to the travel speed as the formula given by:

$$H = \frac{\eta VI}{S} \cos \Phi \text{ J/mm}$$

Where,

H = heat input per unit length, J/mm

η = Heat transfer efficiency

V = Arc voltage, volts

I = Welding current, amperes

S = Welding speed, mm/sec

$\cos \phi$ = Power factor

The higher the linear heat input for a given joint thickness, the lower the cooling rate of the weld metal and heat affected zone of the parent metal, and vice versa. The linear heat input has a significant impact on the weld metal microstructure and the final microstructure of HAZ, and thus on toughness (Sharma & Chibber, 2020).

1.5.7 Electrode Polarity

In submerged arc welding, polarity has a considerable impact on the weld bead characteristics (Chandel, 1987). In DCEP polarity, weld bead properties such as bead width, penetration, and dilution had increased values than in DCEN polarity (Singh, 2016). Figure 1.4 shows cross sections of weld bead profile for (a) DCEP polarity (b) DCEN polarity. It also has an impact on the quantity of heat produced at the electrode and on the work piece, as well as the rate of deposition and mechanical properties (Singh, 2007). Polarities are classified into three types: DCEP, DCEN, and AC. DCEP, also known as reverse polarity, has an electrode connected with positive end

of the power source. As a result, the heating action at the electrode tip increases, resulting in a shallow weld (Kou, 2003). It creates an exceptionally stable arc and a smaller weld puddle, allowing for improved control of the welding bead profile. Direct-current electrode negative (DCEN) or straight polarity, on the other hand, gives the highest metal deposition rates when the weld metal is connected to the positive end of the power source. Renwick and Patchett (1976) found that the DCEN polarity has the highest melting rate, the DCEP polarity has the lowest melting rate, and the AC polarity has a melting rate that is in between the other two polarities.

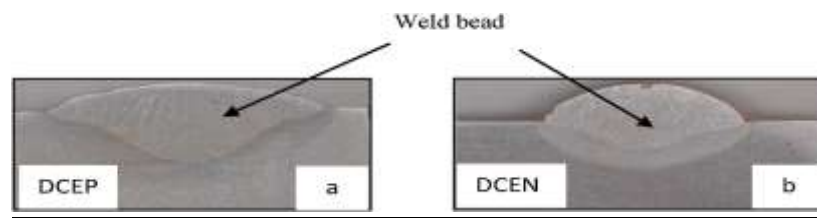


Figure-1.4: Cross sections of weld bead profile for (a) DCEP polarity (b) DCEN polarity (Singh, 2016)

1.5.8 Flux Depth

The depth of the flux is often ignored and the powder is heaped around the wire until the arc is completely covered. If optimal results are to be obtained, the flux depth should be just enough to form a layer to shield the arc, with light reflected from the arc visible at the point where the electrode enters the flux bed. A shallow flux bed allows for flash-through and can result in porosity due to insufficient metallurgical protection of the molten metal. A shallow flux bed produces a poor bead appearance and can cause spillage on circumferential welds. It is especially essential to keep the flux depth to minimum during deep preparations in thick plate, otherwise the weld bead shape and slag removal can be unsatisfactory.

1.5.9 Electrode Angle

Since the angle between the electrode and the plate determines the point of application and direction of the arc force, this affects penetration and undercut. Figure 1.5 describes the effect of electrode angle on butt weld. This figure compares the effects such as penetration, reinforcement and tendency to undercut produced by vertical arc with those obtained by leading and trailing arcs. Figure 1.6 presents effect of electrode angle on fillet weld. Figure 1.6 presents effect of electrode angle on fillet weld.

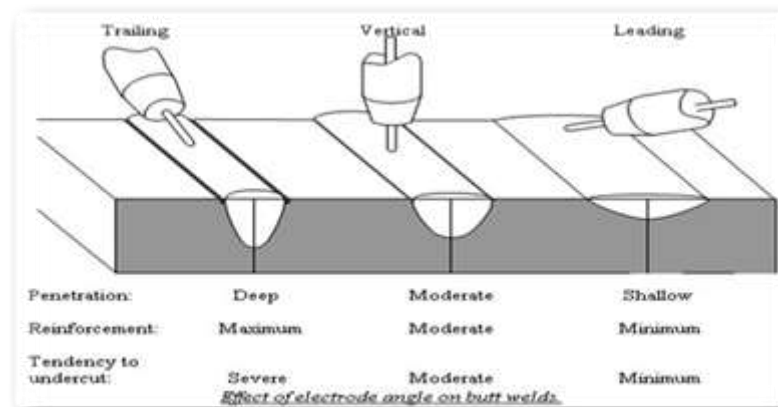


Figure-1.5: Effect of electrode angle on butt weld (Courtesy: TWI Ltd.)

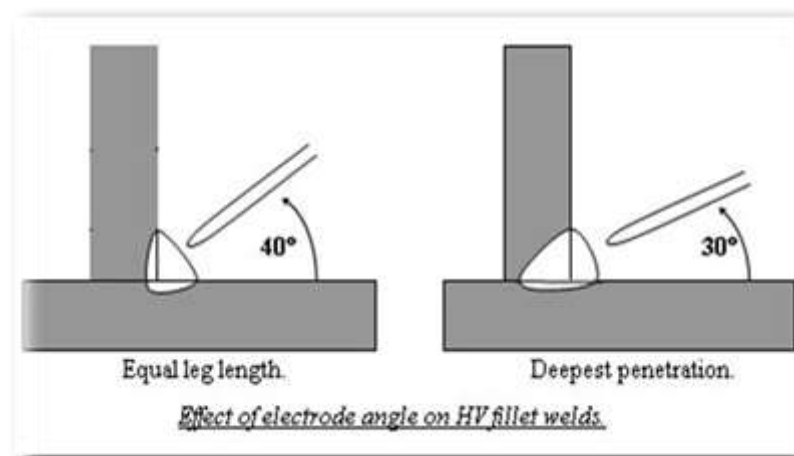


Figure-1.6: Effect of electrode angle on fillet weld (Courtesy: TWI Ltd.)

1.6 Advantages of SAW Process

- It is the most economical process as it employs the use of slag with fresh flux.
- It improves comfort for welding operator.
- Welds produced are sound, uniform, ductile, and corrosion resistant, and have a good impact value (Brien, 2004).
- Due to high deposition rate, welds are produced on thick plates with normal equipment (Kou, 2003).
- A blanket of flux shields the arc which reduces the spatter, arc flash and fumes thus making process environmental friendly (Kou, 2003).
- Sound welds are readily made (with good process design and control).
- Welding of thin steel sheets can be done at high speed of up to 5 m/min (16 ft. / min).
- Due to high current density, penetration increases and thus decreases the need for edge preparation.

1.7 Limitations of SAW process

- Flux obstructs the view of the joint during welding.
- The process is often limited to flat position welding and circumferential welding of pipes due to large volume of molten slag and metal pool (Kou, 2003)
- The electrode "stick out" is normally maintained between 25–35 mm to maintain the optimum process control.

- It requires relatively troublesome flux handling systems.
- Flux and slag residue are to be managed carefully as they cause health and safety hazards (Beck and Jackson, 1996).
- It is not suitable for welding thin material due to high deposition rates (Kou, 2003).
- It requires inter-pass and post weld slag removal.
- Flux is subjected to contamination such as porosity.
- Weld discontinuities such as solidification cracking, undercuts, incomplete fusion occurring in this process are common (Parmar, 1997).
- Due to high heat input, poor weld quality is obtained with increase distortions (Kou, 2003).

1.8 Applications of SAW process

SAW is commonly used for welding carbon, carbon manganese alloys, and stainless steel. It is also used for welding some nickel based alloys. The ability to produce high quality, defect free welds at high deposition rates with deep weld penetration makes the SAW process highly suitable for all mechanised and automatic welding and surfacing applications.

- With longitudinal and spiral welded pipes, the longitudinal welds are carried out by using a two-pass welding procedure. Spiral welded pipes are produced from a continuous coil of strip that is folded into a spiral. One welding head deposits a single weld inside, and another completes the joint from outside (Jeffus, 2004).

- Welding carbon steels, stainless steels and high strength structural steels (Brien, 2004).
- Low alloy structural steel welding applications, including mass production of repetitive short welds (Brien, 2004).
- Propane cylinder manufacturing with a copper backing system.
- For welding mild steel, medium and high-tensile low alloys (Brien, 2004).
- Fabrication of pipes, ships, pressure vessels, bridges and railroads (Parmar, 1997).
- Automotive, aviation, and nuclear industries (Parmar, 1997).
- Surfacing applications (wear-facing, build-up, and corrosion resistant overlay of steels).

1.9 Organisation of Thesis

Chapter 1: Introduction

Chapter one describes a brief introduction of submerged arc welding, its process variables, and SAW components. It also describes various fluxes with their classification and the effect of different process variables on response parameters.

Chapter 2: Literature Review

This chapter comprises the literature review on various aspects, such as recycling of slag in submerged arc welding; element transfer behaviour; weld bead geometry and shape relationships; metallurgical studies and cost analysis of recycled slag. This chapter also deals with the research gap, research objectives, and motivation of the research work and the statement of the problem.

Chapter 3: Experimental set up and Methodology

Chapter three explains the experimental set-up and process parameters used to perform submerged arc welding. Material selection, flux composition, and slag composition is discussed briefly in this chapter. The methodology required to accomplish given research work has also been discussed. In addition, this chapter explains how the design of experiments has been selected and utilised to obtain optimal results. It also includes the procedure to develop an empirical model using half factorial design. Moreover, it also describes the technique for checking the adequacy of the model using 'F' test and 't' test.

Chapter 4: Recycling of Slag and Weldability

This chapter deals with the technology applied to processing slag so as to obtain recycled slag. Different compositions of slag produced by adding different percentages of slag, additives, and binders are mentioned in this chapter. These different slag compositions developed are used to prepare a weld pad as per the ASME SFA 5.17 standard. Various trials are performed until the slag compositions achieved is similar to that of virgin flux. Selection of the best suited slag composition has been achieved by performing spectro analysis of the weld pad, prepared using fresh flux, pure slag, and three types of slag composition. Furthermore, this chapter presents various destructive and non-destructive tests performed on weld metal prepared using recycled slag, pure slag, and fresh flux. These tests involve visual inspection, dye penetrant, slag detachability, and arc stability. Apart from these tests, tensile tests, impact tests, and radiography tests are also evaluated to confirm the weldability of welded specimens prepared using recycled slag.

Chapter 5: Element Transfer Behaviour

This chapter describes the effects of welding parameters on element transfer behaviour using recycled slag. It deals with identifying the input parameters along with their upper and lower limits in order to develop the design matrix. Experimentation was performed using the design matrix. Empirical models were developed for response parameters and have been tested for adequacy by using 'F' test and 't' test. A comparison between predicted and actual values has been presented in graphical form. Moreover, the effects of welding parameters on various response factors such as carbon, manganese, silicon, sulphur, and phosphorus were presented graphically.

Chapter 6: Weld Bead Geometry and Shape Relationships

This chapter describes the effect of process variables on weld bead geometry and shape relationship when using recycled slag. In addition, it includes the development of an empirical model from the response values obtained. These models were tested for adequacy and significance of coefficients by 'F' test and 't' test, respectively. The influence of various input parameters on responses, such as bead width, bead height, bead penetration, WPSF, and WRFF, have been presented in graphical form.

Chapter 7: Metallurgical Studies

This chapter provides a detailed study on the metallurgical testing of welds. It includes microstructure and micro hardness test results obtained for weld metal deposited with fresh flux, pure slag, and recycled slag. Furthermore, graphical representations of micro hardness test results, obtained using recycled slag, pure slag,

and fresh flux, were shown for better understanding. Comparative studies of the microstructure at the fusion boundary were also discussed.

Chapter 8: Cost Analysis

This chapter deals with the detailed cost comparison of recycled slag with fresh flux. It evaluates the processing cost by adding all the costs involved in producing suitable recycled slag.

Chapter 9: Conclusions and Scope for Future Work

This chapter comprises conclusions obtained with respect to recycling of slag, weld qualification tests, element transfer behaviour, weld bead geometry and shape relationship, metallurgical studies, and cost analysis of recycled slag. It also deals with the scope of future work related to recycling of slag in submerged arc welding.

LITERATURE REVIEW

2.1 Introduction

Submerged arc welding is the most versatile type of welding where lots of research has been performed so far. Based on the review of the relevant information available on submerged arc welding, the literature has been categorised as follows:

- Recycling of slag and weldability
- Weld bead geometry and shape relationships
- Element transfer behaviour
- Metallurgical studies

2.2 Recycling of Slag and Weldability

Submerged arc welding involves the consumption of huge amount of flux to shield and join the weld metal. It was estimated that 2,500 tonnes of flux were consumed every year (Visvanath, 1982). This quantity increased to 10,000 tonnes in 2006 (Honavar, 2006) and continues to approximately 20,000 tonnes in the year 2020. During welding, when flux interacts with impurities it produces equivalent amount of slag. Because of its non-biodegradable nature, this slag is considered as scrap and discarded. To recycle slag, this crushed slag was first mixed with iron fillings for its use in the hard facing process, where it was proved to be more effective. Magnetic separation is also used during processing of slag to eliminate magnetic contaminants, which are then discarded as waste (Livshits and Shiryaev, 1960). Beck and Jackson (1996) found that the slag produced from the flux proves reliable and repeatable.

Also, this slag can result in cost saving up to 50% and is environmentally more amicable. Recycling slag helps the environment by reducing the amount of non-renewable resources used and the amount of waste that must be disposed of in landfills (Tiwari et al., 2016). However, it should be noted that most recycling methods result in some weight loss, and not all slag is converted into reusable flux. It was estimated that this loss amounts to 25% of the entire weight handled. Moi et al. (2001) conducted a study on slag consumption in the traditional SAW technique. Their research invented the use of slag-mix percent as welding parameter. Slag-mix percent refers to the combination of slag percentage with fusion of fused flux and fresh flux. Using the analysis of variance approach, the main and interactive effects of input factors (including slag-mix %) on aspects of weld bead geometry and HAZ, were assessed. However, their research did not identify the best combination of factors to produce satisfactory results and the suitable slag-mix percent that may be used without impacting weld bead geometry. In addition, the outcomes of conventional submerged arc welding were compared with a combination of virgin flux and fused slag by conducting microstructural investigations. Similarly, Pandey and Mohan (2003) conducted the study to find the correlation between the amount of flux consumed and the amount of slag produced. Pal et al. (2001) discovered that mixing 20% slag with fresh flux can result in weld metal chemistry that is comparable to that of virgin flux. Later, Singh and Singh (2006) conducted the study by combining slag with flux in various percentages and then investigated weld metal obtained using various weld qualification tests. The findings demonstrated that, in general situations, reclaimed slag can be used instead of flux.

Simultaneously, several researchers investigated ways to replenish the slag. They have used agglomeration process to recycle slag. Singh and Pandey (2009) found that the mechanical qualities and weld metal composition were acceptable and within the limits specified by AWS (American Welding Society) when welded using slag and EL 8 filler wire. Similarly, Sahni et al. (2009) conducted experimental runs using crushed slag and fresh flux mixed in different proportions. They have investigated the influence of mixing flux and slag on weld chemistry. Results revealed that using a slag flux mixture has no harmful effect on the weld metal chemistry. Another study comparable to this one was conducted by Singh et al. (2011), who reported that 60% slag mixed with fresh flux was the most suited mixture for achieving mechanical qualities acceptable to AWS standards. Additionally, it was noted that welded specimen prepared using 20% slag mix in virgin flux have passed radiographic examinations. Thirunavukkarasu et al. (2020) claimed that slag can be utilised with new flux in weight percentages as low as 20% and as high as 30%. This mixture aids in attaining optimal tensile strength, impact strength, hardness, and cost savings.

Garg and Singh (2010) stated two primary reasons for recycling slag: cost savings and environmental protection. It was discovered that the fresh flux has considerably higher cost than that of recycled slag. Additionally, because the slag is non-biodegradable, recycling it helps the environment. By recycling SAW slag, Mahto and Kumar (2010) developed an innovative approach for increasing productivity and reducing waste. They have recycled slag and then characterised it using a variety of weld qualification tests. The results indicate that the weld metal chemistry and mechanical qualities met AWS requirements. Furthermore, the results show that

recycled slag is 70.73 percent more cost effective. Similarly, Chandgude and Asabe (2014) observed that slag is efficient by 43.60% when compared to fresh flux. Garg and Singh (2012) were inspired by the concept of recycling of slag and studied the possibility of reusing the submerged arc welding slag produced during stainless steel cladding applications. SA-516 (Grade 70) base plates were welded with a slag-flux mix. The study demonstrated that pure slag provides inferior claddings when compared to fresh flux. Since this slag does not meet the AWS requirement, it must be reclaimed by adding appropriate additives and deoxidizers. The reclaimed slag obtained produces good results. Similarly, Garg and Singh (2016) investigated the effects of reclaimed slag on the quality of stainless steel claddings. Figures 2.1 (a) and (b) shows slag collected from the factory and slag crushed to the particle size of the original flux, respectively. They have conducted a comparative study between reclaimed slag and flux, the results obtained were satisfactory (Saini and Singh, 2020). Micro hardness of single layer claddings prepared using flux and reclaimed slag is shown in Figure 2.2.

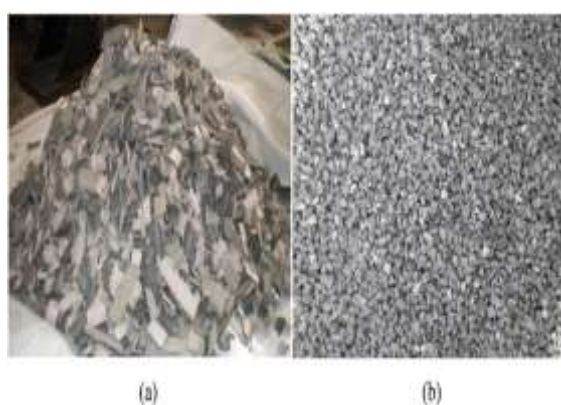


Figure-2.1: (a) Slag as collected from the factory and (b) after crushing to particle size of original flux (Garg and Singh, 2016)

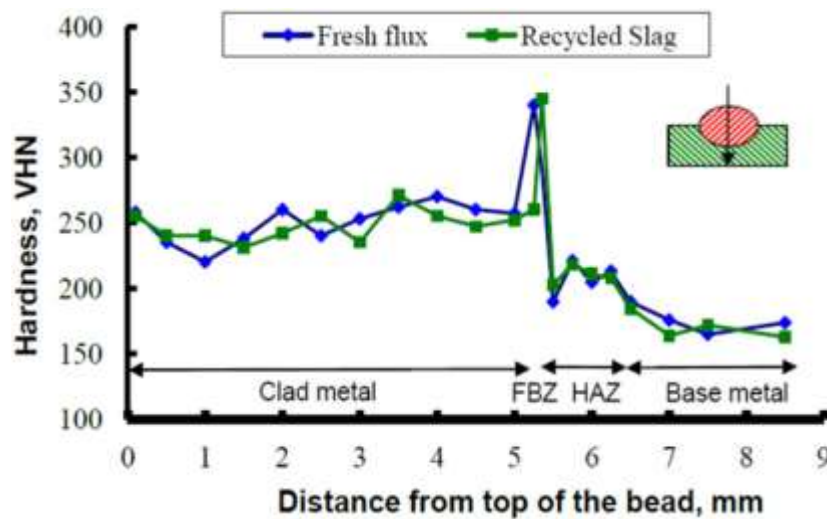


Figure-2.2: Micro hardness of single layer claddings prepared using flux and reclaimed slag (Garg and Singh, 2016)

Wang et al. (2017); Wang and Sohn (2019) discovered that slag up-cycling and recycling are critical for the long-term viability of the metallurgical industry, which generates a considerable volume of iron and steel slags. If correctly treated, slag can be reused as additives or as a stand-alone product and thus employed in civil construction and building materials (Morete et al., 2007). According to Fisher and Barron (2019), steelmaking slag can be used as a raw material, reducing its environmental impact. They discovered that by products can be employed in a way that saves resources while also providing additional benefits like CO₂ sequestration. Similarly, Dippenaar (2005) proposed methods for reducing slag generation in iron and steelmaking processes and then effectively reusing the slag left. This was accomplished by optimising various activities carried out in metallurgical reactors to improve the compositional and physical qualities of slag. According to Shen and Forssberg (2003), slag is classified into ferrous slag, non-ferrous slag, and incineration slag. They examined and explained the production, features, and applications of numerous slags, as well as its possible environmental hazards.

Similarly, Das et al. (2007) investigated the characterization, beneficiation, and usage of blast furnace flue dust, blast furnace sludge, Linz-Donawitz (LD) sludge, and LD slag from various steelmaking industries. Min and Tsukihashi (2017) investigated the structure of slag as well as physical parameters such as viscosity, electrical conductivity, and surface tension to find structure-property and inter-property relationships.

In a study conducted by Kumar et al. (2015), it was discovered that, in addition to machining parameters, flux composition has a key impact on weld quality in SAW. The $\text{SiO}_2\text{-Al}_2\text{O}_3\text{-CaO}$ flux system was employed in this investigation. In addition to alloying materials, SiO_2 based flux system has NiO , MnO , and MgO added in varying quantities with altering voltage at two levels. They have employed Taguchi L9 orthogonal array to design these experiments where voltage was regarded as a source of noise. ANOVA was used to test the model's adequacy. For a given flux composition, mechanical properties of the weld was determined to study the influence of various alloying elements on the weldment. Results revealed that the outcomes of optimal settings were acceptable with voltage having greatest influence on the impact strength. Kumar et al. (2009) reused flux dust by developing agglomerated flux without affecting the weld quality. They found that developed agglomerated flux has satisfactory mechanical properties. Also, this flux proves to be cost effective when compared with the original flux. Similarly, Kozyrev et al. (2016) developed a new flux by adding carbon-fluorine with slag from the silicon-manganese smelting process. After conducting various experiments, they found that the new flux had better strength properties than the commonly used AN-348 type flux.

Sirin et al. (2016) discusses the importance of inter-pass temperature and cooling rate with $t_{8/5}$. This $t_{8/5}$ is critical for estimating the mechanical characteristics, microstructure, and size of the weld metal and HAZ. Its value is determined by the amount of heat generated by the changes in process variables and the temperature of the base metal (BM). They have discovered that changing the inter-pass temperature of the weld region can be accomplished by either interrupting the welding machine for a while or repositioning the external weld head after internal welding. While stopping the welding machine after internal welding, notch impact toughness improves by 24.5%, thus changing the external weld point improves it by 17.7%.

2.3 Weld Bead Geometry and Shape Relationships

Extensive research has been done so far to study the effects of process variables and recycled slag on weld bead geometry and shape relationships. Gunaraj and Murugan (1999) used response surface methodology technique to study the influence of SAW parameters on heat input and the area of HAZ of bead-on plate and bead-on-joint low carbon steel. They concluded that for the same heat input, the region of HAZ for bead-on-plate is higher than that for bead-on-joint. Yang et al. (1999) developed linear-regression equations for evaluating weld characteristics from responses by using DCEP and DCEN polarity. The results revealed that linear regression equations are quite useful for analysing SAW process features. Gunaraj and Murugan (2000) used the five-level factorial technique to study the influence of process variables such as voltage, wire feed rate, welding speed, and nozzle to plate distance on responses such as penetration, reinforcement, bead width, weld bead volume, and dilution. The

model so developed was graphed to show the main and interaction effects of input factors on weld bead parameters.

Karadeniz et al. (2007) evaluated the effect of different process variables on bead penetration obtained by robotic GMAW. Welding currents of 95, 105, and 115 A were chosen for this experiment whereas arc voltages of 22, 24, and 26 V and welding rates of 40, 60, and 80 cm/min, respectively. The results revealed that depth of penetration varies proportionally with the welding current. However, welding voltage had no influence on weld penetration.

Response Surface Methodology (RSM) is a software tool that combines a mathematical and statistical method for modelling and analysing problems with a few input factors that affect the response of the structure. This methodology aids in optimising the problem within the constraints of the experimental setting. As a result, this procedure necessitates careful selection of design of experiment. Datta et al. (2008) and Myers (1990) investigated the optimal parameter combination for achieving good weld bead properties on mild steel bead on plate using a combination of virgin flux and fused slag. They developed mathematical models using the RSM approach, which was followed by the multiple linear regression method. The effect of welding input variables on various responses has been presented graphically. Furthermore, parametric optimization was performed using a combination of grey relational analysis and the Taguchi approach. As a result, they concluded that the slag flux mixture and the flux basicity index have a predominant effect on the weld reinforcement form factor, area of reinforcement, area of penetration, total bead cross sectional area, and percent dilution. In another paper, Datta et al. (2008) employed

grey relational grade to carry out parametric optimization, providing the appropriate weld bead geometry and heat affected zone characteristics using slag mix percent as another welding parameter. During research, it was found that the proposed method for SAW process quality improvement had no effect on weld bead quality. In a separate study, Datta and Mahapatra (2010) provided a method to deal with simultaneous optimization of multiple responses in submerged arc welding. Individual desirability for each response was calculated by picking a suitable desirability function. By using an appropriate desirability function, the responses were converted into their individual desirability values in this technique. The quadratic response surface methodology (RSM) was used to describe overall desirability as a function of process control parameters linear, quadratic, and interaction effects (Rao, 2001). The particle swarm optimization (PSO) technique was used to optimise this model. A confirmatory test revealed satisfactory results. Another method is to use the Derringer and Harrington desirability function to optimise weld parameters including weld bead form factor, dilution, micro hardness, and diffusible hydrogen content of structural pipelines (Jindal et al., 2014). This method determined that, apart from micro hardness, arc voltage varies proportionally with all other factors, but welding current plays an important role in influencing welding response parameters. Dhas and Kumanan (2011) proposed taguchi experimental design and regression analysis to determine the correlation between process variables and responses of the process. This study helped in decreasing the weld bead width by employing optimization techniques such as genetic algorithm (GA) and PSO to discover the ideal weld parameters. The results indicated that the optimised values were comparable. Another method for optimising weld bead geometry was weighted principal component

analysis, which used a Taguchi L25 orthogonal array design to introduce a multi-response performance index in order to achieve a single objective function (Ross, 1996). According to the confirmatory test conducted by Biswas et al. (2011), the proposed method is highly effective in achieving optimal results. The Taguchi method, based on multi-regression and artificial neural network was also used to develop mathematical models. This model was graphically represented, demonstrating its ability to select the optimal welding parameters (Reddy et al., 2013).

Kanjilal et al. (2006) proposed rotatable designs for mixtures based on statistical tests to calculate the combined effect of flux mixture and process variables on the weld metal composition and mechanical properties of weld metal. On low carbon steel plates, experiments were carried out with various flux compositions and welding parameter combinations. They discovered that the flux mixture related variables, namely weld metal chemical composition and mechanical properties, had independent as well as interaction effects on responses. Polarity was determined to be the most significant reaction among welding factors. Figure 2.3 depicts a bar graph illustrating the variation of weld metal manganese, silicon, nickel, sulphur, carbon, phosphorus, and oxygen content in electrode positive (EP) and electrode negative (EN) polarities. Using regression analysis, Bahrami and Kolahan (2010) investigated the input output connections in SAW using fresh flux-fused slag mix. Different linear and curvilinear regression functions were used to build mathematical models, out of which the best set of model was chosen. Then, simulated annealing (SA) was utilised to ideally evaluate the welding parameters in order to get the suitable set of responses. They

have observed that the suggested method is very good at identifying and optimising welding inputs for a preferred weld bead geometry.

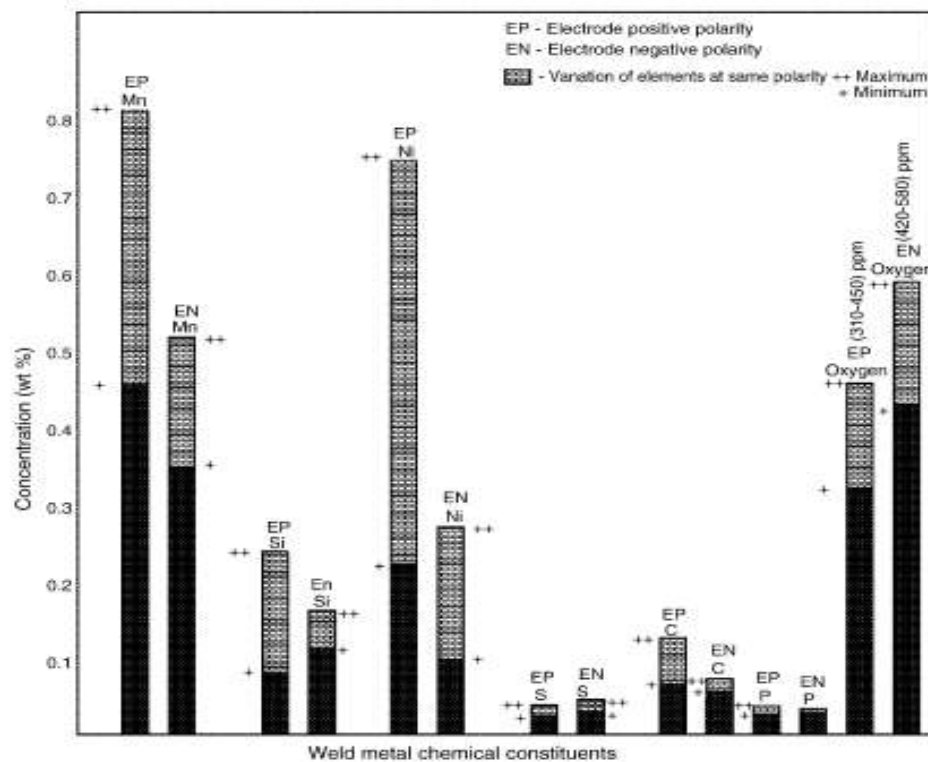


Figure-2.3: Bar chart showing variation of weld metal manganese, silicon, nickel, sulphur, carbon, phosphorus and oxygen content in electrode positive (EP) and electrode negative (EN) polarities (Kanjilal et al., 2006)

Srivastav et al. (2010) evaluated the impact of process parameters on the mechanical characteristics of ferrous metals. Their study revealed that the most important means of achieving adequate HAZ attributes, optimal bead shape, and minimal residual stresses is through the selection of appropriate process parameters.

Ghosh et al. (2011) optimised the SAW process in order to identify the areas of quality engineering that are employed in critical manufacturing processes. They used the design of experiments USP (Universal Sampling Plan) approach to construct a functional relationship for a complex set of process variables. They have found that

the important parameters such as welding bead dimensions, current, wire feed rate, travel speed, and stick out, have influence of their interactions among the main factors, in order to find their optimal values. The interactions illustrated the level of confounded character of the main factors, with respect to the important yield parameters of the process.

Shen et al. (2012) conducted a series of measurements on weldments to determine the influence of changing heat input via single and double wires on weld bead geometry, contact angle, HAZ size etc. They have calculated the % dilution and melting efficiency in order to analyse the change in heat input. They have found that the melting efficiency of the filler wire varies progressively for a certain duration before decreasing as heat input increases. The cooling time was found to have an explicit linear relation with the total nugget area, the length of the heat transfer boundary, and the nugget parameter. Figure 2.4 illustrates a typical SAW welded butt joint with no bevel or a gap.

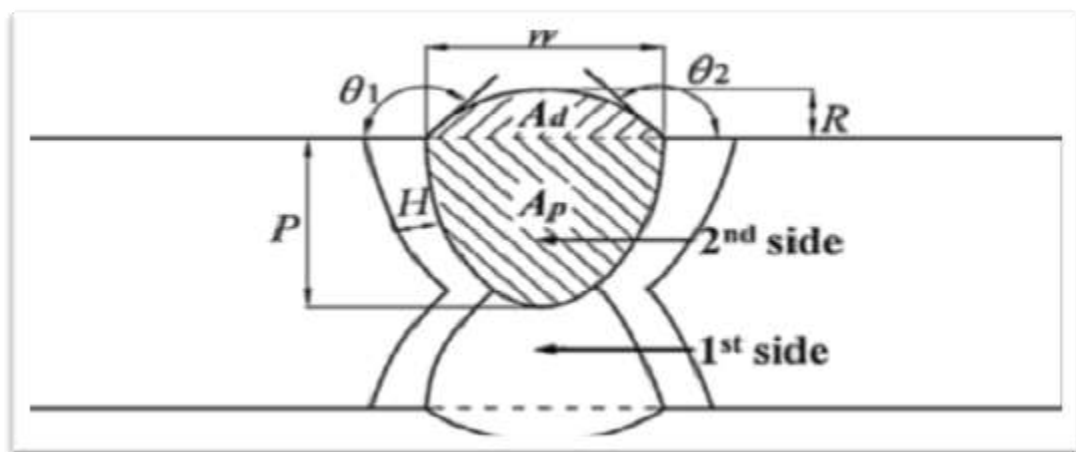


Figure-2.4: A schematic diagram of typical SAW welded butt joints with no bevel or gap (Shen et al., 2012)

Sharma et al. (2009) compared twin wire and single wire welding by analysing the influence of input variables such as current, voltage, wire diameter, and polarity on flux consumption. During this study, they found that wire diameter has a significant effect on flux consumption. The results obtained for a given heat source model were acceptable.

Moradpour et al. (2015) proposed a novel approach for optimising process variables and predicting bead geometry using fuzzy logic and the non-dominated sorting genetic algorithm II (NSGA-II). They have used this approach to weld large diameter gas transmission pipe lines and high G pressure vessels. Initially, SAW was performed on API X65 steel plates by changing the welding voltage, current, and speed. Then, weld bead geometry was predicted using a fuzzy model. The results indicate that the proposed fuzzy model's mean percentage error for depth of penetration, weld bead width, and height was 6.06 %, 6.40 %, and 5.82 %, respectively. Following fuzzy logic, the NSGA-II algorithm was utilised to calculate the desired convexity and penetration index values. Additionally, a set of optimal vectors were produced for ideal convexity and penetration index values in the ranges of (0.106, 0.168) and (0.354, 0.561), which were more applicable in real conditions.

Singh et al. (2016) studied the influence of polarity on bead geometry during submerged arc welding. They suggested a RSM technique for determining the crucial measurements of weld bead geometry and shape relationships in both DCEN and DCEP polarity. They used 'F' and 't' tests to test the model adequacy and its significance. The results were represented graphically, which helps in achieving control over weld quality through the selection of appropriate process parameters.

2.4 Element Transfer Behaviour

Several researches on the element transfer behaviour in SAW using recycled slag discovered that flux composition and weld metal inclusion were the primary cause of the complex changes in submerged arc weldments.. Until now, relatively few researchers have investigated about slag recycling. The current study makes an attempt to forecast the element transfer behaviour in SAW using reclaimed slag. As a result, there is an opportunity to determine the influence of the weld metal integrity of the base metal, filler wire, and flux on many features of SAW weld zone. Another researcher investigated the effect of flux composition on the oxygen concentration of weld deposits. Results revealed that fused flux composed of CaF_2 , Al_2O_3 , and CaO produces less oxygen than agglomerated flux. Oxygen pickup was primarily identified by gas/metal interactions takes place at the tip of filler wire. Patchett and Milner (1972) conducted a study and found that slag metal reactions can be controlled by thermodynamic driving force such as concentration, and gradient causing diffusion across the boundary layer. Mitra and Eagar (1984) aims to establish a correlation between the consumables, process variables, and chemical composition of weld. They introduced the concept of solidification processing, fundamental concepts of chemical metallurgy, and key characteristics of the SAW process. They assumed that there exists a relationship between the effective reaction temperature and the equilibrium constants K_1 and K_2 . Metallurgical thermodynamics has demonstrated that the electrode and base plate composition has a negligible effect on the weldments. Additionally, they examined the composition of the weld metal, droplet reaction time theory, and oxygen transfer affected by the input factors during SAW.

Lau et al. (1986) discovered that by altering the composition of the flux, electrode wire, and base plate, it is possible to evaluate the various types of reactions that occur throughout the welding process. Additionally, they discovered that oxygen absorption occurs primarily at the electrode tip and metal droplet stage. Mohan and Pandey (2005) studied the impacts of process variables on weld metal composition. Results revealed that the process variables and basicity index had an influence on the Mn, Si, and C content of the weld metal (Bang et al., 2009). Similarly, Singh et al. (2018) utilised developed agglomerated flux to investigate the element transfer behaviour of weldment. They found that the transfer of C, Mn, S, P, Si, and Ni varies with flux composition, dilution, and slag metal reactions. Sharma and Chibber (2019) designed welding flux by using $\text{TiO}_2\text{-SiO}_2\text{-MgO}$ and $\text{SiO}_2\text{-MgO-Al}_2\text{O}_3$ flux systems to evaluate its physiochemical and thermo-physical properties. Results revealed that each individual flux component varies proportionally with density but shows anti-synergistic behaviour with others. Here, $\text{SiO}_2\text{-MgO}$ is the only binary flux constituent that tends to increase the grain size number (Kanjilal et al., 2007).

The SAW process is the most versatile process in the industry, it is described by number of welding inputs that determine performance outputs, all of which have an effect on the weld quality. According to an intensive review of the literature, it was found that few control parameters, namely welding current, arc voltage, travel speed, electrode extension, and preheat temperature, had major effect on weld quality. Patnaik et al.(2007) carried out a research which determines the influence of welding inputs on the outputs using the Taguchi technique. They have used nonlinear regression analysis along with the concept of genetic algorithm (GA) to optimise the

welding process with multiple objectives. Similarly, Jindal et al. (2014) optimised weld bead parameters and conducted this investigation on structural steel pipe (API 5L X65 grade) using the desirability function approach designed by Derringer and Harrington. As a result, it was found that welding current can easily control all the responses, and arc voltage is directly proportional to all the responses apart from micro hardness. Figure 2.5 shows direct effect of welding current on (a) form factor and dilution and (b) width, height, A_r (area of reinforcement) and A_p (area of penetration). Figure 2.6 presents direct effect of arc voltage on (a) form factor and dilution and (b) width, height, A_r and A_p .

Cho et al. (2015); Gott et al. (2016); Li et al. (2017); Mendez et al. (2015) conducted a study to simulate metal transfer in SAW by utilising a high speed video camera via a pre-set tunnel to acquire the welding electric signal. It indicates that the welding process was more stable at medium current, but the metal transfer behaviour was not completely clear. Using high speed welding videos and physical modelling experiments, it was concluded that as the welding current increases, three different metal transfer modes occurred. Also, the arc burns constantly at high current while the short circuit is active.

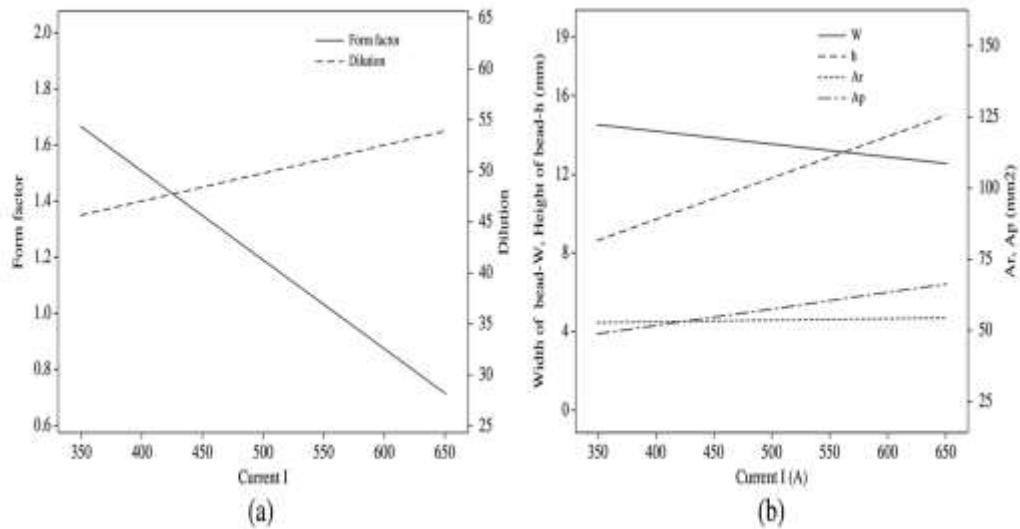


Figure-2.5: Direct effect of welding current on (a) form factor and dilution and (b) width, height, A_r and A_p (Jindal et al., 2014).

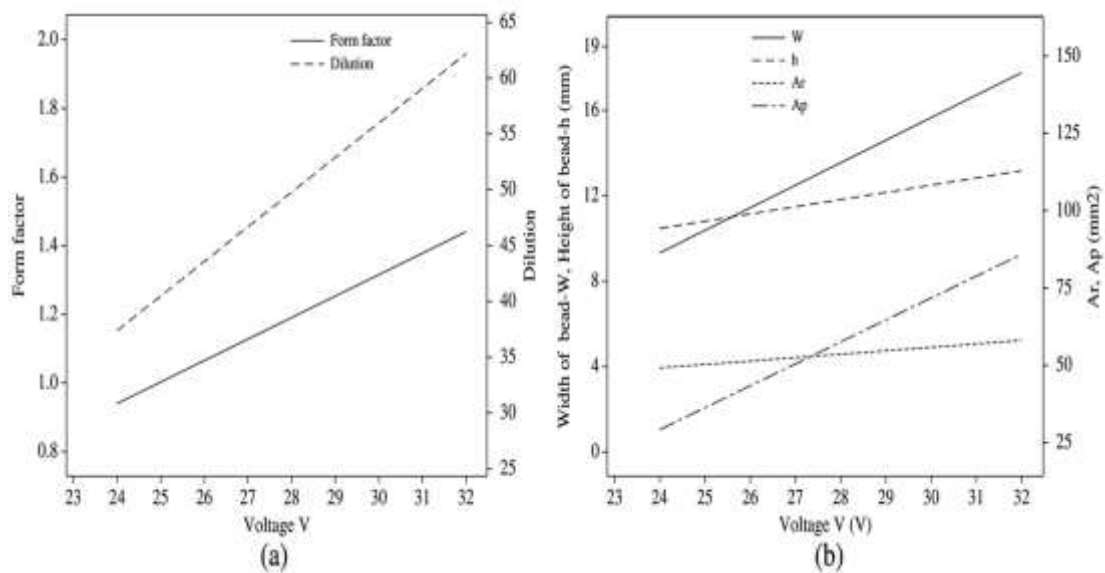


Figure-2.6: Direct effect of arc voltage on (a) form factor and dilution and (b) width, height, A_r and A_p (Jindal et al., 2014).

2.5 Metallurgical Studies

Eroglu et al. (1999) studied the effect of grain size on the metallurgical and mechanical properties, and heat affected zone of low carbon steel. The original and grain coarsened specimen were welded with heat inputs of 0.5, 1, and 2 KJ/mm using

submerged arc welding machine. After welding, the microstructure, hardness, and toughness of weld metals and heat affected zone were studied. They attempted to establish a correlation between the initial grain size, microstructure, hardness, and toughness of weld metals and heat affected zone using the data. Taking into account the heat input, it was discovered that the coarse initial grain size had a significant effect on the response parameters such as microstructure, hardness etc.

Gunaraj and Murugan (1999) compared the region of HAZ in SAW of pipes using mathematical models. They concluded that voltage, wire feed rate, or both varies proportionally with the amount of heat applied to the weld metal. This heat applied reduces as the travel speed increases. Therefore, it was concluded that HAZ area increases with the increase in voltage and wire feed rate whereas it decreases with the increase in travel speed and nozzle to plate distance.

Mercado et al. (2005) conducted a study to analyse the effect of flux mixture on the microstructure and tensile properties of AISI 1025 steel prepared using SAW. Under the same welding conditions, they employed three flux compositions with low carbon electrodes. They have also used commercial flux for comparison. Scanning electron microscopy (SEM) was utilised to analyse the microstructure and macrostructure of the weld metal. It was discovered that flux containing a greater concentration of titanium oxide exhibits the presence of acicular ferrite in weld metal. The yield strength and ultimate tensile strength has increased as a result of the use of acicular ferrite. Figure 2.7 shows a plot of acicular ferrite volume fraction of weld metal vs. titanium content of the flux whereas Figure 2.8 presents a plot of acicular ferrite length vs. titanium content of the flux.

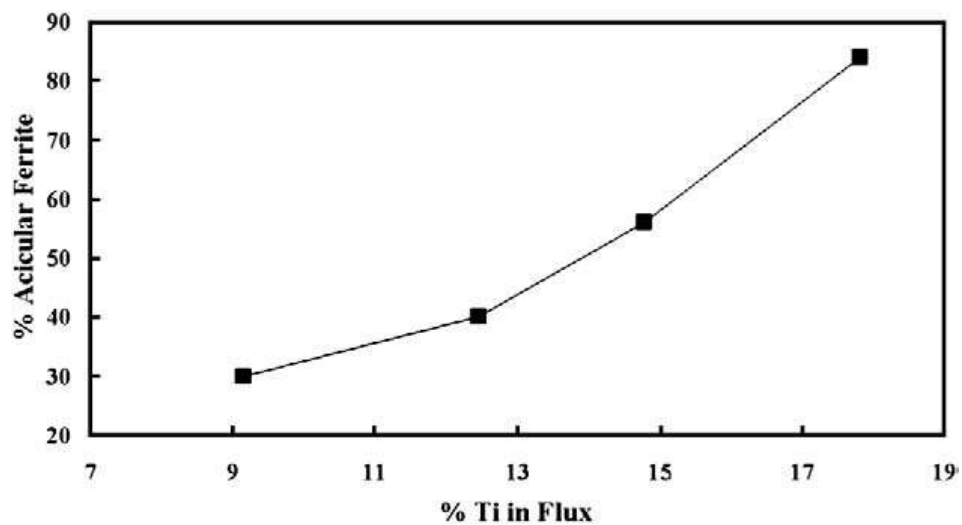


Figure-2.7: Plot of acicular ferrite volume fraction of weld metal vs. titanium content of the flux (Mercado et al., 2005).

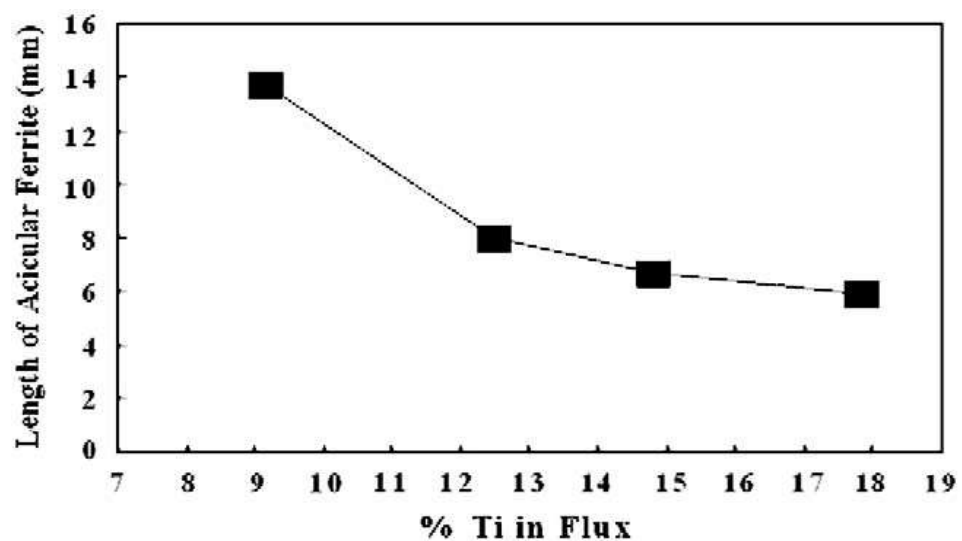


Figure-2.8: Plot of acicular ferrite length vs. titanium content of the flux (Mercado et al., 2005).

In order to manage HAZ dimensions and achieve the requisite weld bead dimensions and quality, it is necessary to select suitable process variables. Also, input parameters must be selected in such a way that it will ensure an acceptable weld bead, which is essential for achieving high quality weld. Kumar and Singh (2007) investigated the effects of process parameters and heat input on metallurgical parameters including weld interface, grain refinement regions of the HAZ, HAZ width, and grain

development. Furthermore, for analysis, they have used the colour metallographic technique and the response surface methodology. The results indicate, firstly, that heat input and wire feed rate varies directly whereas welding speed varies inversely with the HAZ characteristics. Secondly, as arc voltage increases, the width of the grain growth and grain refinement zones increases and the weld interface decreases; and the width of the HAZ is maximum (about 2.2 mm) when wire feed rate and welding speed are at their minimum limits.

Kolhe and Datta (2008) conducted a thorough investigation of the phase analysis, microstructure, and mechanical properties, as well as the HAZ width of a SAW multi-pass joint. They have observed that various sub-zones in heat affected zone are spheroidized, partially transformed, grain refined, and grain coarsened. The phase percentage in welded structures can be regulated by the welding heat input. It was observed that graphitic phase % varies inversely with the heat input whereas the ferrite % varies in direct proportion to the heat input, therefore results in ferritic structures were observed. The proportionate value of micro hardness for low heat input whereas for increased heat input, changes in hardness value were noticed. Also, the bulk hardness of fractured specimen varied more than that of welded samples. It was found that the upper area of the welded specimen has more HAZ width than the bottom region.

Lee et al. (2000) studied the effects of welding parameters on the size of HAZ and the ratio of HAZ size to bead size. They concluded that welding current has the maximum effect on HAZ size and HAZ size to bead size, whereas welding parameters such as heat input and polarity have less effect on both HAZ size and HAZ size to bead size

ratio. Other than this voltage, electrode stick out and diameter have no effect on HAZ size or HAZ size to bead size ratio. Prasad and Dwivedi (2008) investigated the effects of SAW process parameters (welding current and travel speed) on the microstructure, hardness, and toughness of HSLA (high strength low alloy steel) steel weld joints having 16 mm thickness. These specimens were welded with comparatively high heat input (3.0 to 6.3KJ/mm) by changing welding current (500–700 A) and travel speed (200–300 mm/min). The results showed that increasing the heat input coarsens the grain structure in both the weld metal and the heat affected zone. The hardness varied from the weld centre line to the base metal, with the HAZ having the highest hardness. Furthermore, it was observed that an increase in welding current and a decrease in welding speed result in a decrease in hardness, although toughness exhibits a mixed pattern. Increased welding current from 500A to 600A at a certain welding speed (200 mm/min or 300 mm/min) increased toughness, but increasing welding current up to 700A decreased toughness. Figure 2.9 depicts the influence of heat input on (a) tensile strength and (b) % elongation. Scanning electron microscopy was performed to examine the fracture surfaces of impact specimens whereas electron probe micro analysis (EPMA) was implemented to observe the change in weight percent of different elements in the weld metal and HAZ.

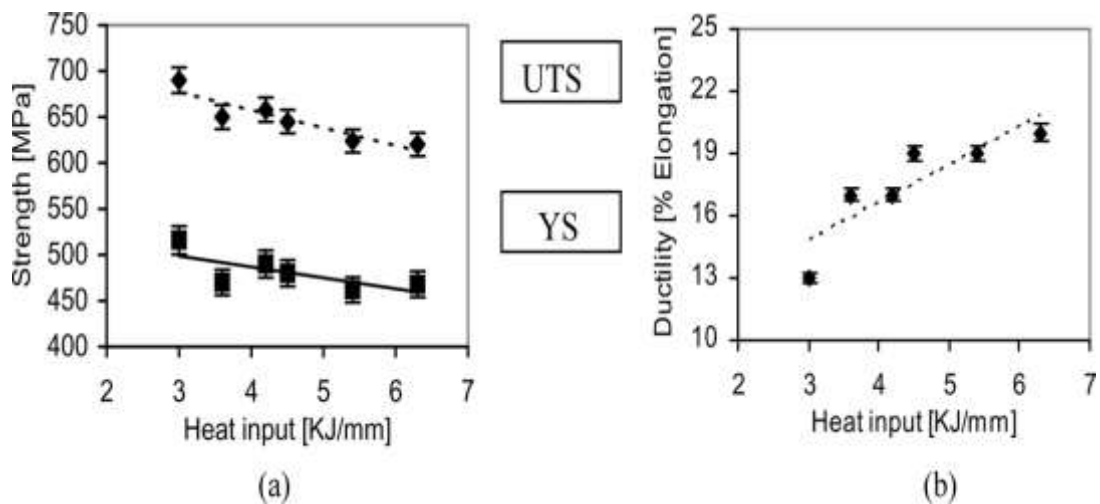


Figure-2.9: Influence of heat input on (a) tensile strength and (b) % elongation (Prasad and Dwivedi, 2008)

According to Singh and Pandey (2009), it is possible to recycle slag through the method of agglomeration. This process includes adding certain suitable alloying elements or deoxidisers to the slag. This replenished slag is known as "recycled slag." They studied the effect of process variables on flux consumption using a two-level factorial technique. The 't' test and 'F' test were used to determine the significance of the coefficients and the adequacy of the developed model. They have graphed the main effects of welding parameters on recycled slag consumption. The developed model can be used to control and predict slag consumption in submerged arc welding. They have studied the physical behaviour of recycled slag as well as the microstructure of the weld metal.

Calik (2009) studied the effect of cooling rate on the microstructure and mechanical properties of steels with AISI 1020, AISI 1040, and AISI 1060. The samples were heat treated at 1250°C for 4 hours before being cooled using three different techniques. Optical microscopy and hardness tests were used to analyse the micro hardness and microstructure of these steels after heat treatment. Experimental results

reveal that by altering the cooling rate, the microstructure of these steels may be changed and greatly improved. Thus, heat treatment (heating and cooling) was used to achieve desirable qualities in steels, such as increased toughness, ductility, or removal of residual stresses (Arya et al., 2018). Because of solid solution hardening and the formation of the martensitic phase, the micro hardness increases with increasing cooling rate and carbon content. In another study, it was found that an increase in cooling rate can prevent the process of crystallisation, thus increasing the time-temperature transformation (TTT) and continuous-cooling-transformation (CCT) of welded specimens (Esfahani and Barati, 2016).

Kiran et al. (2012) analysed the weld bead quality of HSLA steel affected by welding parameters using two-wire tandem SAW. Five different combinations of welding conditions were employed using two-level, five-factor central composite rotatable design. They investigated the effects of trailing wire current pulses and negative current pulse duration, leading wire current, and welding speed on weld bead geometry and mechanical properties. They have concluded that the wire current has the predominant effect on the final weld bead width and reinforcement height, whereas the leading wire current has the greatest influence on the penetration, with all other process parameters remaining constant. Increase in travel speed reduces the weld pool size, thus resulting in a faster cooling rate, which promotes a higher volume percentage of acicular ferrite phase and improves weld bead mechanical properties. The predictions of weld dimensions and mechanical properties from the empirical relations, which were developed based on the experimental results, are in fair agreement with the corresponding measured values within the ranges of the welding

conditions considered in the work. Similarly, Singh and Singh (2020) studied the effects of welding parameters on the mechanical properties of the weld in the case of SAW. They have concluded that the macro as well as microstructure of welds helps in predicting the mechanical properties. Also, the increase in the number of passes in welding results in a good quality weld with high tensile strength. This is because of lower amount of delta ferrite transforming into austenite. Moreover, welding current and arc voltage varies directly proportional with the increase in the hardness and, therefore, the impact value of the weld. On the contrary, welding current was found to be more effective than arc voltage in terms of hardness and HAZ of the weldment. It was found that quenching increases the hardness as well as HAZ of the weld, whereas annealing leads to a decrease in hardness and HAZ (Singh et al., 2020). Verma and Taiwade (2017) investigated the effects of various welding processes and conditions on the microstructure, mechanical properties, and corrosion resistance of duplex stainless steels. In all the welding processes, plasma arc welding exhibits improved weldability, which leads to improved welding speed as well as productivity.

Sailender et al. (2020) proposed a model to build a correlation among parameters such as open circuit voltage (OCV), wire feed rate (WFR), welding speed (WS), and nozzle to plate distance (NPD). They have optimised the results using grey relational analysis (GRA). Results reveal that HAZ can be minimised by maintaining OCV at a lower level and WFR, WS, and NPD at a higher level.

Lan et al. (2012) used optical microscope, transmission electron microscope, and scanning electron microscope equipped with electron back scattered diffraction to investigate the microstructural variation in high strength, low carbon bainite steel

weldment. According to the results, the welded joint exhibits a variety of microstructures, including acicular ferrite, coarse granular ferrite, and fine polygonal ferrite, among others. In each subzone, the martensite austenite (MA) composition has a varied structure that comprises of complete martensite and fully preserved austenite. Meanwhile, the fine-grained heat affected zone has a higher content of retained austenite than the welded metal (WM) and coarse-grained heat affected zone (CGHAZ). In the WM and CGHAZ, the orientation relationship between retained austenite and product phases is similar to the Kurdjumov Sachs relationship. It was discovered that coarse grained regions have lower toughness than WM because coarse bainite contains numerous large MA constituents that aid in the nucleation of micro fractures, and coarse cleavage facet has a lesser ability to inhibit crack propagation. Figure 2.10 depicts optical micrographs of the microstructures in different regions of the welded joint.

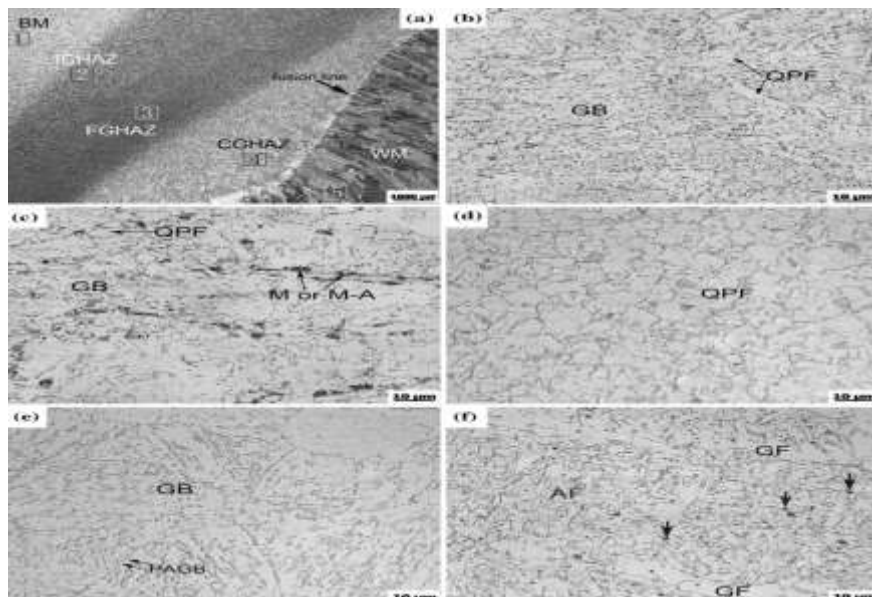


Figure-2.10: Optical micrographs showing the microstructures in different regions of the welded joint (Lan et al., 2012)

Kumar et al. (2012) studied the hardness of weldment produced using developed agglomerated fluxes during submerged arc welding. The trials were carried out using the response surface methodology (RSM) technique. The flux constituents MnO, CaF₂, NiO, MgO, and Fe-Cr were chosen as variables to be added to the primary constituents CaO, SiO₂, and Al₂O₃ to study the performance in terms of hardness. It was determined that the elements that favour hardness include MnO, MgO, NiO, and Fe-Cr, whereas CaF₂ has no effect on hardness.

Wang et al. (2008) studied the effect of alloying elements on the microstructure and wear properties of Fe-based hard facing layers. They discovered that increasing the amount of Fe-Ti, Fe-V, Fe-Mo, and graphite increases the hardness and wear resistance of the hard facing layer, but it also increases the crack sensitivity of the hard facing layer.

2.6 Need of this Research Work

The function of the flux are: arc striking and stability, generate a slag that protects and shapes the weld bead, and to form a gas shield that protects the molten filler metal projected across the arc gap. The following are the reasons that define the need for this research work:

- Submerged arc welding flux is converted into slag during the welding process, which is basically a waste product.
- About 2500 tonnes of flux were consumed in India alone in the year 1982 (Visvanath, 1982), which has risen to more than 10000 tonnes in the year 2006 (Honovar, 2006) to approximately 20000 tonnes in the year 2020.

- Such a large quantity of flux, after welding, becomes slag and has to be disposed-off in a land fill space.
- It is non bio-degradable and will not decay with time.
- Being brittle and glassy material it cannot be used as a filling material in building construction.
- Disposal cost will increase, apart from environmental pollution.
- Non-renewable resources may be exhausted due to continuous mining.
- Thus, slag generated during submerged arc welding is a waste and imposes a number of problems.
- Higher the amount of slag generated, higher is the wastivity.
- It is not possible to stop the generation of slag because it is a by-product of the process, but slag can be reused as a flux in the same submerged arc welding process. Wastivity can be decreased by recycling the slag, thus resulting in higher productivity.
- Furthermore, the slag can be processed according to one's requirements and applications.

2.7 Motivation

1. The motivation is provided by the desire to explore the potential of recycled slag in submerged arc welding process.
2. For exploring the potential of the slag in submerged arc welding process to greater extent possible, basic understanding of the composition and its influence as compared to fresh flux is necessary.

2.8 Research Gaps in Literature Review

Following gaps have been identified after the Literature review:

- Technology for reusing / recycling the slag
- Number of times slag can be recycled
- Environmental Aspects of recycled Slag
- Reutilization and Optimization of slag
- Techno-economic analysis of recycled slag

2.9 Research Objectives

The existence of gaps in the literature was used for deciding the objective of the present research. Therefore, the main objective of this research is to define a technology for recycling slag in submerged arc welding. These research objectives are as follows:

- To define a technology for recycling of submerged arc welding slag.
- To characterize the fresh flux.
- To develop flux using the slag and its qualification as per AWS 5.17.
- To analyse the effects of welding parameters on weld bead geometry & shape relationships using the developed flux and comparison with fresh flux.
- To perform a techno-economic analysis of recycled slag and compare it with fresh flux.

2.10 Statement of problem

"Recycling of Slag in Submerged Arc Welding"

This research work describes the technology developed for recycling of slag such that the weld metal elemental composition qualifies as per AWS 5.17.

EXPERIMENTAL SET-UP AND METHODOLOGY

3.1 Introduction

This research work describes the technology for recycling slag in such a way that the weld metal elemental composition meets the requirements of AWS SFA 5.17 after carrying out SAW using recycled slag. Figure 3.1 depicts a flow chart diagram of slag recycling process.

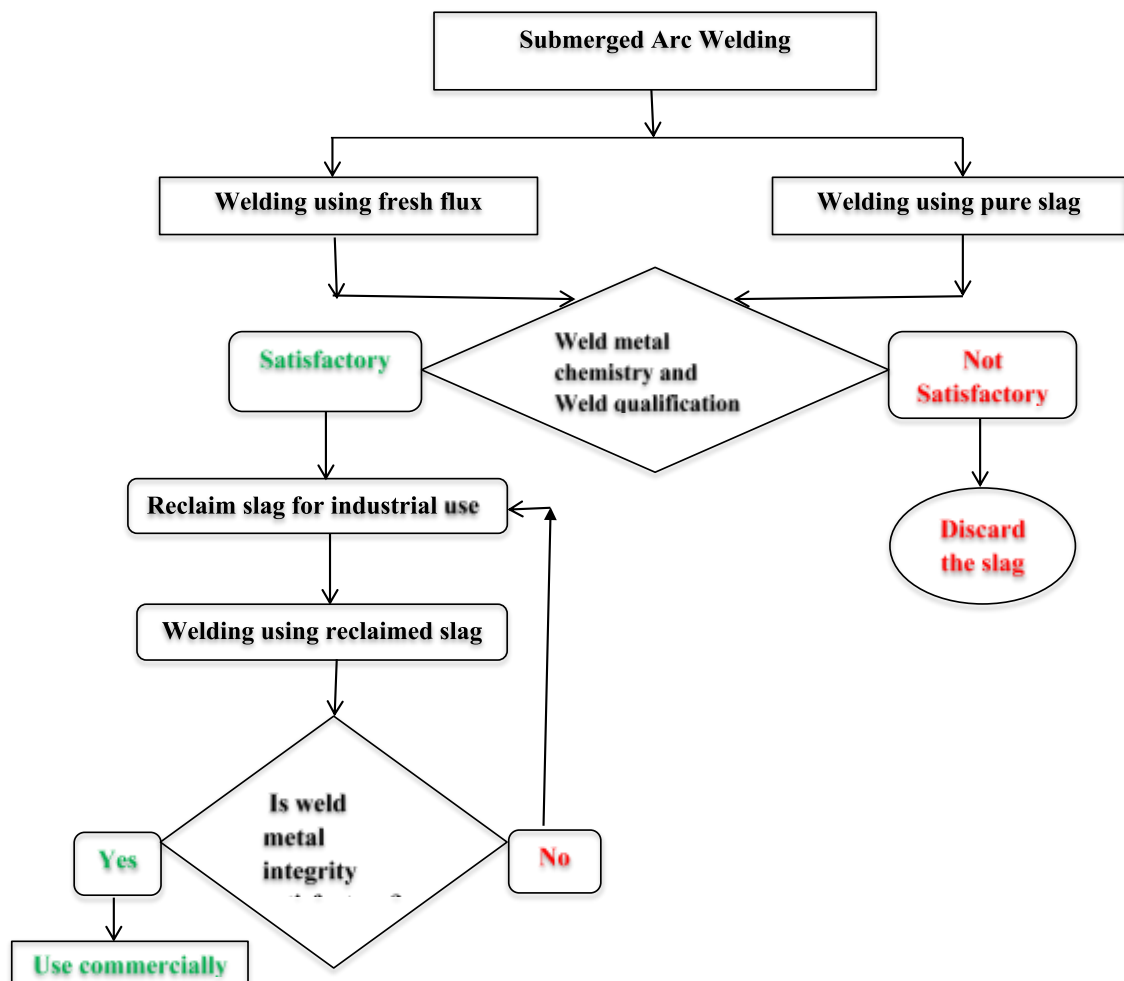


Figure-3.1: Flow chart diagram of slag recycling process

3.2 Material Selection

3.2.1 Base Metal

The base metal for the experiments was mild steel, which contains 0.197 percent carbon. Mild steel is also highly prone to oxidation, and if not properly coated, it becomes more magnetic as its iron and ferrite content rises. Therefore, these plates were cleaned properly to eliminate any impurities like oxide layer and any other source of hydrogen. To study the effect of welding parameters on element transfer behaviour and weld bead geometry and shape relationships, weld bead on mild steel plates measuring 12 x 70 x 160 mm were prepared. Weld pads were prepared on mild steel plates to perform spectro analysis of weld metal. These weld pads were prepared as per ASME SFA 5.17 standard.

3.2.2 Filler Wire

The filler wire used was EH 14 in combination with fresh flux F7A4, pure slag and recycled slag. It is commonly used in industries for welding of boilers, pressure vessels etc. Table 3.1 describes the chemical compositions of the base metal and the filler wire.

Table-3.1: Chemical composition of base metal and filler wire (wt. %)

	C	Mn	Si	S	P
Base Metal	0.197	0.412	0.152	0.028	0.029
Electrode	0.10	1.70	0.10	0.030	0.030

3.2.3 Flux Type

The specification of the flux-wire combination from which slag has been generated is EH14 F7A4. This study was performed by using available flux, i.e., an agglomerated flux

manufactured by ESAB INDIA LTD. The specification of the flux was auto-melt Gr. II, Coding-AWS SFA 5.17. The chemical composition of the fresh flux is shown in Table 3.2.

Table-3.2: Chemical composition of fresh flux (wt. %)

	C	Mn	Si	S	P
Fresh flux	0.092	1.901	0.463	0.012	0.025

3.2.4 Slag Composition

The slag was taken from the dump yard of Cheema Boilers Ltd. Kurali, Punjab. They are manufacturing boilers and pressure vessels in accordance with IBR, ASME-Sec VIII Division. This slag has been generated from plates (SA 516 Grade 70) welded with F7A4 EH14 flux wire combination. These boiler plates were welded for fabrication of boiler (steam and mud drum). The chemical composition of pure slag is shown in Table 3.3.

Table-3.3: Chemical composition of pure slag (wt. %)

	C	Mn	Si	S	P
Pure slag	0.108	1.567	0.364	0.016	0.025

3.3 Welding Equipment and Process Parameters

3.3.1 Submerged Arc Welding Machine

The investigation was conducted using a carriage type fully automated submerged arc welding equipment (Model-QSW800) manufactured by Quality Engineer Baroda Pvt. Ltd., A/18, Gujarat Estate, Dharam Singh Desai Marg, Chhani Road, Baroda-390002. The power supply used was a constant potential transformer-rectifier with a current

capability of 800 amps and an open circuit voltage range of 12-48 volts. The machine was equipped with an electrode with a diameter of 3.15 mm and a wire made of mild steel. Additionally, this machine has the ability to control the wire feed rate and travel speed. A submerged arc welding machine is shown in Figure 3.2. Arc voltage (V), wire feed rate (W), travel speed (S) and contact tube to plate distance (N) were selected as the independently controllable process parameters. Welding was conducted on 12 x 70 x 160 mm mild steel plates. Chemical and mechanical cleaning was used to remove the oxide layer and any remaining foreign particles from these mild steel plates. Table 3.4 gives the welding conditions for a given submerged arc welding machine. Experimental studies were conducted on bead on plate in this work to investigate the weld bead geometry and shape relationships along with element transfer behaviour, and metallurgical studies.

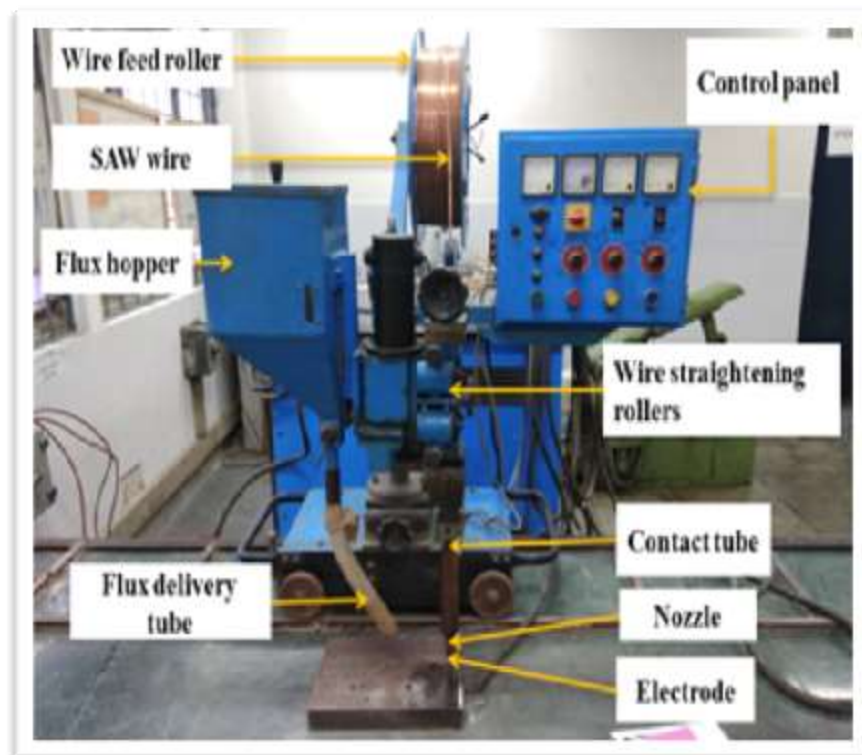


Figure-3.2: Submerged Arc Welding Machine (Welding Laboratory, DTU Delhi)

Table-3.4: Welding Conditions for SAW set up

Base Metal	Mild Steel
Wire material	Mild steel
Filler wire coding	EH14
Flux type	F7A4
Flux coding	F7A4 EH14

3.3.2 Process Parameters

Welding parameters generally affect the weld quality and quantity. To maximise productivity while maintaining excellent quality, the most effective welding parameters must be selected. As a result, the selected parameters effect on the overall soundness of the welded specimen. The following is a list of various types of parameters, such as direct, indirect, and response parameters that need to be set before the execution of the welding process:

3.3.2.1 Indirect Parameters

These parameters have an insignificant effect on the weld quality and yield. It is usually essential to have a highly experienced and skilled operator to select these parameters. These parameters are selected at the initial stages of the welding process. Indirect parameters such as the electrode angle have insignificant effect on the welding process.

3.3.2.2 Direct Parameters

Parameters having a significant influence on the welding operation are known as "direct parameters." Additionally, these are called input parameters. Once the indirect

parameters are set, the operator may easily manipulate these parameters, which define the entire welding technique. Wire feed rate, travel speed, contact tube to work distance, flux depth, and arc voltage are few of those parameters.

3.3.2.3 Response Parameters

These parameters are used to analyse the weld joint soundness, weld metal integrity, and weld bead geometry of the welded specimen. These are also known as output parameters. Submerged arc welding utilises independently variable direct and input parameters such as arc voltage, wire feed rate, travel speed, and contact tube to plate distance to examine the effects on weld bead geometry, element transfer behaviour, and weld metal composition.

3.4 Methodology

The various steps commonly involved in performing the submerged arc welding process using recycled slag for different response parameters are as follows:

1. Prepare weld pad with fresh flux.
2. Prepare weld pad with pure slag.
3. Processing of slag with different compositions.
4. Prepare weld pads with different compositions of slag.
5. Spectro analysis of the weld pads obtained using fresh flux, pure slag, and slag with different compositions.
6. Comparison of weld chemistry of weld pads prepared using fresh flux, pure slag, and different compositions of slag.

7. Validation of one of the compositions of slag.
8. Identifying input factors and determining their upper and lower limits.
9. Developing the design matrix.
10. Conducting the experiments as per the design matrix using recycled slag.
11. Recording the response parameters.
12. Formulating the empirical models.
13. Evaluating the coefficients of the polynomials and their significance.
14. Developing the final model.
15. Analysing the adequacy of empirical models

In the present work, the SAW experiments have been divided into some categories to explore different aspects in order to observe the overall soundness of the weld metal. The details regarding the process and response parameters, experimental designs, limits of the parameters, etc. are described separately in the respective chapters. Figure 3.3 mentions the methodology for submerged arc welding process in this research. As mentioned, this figure clearly explains the various tests performed under the main categories. For example, weld qualification tests include visual inspection, slag detachability, dye penetrant test, tensile and impact tests.

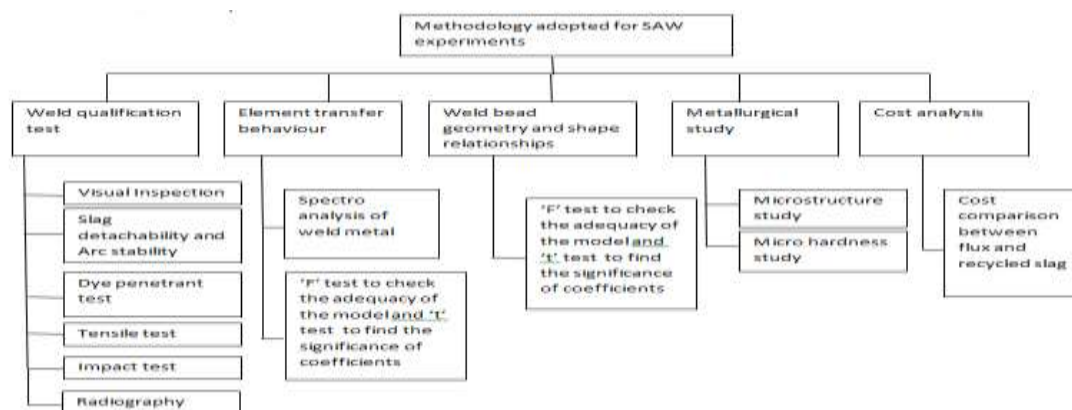


Figure-3.3: Methodology for submerged arc welding process

3.5 Design of Experiments

Design of experiments (DOE) is a useful way of finding the effect of a number of parameters, also the effects of these parameters' interactions, on a specific response variables. In experimentation, the DOE concept is efficiently used to reduce the number of experimental runs and to determine the main effect of welding parameters on response parameters, also the interaction effect of multiple welding parameters on response parameters (Montgomery, 2008).

3.5.1 Selection of the Design

Based on the literature survey it is observed that RSM technique is most widely used by the researcher around the world. Factorial design is one of the most popular techniques used for designing welding experiments, and it is used in the experiments. The number of trials in a full factorial design varies progressively with the number or level of factors. Higher order interactions, which do not have a large impact on the outcome in most cases, account for the increased number of trials. In a factorial experiment, the number of trials is higher than the number of coefficients to be calculated in a linear model. Furthermore, as the number of experiments increases, so

does the cost of experimentation and the amount of time consumed. But the need is to decrease the number of experiments as well as the cost of experimentation. To meet these requirements, a fractional factorial approach was adopted, which allows for a reduction in the number of trials while still providing relevant results. The main effects of the factors are confounded with the effects of higher order interactions in fractional factorial design. The resulting estimates are essentially the main effect estimates because these higher order interaction effects are expected to be statistically insignificant. In order to evaluate the influence of the process variables on the response parameters, two levels for each of the input parameters were chosen in this study. Thus, a two-level half fractional factorial design $(2^{4-1}) = 8$ sets of weld runs was used in the current work to gain a thorough understanding of the main and interaction effects of welding parameters on weld metal chemistry and weld bead geometry. For evaluating the adequacy of the model developed, the design required three sets of eight weld runs.

3.5.2 Selection of levels

The next step in achieving the desired objectives was the careful selection of direct parameters, along with their effects on weld metal chemistry and weld bead geometry due to their extreme range. For ease of recording and processing, parameters were coded as (+1) and (-1) or simply (+) and (-), corresponding to the high and low levels, respectively. Table 3.5 shows welding parameters with their upper and lower limit for element transfer behaviour and Table 3.6 shows welding parameters with their upper and lower limit for weld bead geometry and shape relationships.

Table-3.5: Welding parameters with their upper and lower limit for element transfer behaviour

Parameters	Units	Symbol	Low (-1)	High (+1)
Arc Voltage	Volts	V	25	40
Wire Feed Rate	cm/min	W	111	156
Travel speed	cm/min	S	30	40
Contact tube to plate distance	mm	N	20	25

Table-3.6: Welding parameters with their upper and lower limit for weld bead geometry and shape relationships

Parameters	Units	Symbol	Low (-1)	High (+1)
Arc Voltage	Volts	V	25	40
Wire Feed Rate	cm/min	W	97	156
Travel speed	cm/min	S	32	40
Contact tube to plate distance	mm	N	18	23

3.5.3 Selection of the Model

The response function can be expressed as:

$$Y = f(V, W, S, N) \dots\dots\dots 3.1$$

Where, Y - response parameter i.e. bead geometry and shape relationships (bead width, bead height, bead penetration, WPSF, WRFF) and weld metal composition (C, Mn, Si, S and P) in the wt. %.

V - Arc Voltage,

W- Wire feed rate,

S - Travel speed,

N - Contact tube to plate distance

Assuming linear relationship, the possible two factor interactions are taken into consideration, therefore the above expression rewritten as:

$$Y = b_0 + b_1V + b_2W + b_3S + b_4N + b_{12}VW + b_{13}VS + b_{14}VN + b_{23}WS + b_{24}WN + b_{34}SN \dots\dots\dots 3.2$$

After confounding the given empirical model can be expressed as:

$$Y = b_0 + b_1V + b_2W + b_3S + b_4N + b_5(VW + SN) + b_6(VS + WN) + b_7(VN + WS) \dots\dots\dots 3.3$$

3.5.4 Development of Design Matrix

Experiments were performed for all possible combinations of parameter levels, and these combinations, when written as a table with rows representing distinct trials and columns representing parameter levels, create a design matrix. The design matrix shown in Table 3.7 was designed for the purpose of conducting eight trial runs of a two-level half factorial design. After confounding interaction effects and excluding higher-order interaction effects (greater than two), the design matrix can be represented as shown in Table 3.8.

Table-3.7: Design matrix for two level half factorial design

Trial No.	V	W	S	N
1.	-	-	-	-
2.	+	-	-	+
3.	-	+	-	+
4.	+	+	-	-
5.	-	-	+	+
6.	+	-	+	-
7.	-	+	+	-
8.	+	+	+	+

Table-3.8: Design matrix for calculating coefficients after confounding

Trial No.	b₀	V b₁	W b₂	S b₃	N b₄	(VW+SN) b₅	(VS+WN) b₆	(VN+WS) b₇
1.	+	-	-	-	-	+	+	+
2.	+	+	-	-	+	-	+	-
3.	+	-	+	-	+	-	-	+
4.	+	+	+	-	-	+	-	-
5.	+	-	-	+	+	+	-	-
6.	+	+	-	+	-	-	-	+
7.	+	-	+	+	-	-	+	-
8.	+	+	+	+	+	+	+	+

3.5.5 Evaluating the Coefficients of Polynomials

Coefficients of the empirical model were evaluated according to the design matrix.

This is based on the method of least squares which is as follows:

$$b_j = \frac{\sum_{i=1}^N Y_i X_{ji}}{N}, \quad j = 0, 1, \dots, k$$

Where, Y_i = Value of the response parameter,

X_{ji} = value of a factor in coded form,

N = Number of runs,

K = Number of coefficients of the model

The importance of each coefficient was checked using 't' test. Here the value of 't' from the standard table is 2.3 for confidence level 95% and degree of freedom as 8.

The model coefficients and their significant 't' value can be expressed as following:

$$t = \frac{|b_j|}{S_{b_j}}$$

Where b_j = Absolute Value of Coefficient and S_{b_j} = Standard Deviation of Coefficient

$$S_{b_j} = \sqrt{\frac{S_y^2}{N}}$$

Where S_y^2 = Variance of Optimization Parameter

3.5.6 Analysing the Adequacy of Empirical Models

ANOVA was employed to analyse the adequacy of empirical model. According to this technique, the model is significant when calculated model's F-ratio value is less than tabulated value for a desired level of confidence at 95%. It has been found that all models are significant. Mathematical expression of F ratio of the model is given below:

$$F_{\text{model}} = \frac{S_{ad}^2}{S_y^2}$$

Where S_{ad}^2 = Variance of adequacy

CHAPTER 4

RECYCLING OF SLAG AND WELDABILITY

4.1 Introduction

The submerged arc welding process was designed in many ways to improve its overall efficiency and enhance the weld metal properties. The modifications in the process include the use of three wires, electrode stick out, narrow gap welding, pulsed arc welding, twin arc welding, etc. Apart from these techniques, one of the most preferable methods is the use of recycled slag instead of flux. The thick layer of flux becomes slag after welding, which can be reclaimed further by recycling. When slag is mixed in varying proportions with additives and binder, it can produce satisfactory results.

The present work has been aimed at recycling of slag through a process called agglomeration. One of the most important purposes of carrying out this research is to reduce the harmful effects posed by the large amounts of slag generated after flux is consumed in SAW. This slag can be reused if it is replenished with the correct percentage of additives and binders. The weld pad generated using different compositions of slag helps in finding the right composition required to develop recycled slag equivalent to fresh flux. Different compositions of slag were tried through hit and trial, to achieve the desired composition. In order to replenish the slag, pulverised form (100 mesh size) slag was added with deoxidisers, i.e., CaCO_3 ; Al powder; Mn powder with K_2TiO_3 , which acts as an arc stabiliser, and K_2SiO_3 was added as a binder to bind the mixture. The welding characteristics and conditions used are in accordance with American society of mechanical engineers (ASME) SFA 5.17. Four independently controllable factors were identified as arc voltage (V), wire feed

rate (W), travel speed (S), and contact tube to plate distance (N). The weld pad prepared was 4 layers high with 3 passes per layer using recycled slag with 3.15 mm EH14 wire. In order to avoid systematic error, experiments were conducted randomly. Once the experiments were conducted, the welded specimens were removed from the middle of mild steel plates to perform spectro analysis. The results helped in selecting the best suited slag composition.

4.2 Plan of Investigation

Plan of investigation involves various steps which are as follows:

1. Weld pad preparation using fresh flux.
2. Weld pad preparation using pure slag.
3. Comparison of chemical composition of weld pads prepared using fresh flux and pure slag.
4. Recycling of slag.
5. Weld pad preparation using different compositions of slag.
6. Comparison of chemical composition of weld pad obtained using fresh flux, pure slag and different compositions of slag.
7. Selection of one of the composition as recycled slag.
8. Weld qualification tests for weld joint prepared with recycled slag
 - Tensile test
 - Charpy Impact test
 - Radiographic test

- Metallurgical test

9. Physical properties of recycled slag

- Visual inspection
- Arc stability
- Slag detachability
- Bead geometry and shape relationships
- Element transfer behaviour

10. Cost analysis of recycled slag compared with fresh flux

4.2.1 Welding with Fresh Flux

Four layer high weld pad was prepared with three passes per layer using fresh flux (F7A4) in combination with EH 14 wire having a 3.15 mm diameter. The welding conditions and weld metal dimensions were in compliance with ASME SFA 5.17, where the inter-pass temperature was taken as 150°C approximately. To perform spectro analysis of the weld pad, a 50 mm long welded sample was removed from the middle of the specimen. Table 4.1 shows welding parameters to prepare weld pad. Figure 4.1 shows weld pad for chemical analysis. Weld pad prepared using fresh flux was shown in Figure 4.2.

Table-4.1: Welding parameters to prepare weld pad

S. No.	Factors	Unit	Symbol	Value
1.	Arc Voltage	Volts	V	30
2.	Wire feed rate	cm/min	W	140
3.	Travel speed	cm/min	S	35
4.	Contact tube to plate distance	mm	N	25

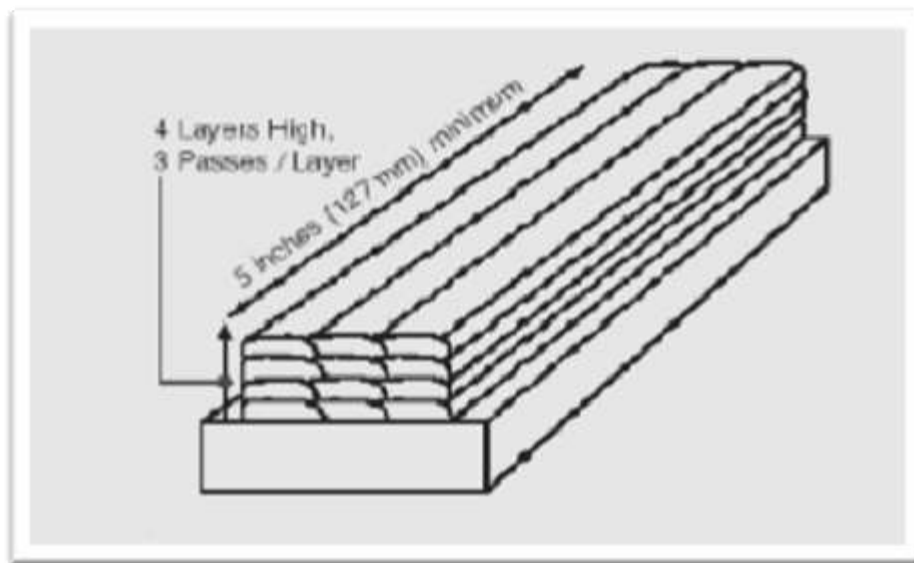


Figure-4.1: Weld pad for spectro analysis (ASME SFA 5.17)



Figure-4.2: Weld pad prepared using fresh flux

4.2.2 Welding with Pure Slag

Slag was crushed and sieved to the same granular mesh size as that of fresh flux. Once the slag was obtained, the weld pad was prepared using pure slag along with EH 14 wire of 3.15 mm diameter. Figure 4.3 presents the weld pad prepared using pure slag.



Figure-4.3: Weld pad prepared using pure slag

4.2.3 Comparison of chemical composition of weld pads prepared using fresh flux and pure slag

Table 4.2 mentions the chemical composition (wt. %) of weld pad prepared using pure slag and fresh flux. The chemical composition achieved was investigated and compared with the AWS standard in order to develop a suitable composition of slag.

Table-4.2: Chemical composition (wt. %) of weld pad prepared using pure slag and fresh flux

S. No.	Responses	C	Mn	Si	S	P
1.	AWS	0.05-0.15	0.80-1.25	0.1-0.35	0.03 max	0.03max
2.	Fresh flux	0.092	1.901	0.463	0.012	0.025
3.	Pure slag	0.108	1.567	0.364	0.016	0.025

4.2.4 Recycling of slag

The chemical configuration of the welded metal attained using pure slag and fresh flux was investigated carefully and compared. During this process, it was found that

pure slag was deficient in various elements, which led to its poor performance during welding. In order to recycle the slag, the method of recycling was defined to achieve similar characteristics to that of fresh flux. The slag was first collected from the welding industry, washed in tap water, and dried. Later, it was grounded and milled in a ball mill having a capacity of 25 kg and converted into powder form. The pulverised form of slag was then mixed with additives such as CaCO_3 , Al powder, Mn powder, and K_2TiO_3 (which act as arc stabiliser), K_2SiO_3 was used to bind the mixture. This wet mixture was then agglomerated and converted into small pellets by passing through a 10 mesh size screen. These pellets were then dried in air for 24 hours and baked at 850°C for around 2 hours in the stir casting furnace. Figure 4.4 shows the small pellets of recycled slag. Baked mass, once obtained, was then crushed and sieved through a 12 mesh size screen to achieve the same grain size as that of fresh flux. This grain size of baked mass slag is obtained as recycled slag. The steps involved in recycling of the slag are summarised in Figure 4.5.



Figure-4.4: Small pellets of recycled slag

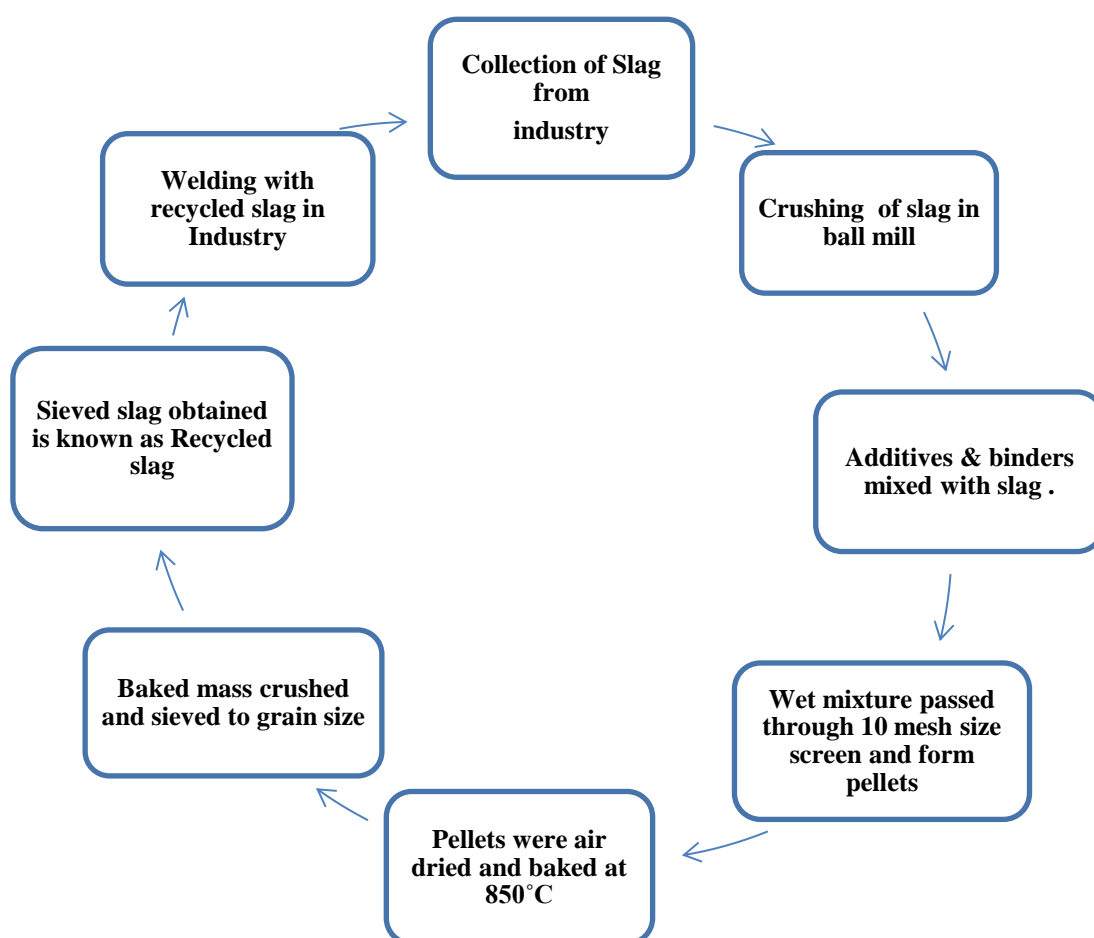


Figure-4.5: Steps involved in recycling slag

4.2.5 Weld Pad Preparation using Different Compositions of Slag

This replenished slag was used to prepare a weld pad, which was examined by the spectroscope for weld metal composition. If the composition obtained does not meet the AWS standards, then the process is repeated again and again by adding deoxidisers and binders in varying percentages till the desired composition is attained. The selection of various ingredients depends on their capability to improve certain properties of the weld metal. The ingredients used were CaCO_3 , Al powder, and Mn powder, which act as deoxidisers; K_2TiO_3 , which acts as an arc stabiliser; and K_2SiO_3 , which acts as a binder. Figure 4.6 shows weld pads prepared using different

composition of slag. Figure 4.7 illustrates a transverse section view of specimen cut from different weld pads. Table 4.3 shows different compositions (wt. %) of slag.

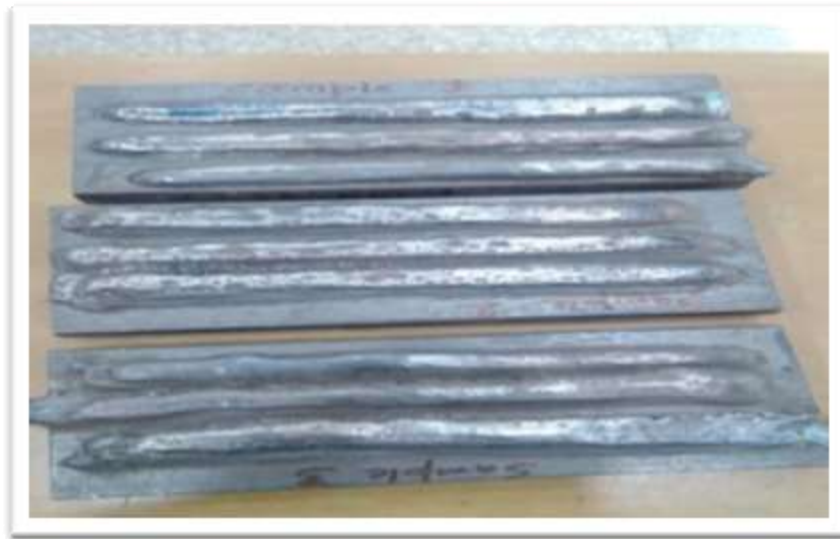


Figure-4.6: Weld pads prepared using different composition of slag



Figure-4.7: Transverse section view of specimen cut from different weld pads

Table-4.3: Different compositions (wt. %) of slag

S. No.	Different slag compositions	Pure slag	CaCO ₃ + Al powder	K ₂ TiO ₃ + Mn powder	K ₂ SiO ₃
1.	Slag composition 1	87.50%	5.50%	7%	Enough to wet the mixture
2.	Slag composition 2	80.70%	8.25%	11%	Enough to wet the mixture
3.	Slag composition 3	74%	11%	15%	Enough to wet the mixture

4.2.6 Comparison of chemical composition of weld pads obtained using fresh flux, pure slag and different compositions of slag

Table 4.4 describes the chemical composition (wt. %) of the weld pad prepared using fresh flux, pure slag and different compositions of slag, compared with AWS 5.17 standard shown. Figure 4.8 illustrates the graphical presentation of weld pads prepared using pure slag, fresh flux and different compositions of slag.

Table-4.4: Chemical composition (wt. %) of weld pad prepared using fresh flux, pure slag and different compositions of slag compared with AWS 5.17 standard

S. No.	Responses	C	Mn	Si	S	P
1.	AWS	0.05-0.15	0.80-1.25	0.1-0.35	0.03 max	0.03max
2.	Fresh flux	0.092	1.901	0.463	0.012	0.025
3.	Pure slag	0.108	1.567	0.364	0.016	0.025
4.	Slag composition 1	0.089	1.101	0.123	0.019	0.02
5.	Slag composition 2	0.086	1.277	0.078	0.015	0.02
6.	Slag composition 3	0.092	1.257	0.064	0.016	0.02

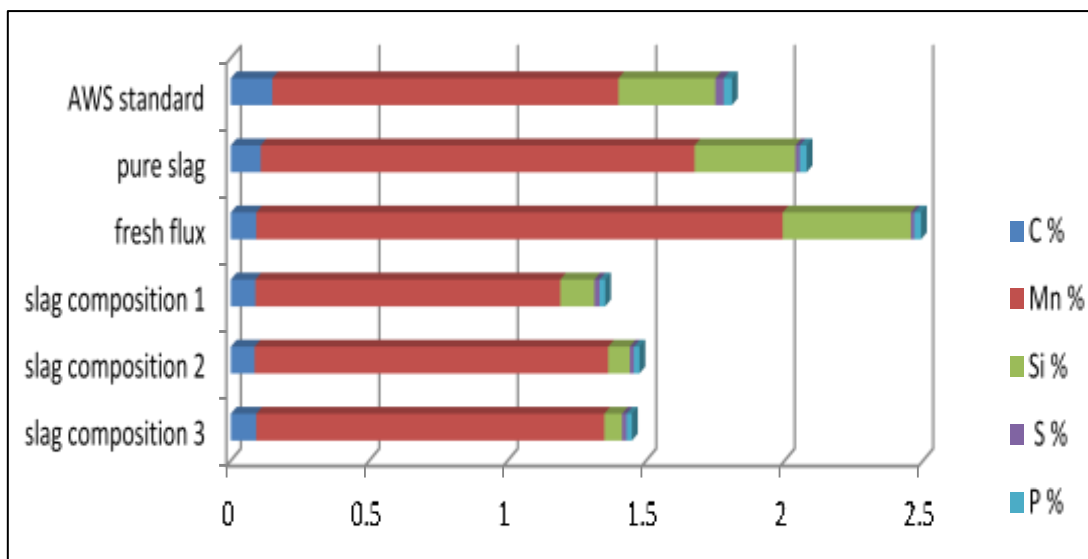


Figure-4.8: Comparison of chemical composition of weld pads prepared using pure slag, fresh flux, and different compositions of slag

4.2.7 Selection of One of the Composition as Recycled Slag

Based on the spectro analysis, slag composition 1 out of three compositions of slag was found to confirm the chemical composition within the range of AWS standard. Therefore, slag composition 1 was selected and utilised further in SAW experiments. This composition of slag is known as recycled slag.

4.2.8 Weld Qualification Tests with Recycled Slag

Once the acceptable chemical composition was achieved, the test assemblies were examined for weld qualification tests.

4.3 Results and Discussions

4.3.1 Weld Metal Chemistry

As mentioned above, Table 4.4 shows the chemical composition of weld pads deposited with fresh flux, pure slag, and different compositions of slag compared with the AWS

5.17 standard. From this table, it was observed that when chemical composition was compared with pure slag, fresh flux, and recycled slag, the composition of recycled slag were in compliance with AWS standard. This may be due to the addition of various additives such as Al powder, Mn powder, CaCO_3 , K_2TiO_3 and binder, i.e., K_2SiO_3 to the slag, all these elements enhances the properties of slag and thus can be used as flux.

Figure 4.9 shows a comparison chart between fresh flux and recycled slag.

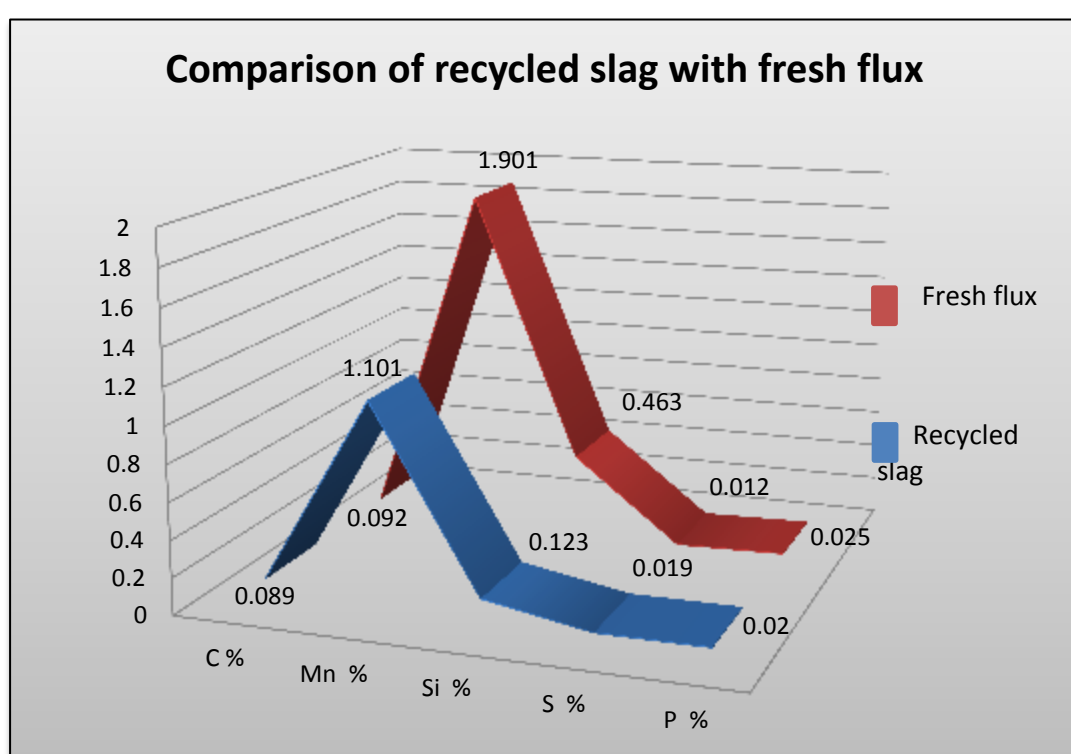


Figure-4.9: Comparison chart between fresh flux and recycled slag

4.3.2 Visual Inspection of the Weld Bead

It was noted that pure slag results in undercuts and porosity on the weld metal. So, the welding performed with pure slag yields an inferior quality weld as compared to reclaimed slag and virgin flux. Welding with recycled slag yields better results, with no apparent cuts and porosity. These results are similar to those of a weld prepared with fresh flux.

The welding input parameters selected as mentioned above in Table 4.1 produced weld beads that were free from the following visual defects.

- a) Undercut
- b) Overlap
- c) Excessive crown height (preferably greater than 20% of plate thickness)
- d) Excessive convexity
- e) Non uniform ripples on the bead
- f) Macro cracking
- g) Surface porosity / dimpled surface
- h) Non uniform width
- i) Excessive spatter

The weld beads so attained also exhibit sound weld metal integrity. It was observed that any combination of welding parameters could be selected as long as the deposited weld beads were free from all the problems mentioned above (a-i).

4.3.3 Slag Detachability and Arc Stability

It was ensured by visual inspection that there was a smooth, detached slag in a welded specimen obtained using virgin flux and reclaimed slag. Slag detachability was also claimed to be self-detachable after each run during welding due to the presence of enough deoxidisers in the virgin flux and reclaimed slag. This results in a rise in the difference between the thermal expansion coefficient of the weld sample and the slag, which aids in slag detachability. On the contrary, the presence of enough silica in slag

results in poor detachability in the weld pads prepared using pure slag. Figure 4.10 shows slag obtained from weld pad prepared using pure slag.



Figure-4.10: Slag obtained from weld pad prepared using pure slag

It was observed that the arc is stable when welding is performed with pure flux and reclaimed slag, whereas in the case of pure slag, the arc was highly unstable. Figure 4.11 and Figure 4.12, illustrate slag after weld pad prepared using fresh flux, and recycled slag, respectively.



Figure-4.11: Slag obtained from weld pad prepared using fresh flux



Figure-4.12: Slag obtained from weld pad prepared using recycled slag

4.3.4 Dye Penetrant Test

A dye penetrant test was done on a test assembly of weld pads prepared with fresh flux, pure slag, and recycled slag to detect various surface defects. It was observed that all the welded samples yielded better results with negligible surface defects.

4.3.5 Tensile Test

The tensile test specimen was cut from the weld pad prepared using recycled slag in mm as per ASME SFA 5.17 requirement. Figure 4.13 shows dimensions of the tensile test and impact test assembly as per ASME SFA 5.17. The tensile test was performed on a 50 KN electro-mechanical controlled universal tensile testing machine (Tinius Olsen) as presented in Figure 4.14. From the tensile specimen, yield strength (YS), ultimate tensile strength (UTS), and percentage elongation were calculated. The tensile test was done by holding the end of the tensile specimen in the universal testing machine and gradually increasing the load on the specimen from both sides until it fractured.

During the test, the tensile load as well as the elongation of a previously marked gauge length in the specimen measured with the help of the load dial of the machine and extensometer, respectively. After fracture, the two pieces of the broken specimen are placed as if fixed together, and the distance between the two gauge marks and the area at the place of fracture are noted.

The minimum yield strength, ultimate tensile strength and percentage elongation of the tensile specimen obtained from welded specimen prepared using reclaimed slag were 366 MPa, 427 MPa and 26.5 percent, respectively as shown in Table 4.5 . The weld specimen obtained using fresh flux accomplishes the AWS specification, whereas weld prepared using pure slag results in 305 MPa and 323 MPa as its yield and ultimate tensile strength, respectively, which is lower than the prescribed value. The decrease in YS and UTS mainly indicates an insufficient quantity of alloying elements in the weld metal, which further increases the chances of oxidation, thus affecting the strength of the weld specimen.

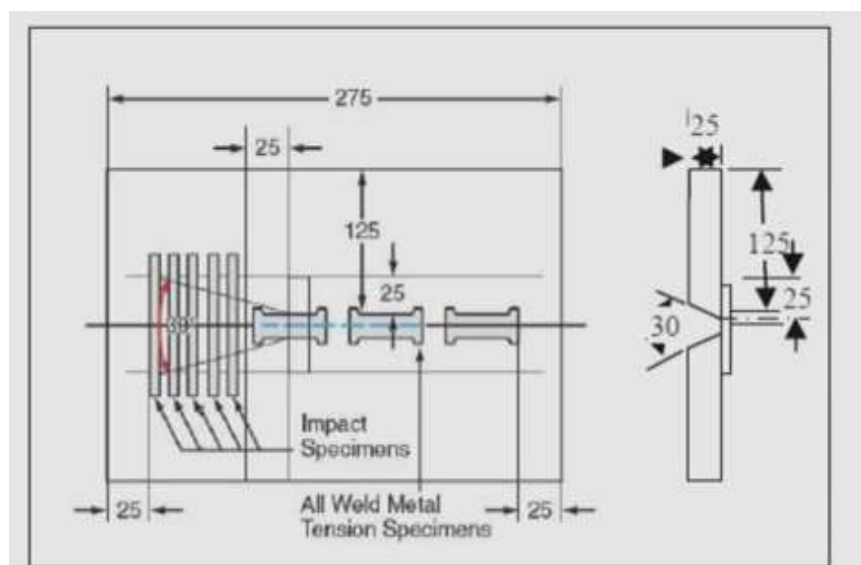


Figure-4.13: Dimensions of tensile test and Impact test assembly in mm as per ASME SFA 5.17

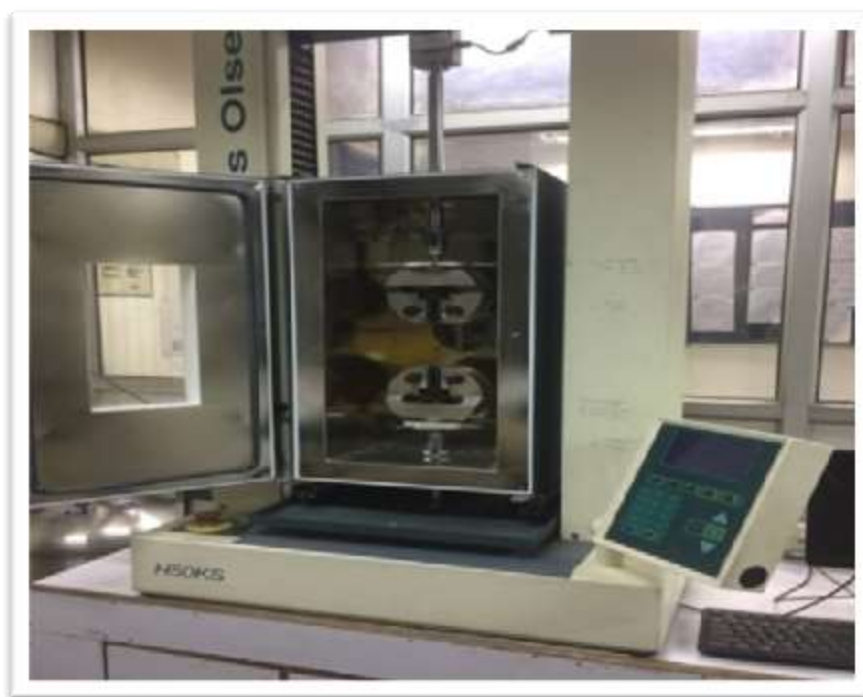


Figure-4.14: Universal Tensile Testing Machine (Metal Forming Laboratory, DTU Delhi)

Table-4.5: Results of weld qualification tests

	YS (MPa)	UTS (MPa)	% Elongation	Charpy Impact (J) (0°C)	Radiography
AWS req.	360	420	24	90	Must pass
Pure Slag	305	323	25	55.3	Failed
Fresh Flux	382.5	454	28.6	114.2	Passed
Recycled Slag	366	427	26.5	101.8	Passed

4.3.6 Impact Test

An impact test was done by preparing five charpy impact specimens as per ASME SFA 5.17. These five specimens were tested according to impact test section of ANSI/AWS B4.0. Impact test results were evaluated as per AWS codes, by discarding the highest and lowest values out of five charpy values. During this test, two of the

remaining three values must be equal or greater than the described energy level of 90 J at 0°C. Moreover, one of the three values may be lower, and the average of the three values should not be less than 90 J (ASME Sec. II, 2010). The average impact value of recycled slag was obtained as 101.8 J, which is within the AWS specification, but in the case of pure slag, the impact value was 55.3 J, which was unacceptable. Figure 4.15 shows impact test specimen. Pure slag consists of oxygen due to which there are chances of slag inclusion, porosity, and lack of fusion, which results in low impact value, whereas reclaimed slag has a reduced amount of oxygen owing to insignificant inclusion. Reclaimed slag thus results in improved toughness, which is due to the presence of acicular ferrite in a higher amount.

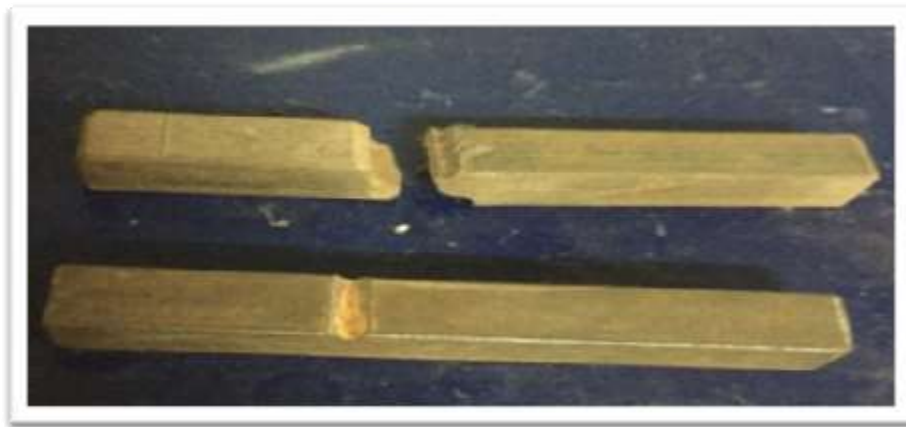


Figure-4.15: Impact specimen of recycled slag

4.3.7 Radiography

The welded specimen infused with fresh flux and reclaimed slag passed the radiographic test. These weld radiographs were obtained in accordance with the AWS standard. The radiographic test was not passed with the pure slag test assembly; this could be due to non-metallic inclusions caused by carbon oxidation.

4.4 Summary

1. Slag recycling proved reliable as the yielding characteristics were found to be equivalent to the flux in the same submerged arc welding process.
2. It was concluded that 87.5% slag when mixed with 5.5% of calcium carbonate and Al powder along with 7% potassium titanate and Mn powder in addition to potassium silicate solution to wet the mixture was suitable composition to be used as recycled slag.
3. Weld metal chemistry for recycled slag was found to be satisfactory as per ASME SFA 5.17.
4. The results of the tensile test and impact test lie within the acceptable range of ASME SFA 5.17.
5. Dye penetrant test was also performed on the specimen and revealed a defect-free surface for reclaimed slag welded specimen.
6. Radiographic test results were comparable to those of fresh flux when observed for recycled slag whereas in case of pure slag, the welded specimen does not pass the radiographic test.
7. Slag detachability and arc stability were both adequate as per the requirement. Both showed an explicit characteristic when observed for recycled slag.
8. Weld beads with an acceptable appearance were observed.

CHAPTER 5

ELEMENT TRANSFER BEHAVIOUR

5.1 Introduction

Several researches on the element transfer behaviour of weldment obtained using recycled slag in SAW discovered that the main causes of the complex changes in the welded specimen were flux composition and weld metal inclusion. According to current slag metal reaction thermodynamics theory, net oxygen transfer is independent of Mn and Si transfer to the weld metal (Pandey et al., 1994). Mohan and Pandey (2005) reported that the weld metal composition was influenced by SAW parameters and flux basicity index. According to Sahni et al. (2009), the open-circuit voltage, welding wire feed rate and basicity index all have a significant impact on weld metal composition. Welding slag can be recycled and reused with varying amounts of flux. The slag-flux mixture has a positive impact on the weld metal chemistry. Some research discovered that it is possible to predict element transfer of C, Mn, Si, and S by designing suitable regression models using statistical designs of mixture experiments (Kanjilal et al., 2007). Wang et al. (2014) explored the effects of wire feed rate and welding current on the metal transfer and arc behaviour. Pandey and Mohan (2003) found the effect of welding current in submerged arc welding and found that there exists a relation between the The transfer of C, Si, Mn, S, and P using formulated flux was achieved by extreme vertices design, which developed an adequate mathematical model using ‘F’ test and ‘t’ test (Jindal et al., 2014). Following this investigation, the model can be developed using a half factorial design and its adequacy can be tested using the ANOVA technique (Montgomery, 2006). So far, it

has been observed that only a few researchers have worked on recycling of slag. The present study attempted to predict the C, Mn, Si, S, and P content transfer in weldment during submerged arc welding with recycled slag.

5.2 Alloying Elements

Weld metal chemistry is primarily affected by welding parameters such as arc voltage, travel speed, voltage, wire feed rate, contact tube to plate distance, and so on during submerged arc welding. In general, weld metal composition varies due to welding parameters in two ways: (i) time spent in interaction between slag and droplet through the arc during welding (ii) slag metal ratio changes with welding parameters. The welding parameters and flux composition have the greatest influence on element transfer behaviour. It is therefore, believed that for determining the weld metal composition and mechanical properties of the weld metal, it is essential to understand the effects of welding parameters on element transfer behaviour. Most commonly, elements like carbon, manganese, and silicon are transferred to the weldments. The addition of these elements plays a crucial role in the mechanical properties of the weld metal. Apart from these elements, there are certain elements such as sulphur and phosphorus that act as impurities in the weldments. The presence of these elements deteriorates the quality of the weld metal. Each element added to the weldments has its own effect, which is explained further in the following paragraphs.

5.2.1 Carbon

Carbon is widely used with Si, Mo, Ni, Cr, and copper to improve weld metal strength and mechanical properties (Wittstock, 1976). In general, increasing the carbon

content, along with other alloying elements, helps to increase strength and hardness. Davis (1980) reported that as the basicity index (BI) reduces for a given flux, the carbon content decreases to a greater extent. Decrease in the carbon content was mainly attributed to oxidation (Mitra and Eagar, 1984).

According to Pandey et al. (1994), carbon percentage increases with increasing welding current and voltage which is attributed to the fact that increase in heat input is mainly caused by increased welding current that results in a larger weld pool size. Weld pool size increases weld pool temperature, which in turn causes higher amount of element transfer from slag to weld pool (Metals handbook, 1983). Similarly, Mohan and Pandey (2005) discovered a linear relationship between carbon percentage and open circuit voltage; welding wire feed rate, and BI basicity index. Chai and Eagar (1980) observed that flux composition has the predominant effect on carbon transfer from flux to the weld metal. Welding parameters have a significant role in carbon content transfer to the weld metal. Kanjilal et al. (2006) observed that the increase in welding speed increases the carbon content, may be because of reduced time for carbon to react with oxygen.

5.2.2 Manganese

Generally, it is believed that the addition of manganese to the low alloy steel results in the increase in the weld metal strength, decreasing the CO porosity. Mn content varies by up to 2% to improve strength, toughness, and welding performance in order to achieve overall weld metal soundness (Wittstock, 1976). Tanaka et al. (1980) observed that, when oxides such as MnO are added to the flux, it improves the chances of Mn transfer to the weld metal. Variations in Mn content in the weld deposits are also

correlated to the transition temperature. North et al. (1978) found that the flux containing alumina, aluminosilicates, and Mn sulphides can cause an increase in aluminium content, which results in increased Mn content in the weld deposits. As a result, Mn content causes an increase in transition temperature of wrought steel with multi-pass GMA welds. Chai and Eagar (1980) found that Mn content varies with change in flux composition and welding parameters such as welding current. Moreover, flux containing a higher concentration of SiO_2 causes an increase in Mn content (Chai and Eagar, 1981). This is due to the reaction of Mn with the silicate anions that increases the percentage Mn transfer from the flux to weld pool (Davis, 1991).

In general, it was observed that apart from flux composition welding parameters play an important role in Mn transfer in the weld metal. Mohan and Pandey (2005) reported that BI and welding parameters such as open circuit voltage, welding speed, and wire feed rate have a predominant influence on weld metal chemistry. Furthermore, it was discovered that Mn content increases as open circuit voltage, wire feed rate, and basicity index decreases. In contrast, Pandey et al. (1994) reported that Mn content is inversely proportional to the welding current and voltage.

5.2.3 Silicon

Silica content is mainly influenced by the silicon content, oxygen content and basicity of flux. With the help of flux basicity and concentration conditions, it is evident that reaction between flux/slag and the metal can be controlled (Potapov, 1978). Silica acts as an alloying element in the weld metal as well as acting as a deoxidiser, which improves oxidation resistance.

Silicon content varies up to 0.7% that helps in improving the welding performance (Wittstock, 1976). Tanka et al. (1980) discovered that silicon content of the flux increases as the SiO_2 content increases. Also, when Mg, Al, and Ti are added to the flux, there is an increase in silicon percentage in the weld metal. Flux containing aluminium additions such as aluminosilicates, alumina, calcium, and aluminium rich compounds etc., results in an increase in aluminium percentage in weld deposits. This leads to an increase in silicon content also from 0.11% to 0.21% that improves the transition temperature of the weld (North et al., 1978). Similarly, Chai and Eagar (1980) concluded that flux composition has a significant role in defining the weld metal chemistry. It was found that silicon content varies with the change in flux composition and the process variables such as welding current and plate thickness. Flux containing MnO results in oxidation of the weld metal and decreases the silicon content of the weld metal. Mohan and Pandey (2005) reported that silicon content is inversely proportional to the open circuit voltage; wire feed rate, and BI. They have observed that silicon content decreases with increasing voltage and welding current.

5.2.4 Sulphur

Sulphur is considered as an impurity present in the welding flux. The quantity of basic and acidic ingredients present in the flux helps in reducing the sulphur content of the weld pool (Davis, 1991). Apart from flux ingredients, Hatch and Chipman (1949) observed that welding parameters and flux basicity index plays a crucial role in affecting the weld metal composition. They have observed various slag/metal reactions that occurs in blast furnace. In this study, they concluded that sulphur content is directly proportional to temperature. In another research, Pandey et al.

(1994) found that sulphur content increases with an increase in welding current and voltage. Also, sulphur content shows a linear relationship with BI. Kanjilal et al. (2006) reported that sulphur content decreases with increase in welding speed, which results in low dilution effect. Later, in 2007, Kanjilal et al. found that the addition of ingredients such as CaO, MgO, CaF₂ and Al₂O₃ cause an increase in sulphur content, whereas binary mixtures such as CaO-MgO, CaO-CaF₂, CaO-Al₂O₃, MgO-CaF₂ and MgO-Al₂O₃ cause a decrease in sulphur content.

5.2.5 Phosphorus

Phosphorus is present as an impurity that serves no purpose other than to decrease the ductility of the weldment. According to Ferrera and Olson (1975), the ability of basic fluxes to remove sulphur and phosphorus results in producing weld metal with good impact properties. It has been observed that phosphorus content of the flux, the basicity index, and the viscosity of the flux has predominant effect on the phosphorus content of weld metal (Solokha et al., 1979).

According to Mitra and Eagar (1984), flux containing higher CaO has less phosphorus content than flux containing MnO. Kanjilal et al. (2005) discovered that as welding speed increases, the phosphorous content decreases. Phosphorus can be found in the filler metal and base plate, where it plays an important role in dilution. Another researcher, Bailey (1977) found that, phosphorus content of the weld metal is directly proportional to the Solidification cracking.

5.3 Plan of Investigation

The element transfer behaviour was evaluated using the procedure as follows:

1. Identifying the input factors and determining their upper and lower limits.
2. Developing the design matrix.
3. Conducting the experiments as per design matrix using recycled slag.
4. Recording the response parameters.
5. Formulating the empirical models.
6. Evaluating the coefficients of the polynomials.
7. Evaluating the significance of coefficients and obtaining the final model.
8. Analysing the adequacy of empirical models.

5.3.1 Identifying the input factors and determining their upper and lower limits

Four welding parameters were identified as wire feed rate (W), arc voltage (V), travel speed (S), and contact tube to plate distance (N). These parameters were considered as direct welding parameters affecting the weld metal integrity because they control the rate of heat input as this is the main cause of melting of flux and filler wire. Many researchers have reported the effect of these parameters on weld metal chemistry. To determine their working range, trial runs were performed by varying one parameter and keeping the others constant. Table 5.1 shows the welding parameters with their upper and lower limits (Montgomery, 2006). The upper limit was coded as +1 and the lower limit was coded as -1.

Table-5.1: Welding parameters with their upper and lower limit

Parameters	Units	Symbol	Low (-1)	High (+1)
Arc Voltage	Volts	V	25	40
Wire Feed Rate	cm/min	W	111	156
Travel speed	cm/min	S	30	40
Contact tube to plate distance	mm	N	20	25

5.3.2 Developing the Design Matrix

The design matrix was developed for a two level half factorial design, where each column and row corresponded to a different level of factors for eight distinct experimental runs. Some researchers discovered that using a two-level half factorial design matrix is effective for modelling the submerged arc welding process because it provides sufficient information at a low cost of experimentation. The design matrix for element transfer is the same as mentioned in Table 3.7 in chapter 3.

5.3.3 Conducting the Experiments as Per Design Matrix using Recycled Slag

As per design matrix, bead on mild steel plate having dimensions as 12 mm X 70 mm X 160 mm were deposited using recycled slag with 3.15 mm diameter EH14 wire. In order to avoid systematic errors, experiments were conducted randomly. Eight sets of experimental runs with three replicates each were performed to prepare the weldments. A Design matrix for calculating coefficients of various responses was mentioned in Table 3.7 of Chapter 3. Design matrix after confounding was shown in Table 3.8 of Chapter 3. Figure 5.1 shows eight sets of submerged arc welding specimens.



Figure-5.1: Eight sets of submerged arc welding specimen

5.3.4 Recording the Response Parameters

After conducting the experiments, the welded samples were removed from the middle of mild steel plates. These samples were then evaluated for their chemical composition with the help of a spectrometer. Table 5.2 shows observed values of weld metal composition (wt. %). The observed mean values of weld metal composition (wt. %) shown in Table 5.3. Table 5.4 represents the predicted and actual values of weld metal composition (wt. %).

Table-5.2: Observed values of weld metal composition (wt. %)

Trial No.	Carbon		Manganese		Silicon		Sulphur		Phosphorus	
	1	2	1	2	1	2	1	2	1	2
1.	0.079	0.081	0.78	0.84	0.32	0.36	0.036	0.032	0.035	0.039
2.	0.082	0.090	0.90	0.82	0.29	0.34	0.034	0.030	0.032	0.028
3.	0.081	0.085	0.60	1	0.20	0.18	0.027	0.029	0.027	0.027
4.	0.073	0.065	1.17	1.09	0.32	0.26	0.035	0.031	0.025	0.029
5.	0.101	0.097	0.81	0.89	0.29	0.31	0.031	0.037	0.037	0.039
6.	0.062	0.058	0.89	0.85	0.32	0.34	0.028	0.032	0.031	0.027
7.	0.062	0.068	0.99	0.93	0.29	0.25	0.027	0.031	0.025	0.031
8.	0.069	0.075	1.1	1	0.34	0.28	0.024	0.026	0.024	0.028

Table-5.3: Observed mean values of weld metal composition (wt. %)

Trial No.	Carbon	Manganese	Silicon	Sulphur	Phosphorus
1.	0.080	0.81	0.34	0.034	0.037
2.	0.086	0.86	0.31	0.032	0.030
3.	0.083	0.80	0.19	0.028	0.027
4.	0.069	1.13	0.29	0.033	0.027
5.	0.099	0.85	0.30	0.034	0.038
6.	0.060	0.87	0.33	0.030	0.029
7.	0.065	0.96	0.27	0.029	0.028
8.	0.072	1.05	0.31	0.025	0.026

Table-5.4: Predicted and actual values of weld metal composition (wt. %)

Trial no.	Carbon		Manganese		Silicon		Sulphur		Phosphorus	
	Predicted	Actual	Predicted	Actual	Predicted	Actual	Predicted	Actual	Predicted	Actual
1.	0.081	0.080	0.84	0.81	0.36	0.34	0.036	0.034	0.035	0.037
2.	0.090	0.086	0.90	0.86	0.34	0.31	0.034	0.032	0.032	0.030
3.	0.085	0.083	1.0	0.80	0.20	0.19	0.029	0.028	0.027	0.027
4.	0.073	0.069	1.17	1.13	0.32	0.29	0.035	0.033	0.029	0.027
5.	0.101	0.099	0.89	0.85	0.31	0.30	0.037	0.034	0.037	0.038
6.	0.062	0.060	0.89	0.87	0.34	0.33	0.032	0.030	0.031	0.029
7.	0.068	0.065	0.99	0.96	0.29	0.27	0.031	0.029	0.031	0.028
8.	0.075	0.072	1.10	1.05	0.34	0.31	0.026	0.025	0.028	0.026

5.3.5 Formulating the Empirical Models

The response function can be expressed as:

$$Y = f(V, W, S, N) \dots\dots\dots 5.1$$

Where,

Y - Response parameter i.e. weld metal chemistry (C, Mn, Si, S and P) in the wt. %.

V - Arc Voltage,

W- Wire feed rate,

S - Travel speed,

N - Contact tube to plate distance

Assuming linear relationship, the possible two factor interactions are taken into consideration, therefore the above expression rewritten as:

$$Y = b_0 + b_1V + b_2W + b_3S + b_4N + b_{12}VW + b_{13}VS + b_{14}VN + b_{23}WS + b_{24}WN + b_{34}SN \dots\dots\dots 5.2$$

After confounding the given empirical model can be expressed as:

$$Y = b_0 + b_1V + b_2W + b_3S + b_4N + b_5(VW + SN) + b_6(VS + WN) + b_7(VN + WS) \dots\dots\dots 5.3$$

5.3.6 Evaluating the coefficients of polynomials

The significance of each coefficient was tested using 't' test. Here the value of 't' from the standard table is 2.3 for confidence level 95% and degree of freedom is 8. Table 5.5 describes coefficients of the model and their significance.

Table-5.5: Coefficients of the model and their significance

Responses	Coefficient	b₀	b₁ (V)	b₂ (W)	b₃ (S)	b₄ (N)	b₅ (VW)	b₆ (VS)	b₇ (WS)
Carbon	value	0.076	0.005	-0.0045	-0.0027	0.002	0.002	-0.001	-0.003
	't' value	54.16	3.56	3.20	1.96	1.42	1.8	0.97	2.13
	significant	Yes	Yes	Yes	No	No	No	No	No
Manganese	value	0.91	0.0612	-0.0687	0.0162	-0.026	-0.026	0.003	-0.033
	't' value	51.60	3.48	3.90	0.92	1.49	1.49	0.17	1.88
	significant	Yes	Yes	Yes	No	No	No	No	No
Silicon	value	0.29	0.0175	-0.0275	0.01	-0.015	0.0175	0.015	0
	't' value	26.85	1.62	2.54	0.92	1.38	1.62	1.38	0
	significant	Yes	No	Yes	No	No	No	No	No
Sulphur	value	0.030	0	-0.0025	-0.0005	-0.0015	0.0002	-0.0012	-0.00075
	't' value	30.61	0	2.55	0.51	1.53	0.25	1.38	0.76
	significant	Yes	No	Yes	No	No	No	No	No
Phosphorus	value	0.030	0.0022	-0.0032	0	0	0.0017	0	-0.0005
	't' value	31.25	2.34	3.38	0	0	1.82	0	0.52
	significant	Yes	Yes	Yes	No	No	No	No	No

5.3.7 Evaluating the significance of coefficients and obtaining the final model

The developed design matrix was employed to establish the significance of coefficients. By putting these values into equation 5.3, we obtain the final developed model for weld metal composition (wt. %) as shown in Table 5.6.

Table-5.6: Final developed model for weld metal composition (wt. %)

S. No.	Responses	Developed Model
1.	Carbon	$C = 0.076 + 0.005 V - 0.0045 W$
2.	Manganese	$Mn = 0.91 + 0.0612 V - 0.0687 W$
3.	Silicon	$Si = 0.29 - 0.0275 W$
4.	Sulphur	$S = 0.030 - 0.0025 W$
5.	Phosphorus	$P = 0.030 + 0.0022 V - 0.0032 W$

5.3.8 Analysing Adequacy of the Empirical Models

Analysis of variance technique was used to analyse the adequacy of mathematical model. According to this technique, the model is significant when the model's calculated F-ratio value is less than tabulated value for a desired level of confidence at 95% confidence level, with 8 as the degree of freedom. It has been found that all models are significant, as shown in Table 5.7.

Table-5.7: Model Adequacy test for weld metal composition (wt. %)

Responses	Degree of freedom S^2_y S^2_{ad}		Variance of optimization S^2_y	Standard deviation of coefficient S_{bj}	Variance of adequacy S^2_{ad}	F-ratio Model F_m	F ratio from table F_t	Whether model significant or not $F_m < F_t$
Carbon	8	3	0.000015	0.001403	0.000042	2.80	4.12	Yes
Manganese	8	3	0.0024	0.17589	0.0066	2.67	4.12	Yes
Silicon	8	3	0.00095	0.0108972	0.00253	2.66	4.12	Yes
Sulphur	8	3	0.00000775	0.0009842	0.00002067	2.68	4.12	Yes
Phosphorus	8	3	0.0000075	0.00096824	0.00002	2.67	4.12	Yes

5.4 Results and Discussions

Experimentation was carried out using half factorial design to analyse the effects of independent variables such as wire feed rate, arc voltage, travel speed, and contact tube to plate distance on the responses such as carbon, manganese, silicon, sulphur and phosphorus.

A linear regression model was suggested to check the adequacy of the model, and for this variance of optimization parameter (S_y^2), variance of adequacy (S_{ad}^2), and standard deviation of coefficient (S_{bj}) were calculated in order to find F value where tabulated F value is 4.12 for the degree of freedom and the confidence interval of 8 and 95 %, respectively. According to this model, if the calculated F-value is less than the tabulated F-value, then the model is significant. It was observed in Table 5.7 that 'F' values for given responses were adequate and less than tabulated F-value. Using Table 5.5, the final equations of developed model were obtained and used to forecast the output. The final developed model was shown in Table 5.6. Based on the diagnostics of model adequacy, a scatter plot diagram was plotted in order to test the goodness of fit or model. Figure 5.2 to 5.6 shows a scatter diagram of various responses where the actual values were drawn on X axis and the predicted values were drawn on Y axis. The points closer to the fitted line indicate a good fit model with a narrow confidence interval.

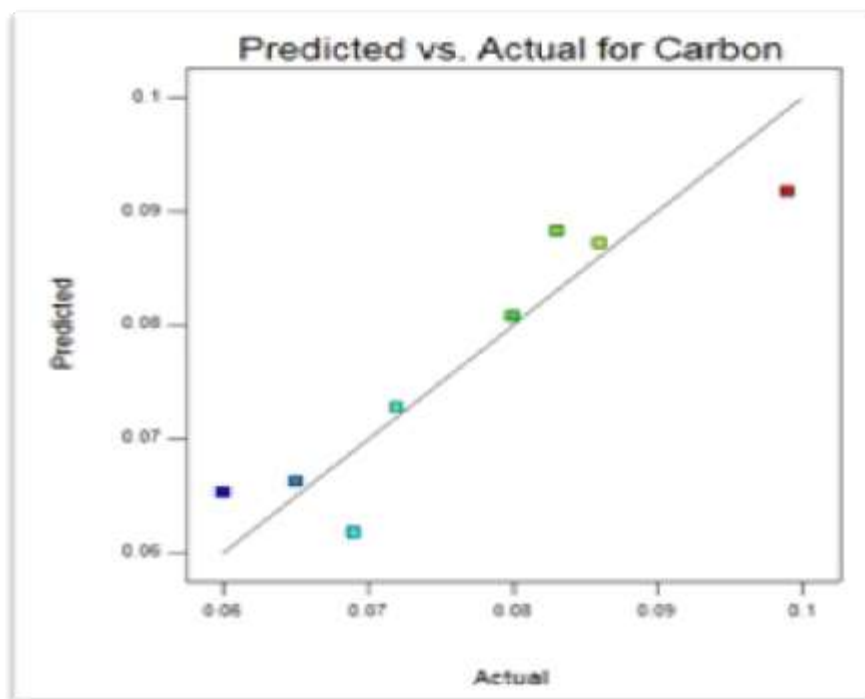


Figure-5.2: Scatter diagram between predicted and actual values of Carbon

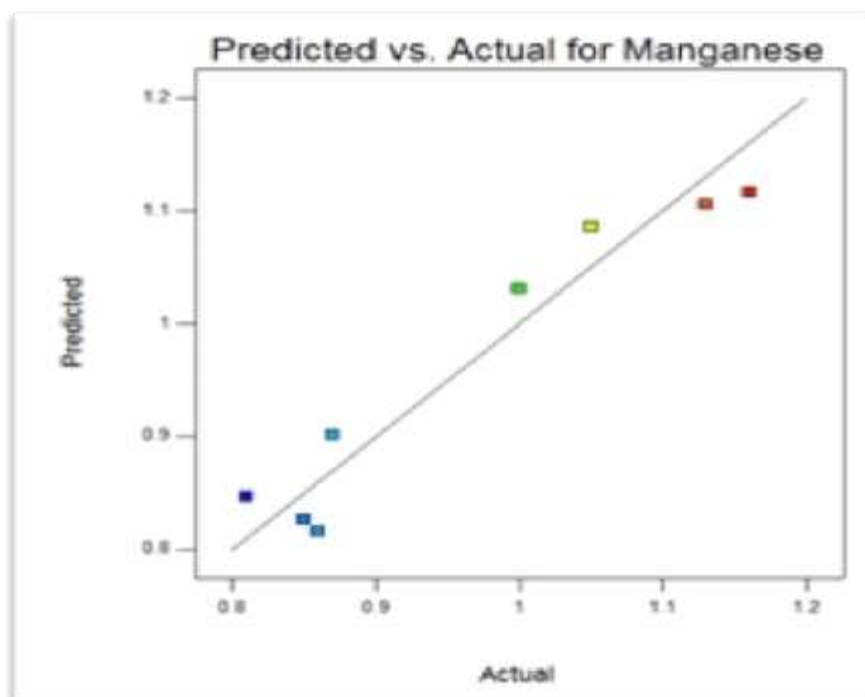


Figure-5.3: Scatter diagram between predicted and actual values of Manganese

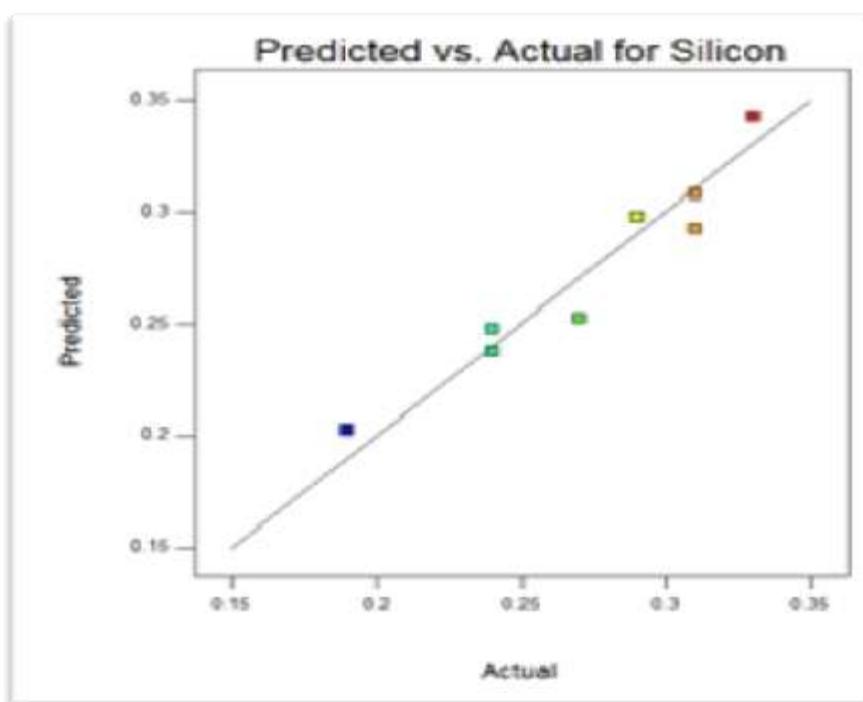


Figure-5.4: Scatter diagram between predicted and actual values of Silicon

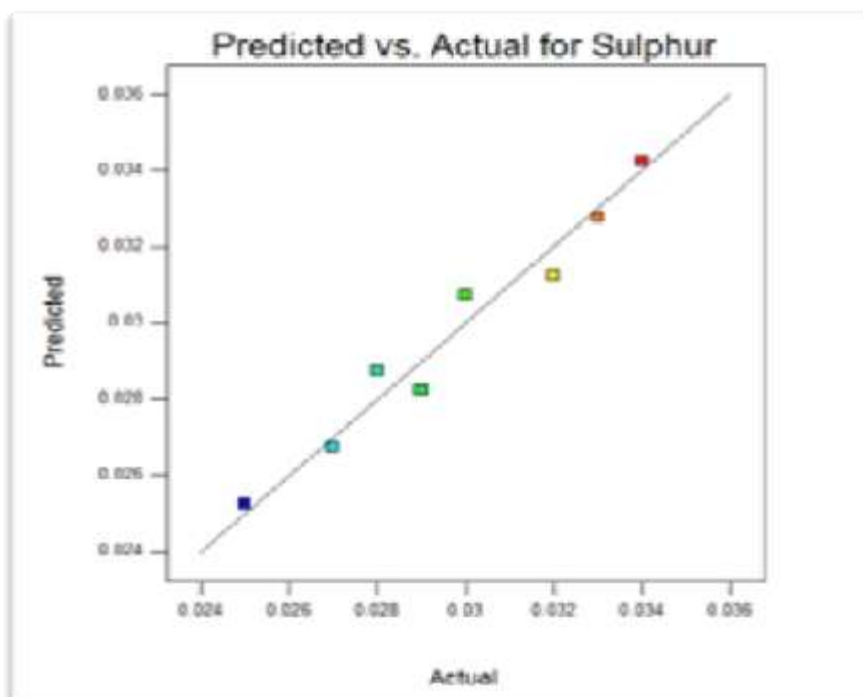


Figure-5.5: Scatter diagram between predicted and actual values of Sulphur

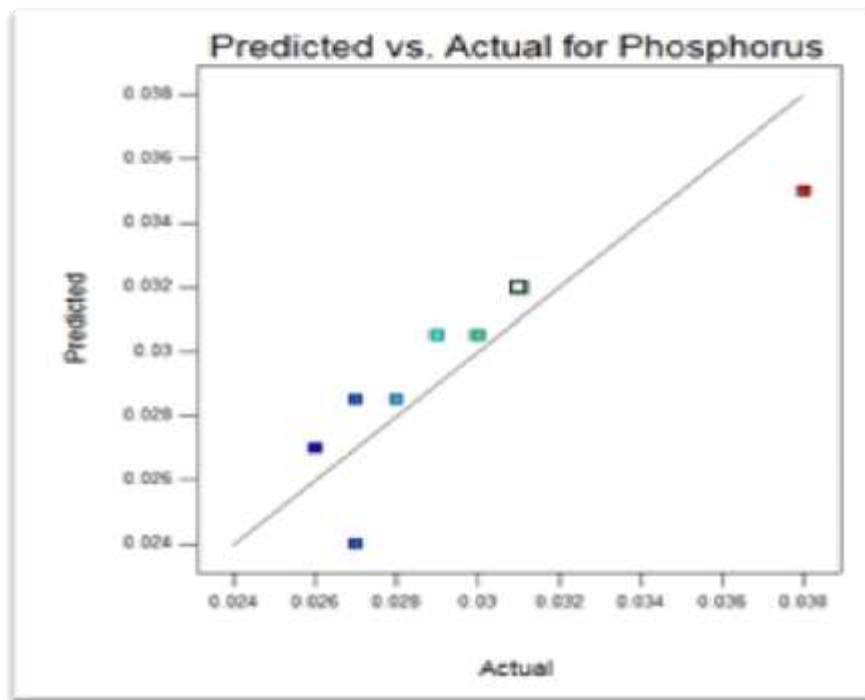


Figure-5.6: Scatter diagram between predicted and actual values of Phosphorus

5.4.1 Effect of welding input parameters on Carbon

As illustrated in Figure 5.7, the carbon content increased from 0.068 to 0.085 as the arc voltage increases from 25 to 40 volts, whereas carbon content decreases from 0.081 to 0.072 as the wire feed rate increased from 111 to 156 cm/min. Figure 5.8 demonstrates the effect of wire feed rate on carbon. The change in carbon content was found to be directly proportional to the variation in arc voltage. This is because an increase in arc voltage results in an increase in arc length, which increases arc spread. However, when flux consumption increased, a higher percentage of carbon was transferred from molten slag to the molten metal.

The decrease in carbon content with increase in wire feed rate can be attributed to the fact that the amount of flux consumption has been reduced. As the flux consumption reduces, it leads to a decreased consumption of carbon from slag to molten metal. Also, the other welding parameters have insignificant effect on the transfer of carbon content.

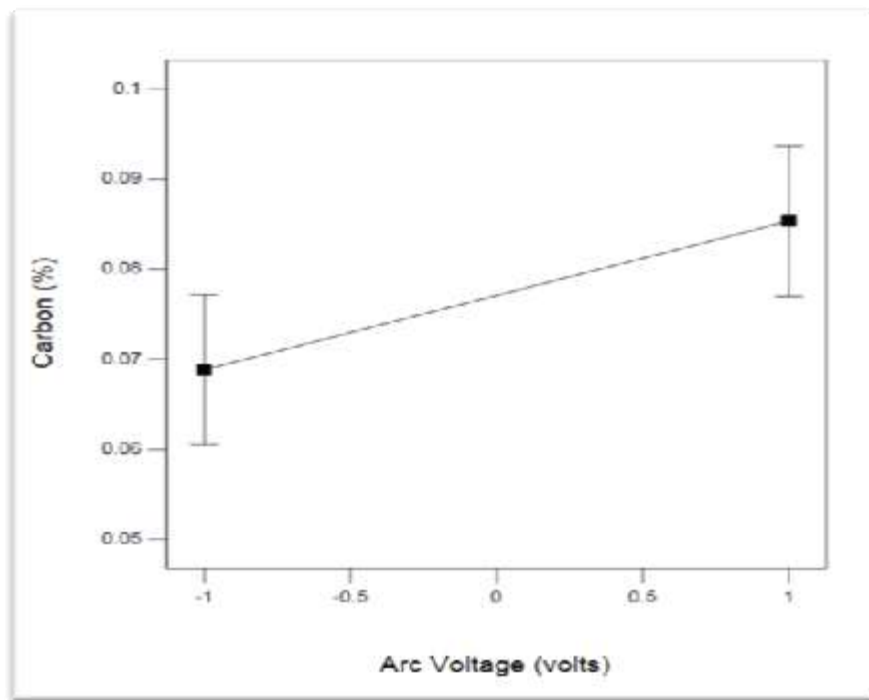


Figure-5.7: Effect of arc voltage on Carbon

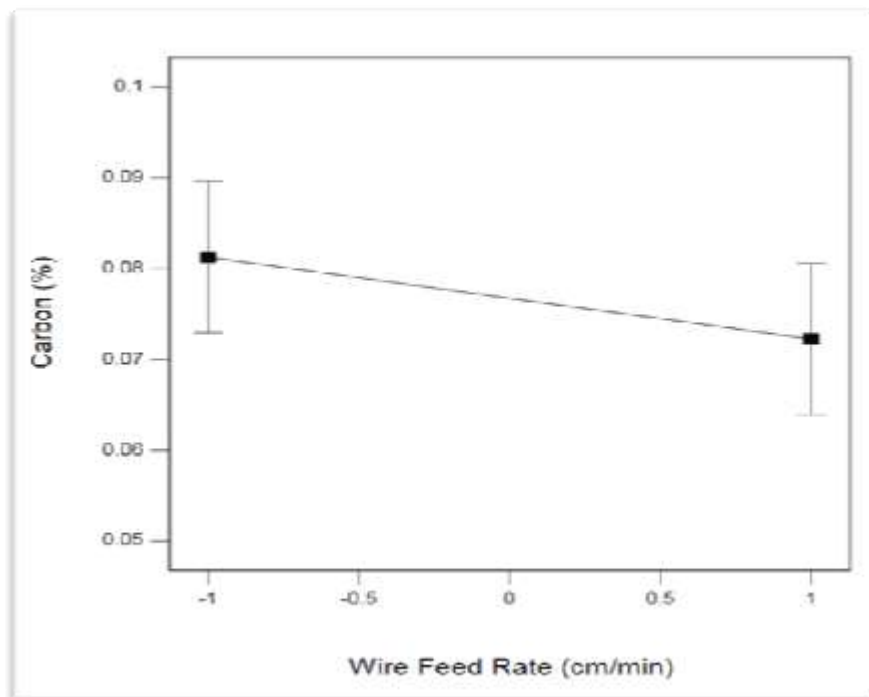


Figure-5.8: Effect of wire feed rate on Carbon

5.4.2 Effect of Welding Input Parameters on Manganese

As depicted in Fig 5.9, the manganese content increased from 0.85 to 0.97 as the voltage increased from 25 to 40 volts, whereas it decreased from 1 to 0.83 as the wire feed rate increased from 111 to 156 cm/min. Increased manganese content with increasing arc voltage may be attributed to increased arc length causing a greater amount of flux to melt along with it, resulting in manganese content transfer from molten slag to the weld metal.

Manganese content decreases when the wire feed rate increases. This is due to the rising welding current during submerged arc welding process, an increase in heat input results in manganese evaporation. Additionally, travel speed and the distance between the contact tube and the plate have insignificant effect on manganese content.

Figure 5.10 shows the effect of wire feed rate on manganese.

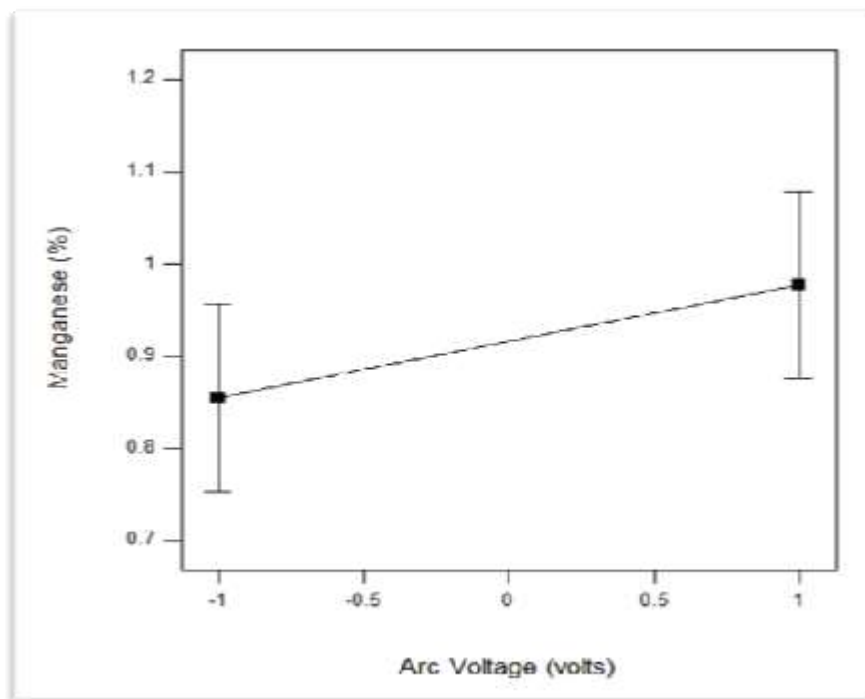


Figure-5.9: Effect of arc voltage on Manganese

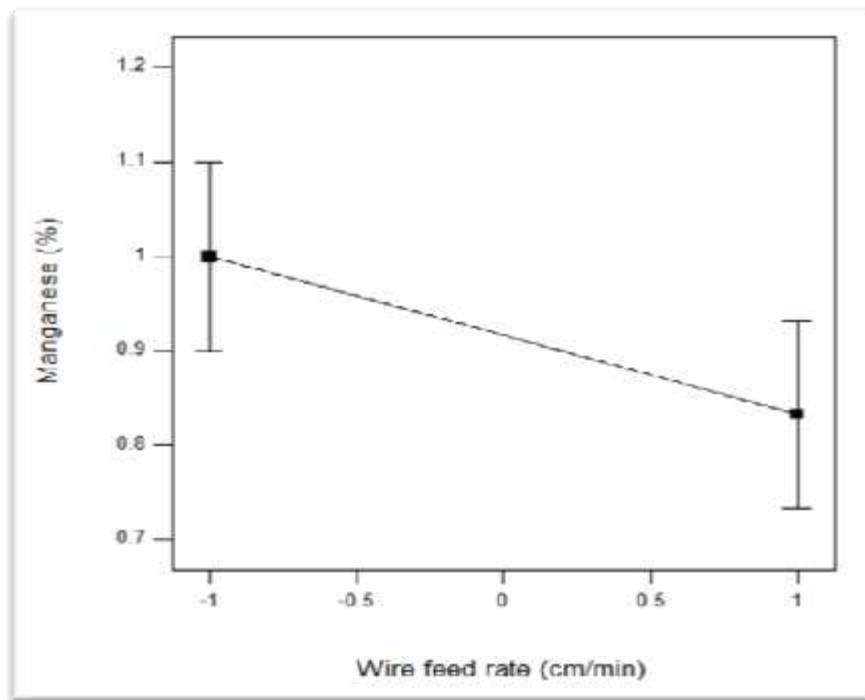


Figure-5.10: Effect of wire feed rate on Manganese

5.4.3 Effect of Welding input Parameters on Silicon

Figure 5.11 shows that the weld metal silicon content decreased from 0.32 to 0.26 when the wire feed rate increased from 111 to 156 cm/min. This decreasing trend was due to the fact that as the wire feed rate increases, it causes less slag metal reaction and thus less silicon transfer occurs in the weld metal. Furthermore, this relationship can also be attributed to the fact that lower the wire feed rate, lower is the welding current, thus requiring less heat input to create a smaller weld pool area. Due to small weld pool area, a lesser amount of silicon content will take place. Travel speed, arc voltage, and contact tube to plate distance have insignificant effect on the transfer of silicon content.

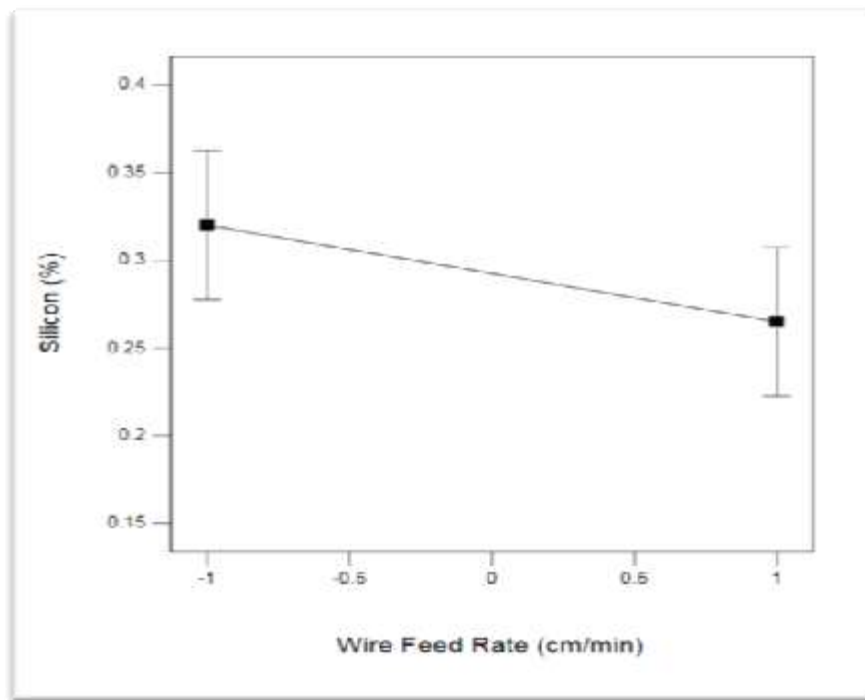


Figure-5.11: Effect of wire feed rate on Silicon

5.4.4 Effect of Welding Input Parameters on Sulphur

As depicted in Figure 5.12, the sulphur content decreased from 0.033 to 0.029 with increase in wire feed rate from 111 to 156 cm/min. An increase in wire feed rate results in increase in welding current, which thus decreases the slag metal reaction and therefore a lesser amount of sulphur content will be transferred from the slag to weld metal.

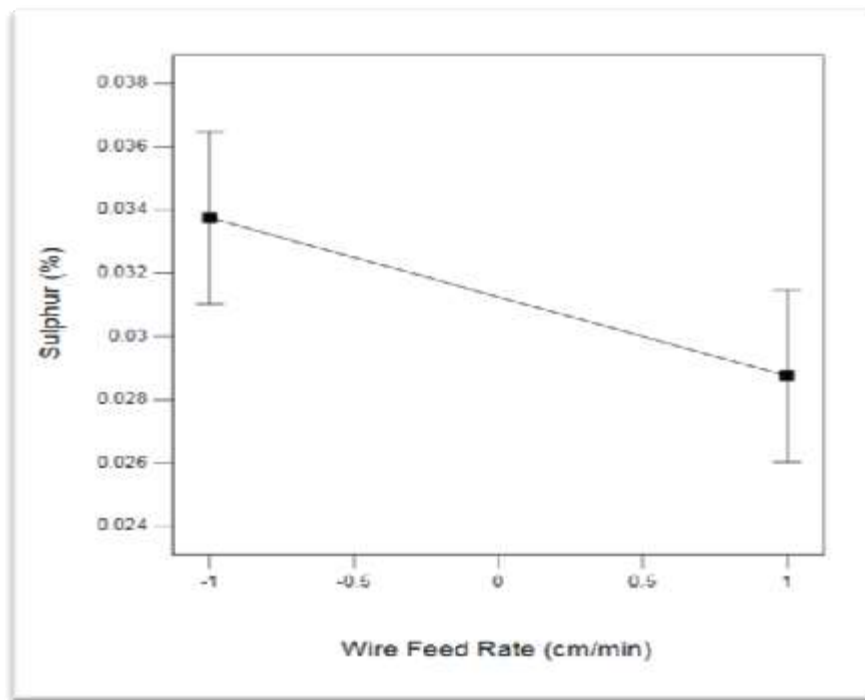


Figure-5.12: Effect of wire feed rate on Sulphur

5.4.5 Effect of welding input parameters on Phosphorus

Figure 5.13 demonstrates that the phosphorus content increased from 0.028 to 0.031 with an increase in arc voltage from 25 to 40 volts and decreased from 0.033 to 0.027 with the increase in wire feed rate from 111 to 156 cm/min. This increasing trend of phosphorus content with arc voltage can be supported by the fact that an increase in voltage will lead to an increase in arc spread, which provides a larger area for melting flux, therefore a higher amount of phosphorus transfer takes place. On the contrary, the decreasing trend of phosphorus content with the increasing wire feed rate was due to increased welding current and then an increase in heat input, resulting in lower cooling rate. However, phosphorus content is reduced in weld metal due to oxidation. As observed, travel speed and contact tube to plate distance have insignificant effect on phosphorus content. Figure 5.14 shows the effect of wire feed rate on phosphorus.

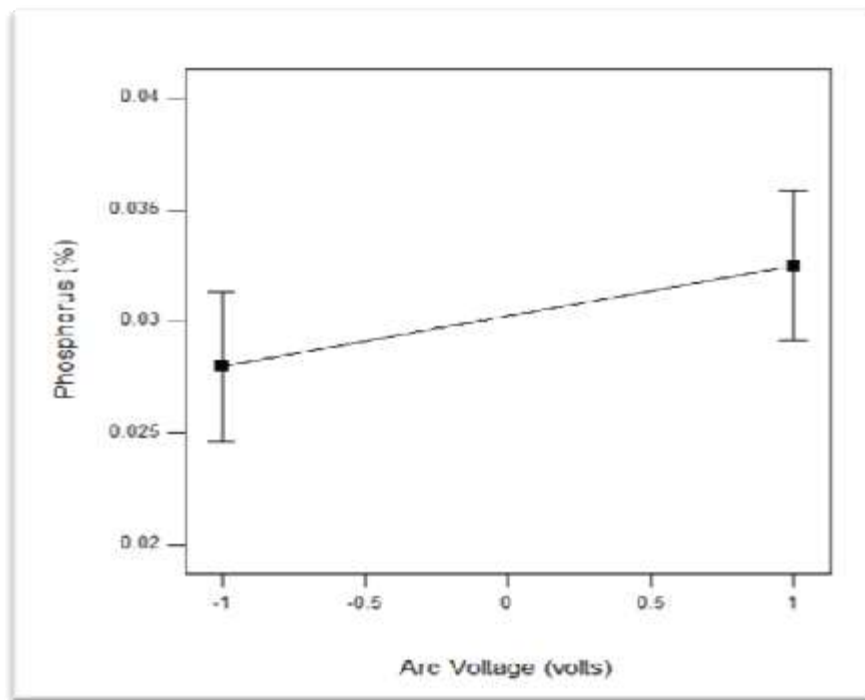


Figure-5.13: Effect of arc voltage on Phosphorus

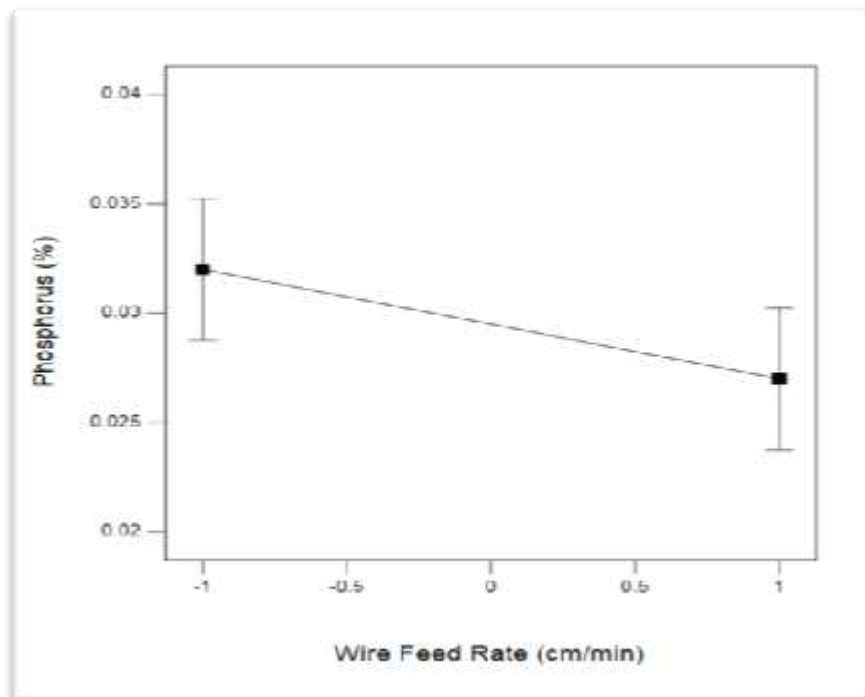


Figure-5.14: Effect of wire feed rate on Phosphorus

5.5 Summary

1. Carbon content is directly proportional to the arc voltage, whereas it is inversely proportional to the wire feed rate. Both welding speed and contact tube to plate distance have insignificant effect on it.
2. Manganese content is directly proportional to the arc voltage, whereas it is inversely proportional to the wire feed rate.
3. Silicon content is inversely related to the wire feed rate but remains the same with varying arc voltage, welding speed, and contact tube to plate distance.
4. Sulphur content decreased with an increase in wire feed rate but remains the same with varying arc voltage, welding speed, and contact tube to plate distance.
5. Phosphorus content increased with an increase in arc voltage and decreased with the increase in wire feed rate but remained almost constant in the case of contact tube to plate distance and welding speed.
6. It was concluded that the contact tube to plate distance has an insignificant effect on weld metal chemistry.

WELD BEAD GEOMETRY AND SHAPE RELATIONSHIPS

6.1 Introduction

Weld bead geometry has a significant role in affecting the load carrying capacity and stress distribution of the weld during solidification. During research, it was found that by the application of high current, straight polarity, small electrode diameter, and longer electrode extension, it is possible to raise the melting rate of weld metal in SAW (Chandel et al., 1987). Kiran et al., (2012) studied the changes that occur in bead geometry of high strength low alloy steel due the effect of welding current, current pulses along with welding speed, and it was concluded that the former two factors affect the weld bead width and reinforcement, while welding current also affects the weld bead penetration. Another study reported that the rate of heat input and welding speed are inversely related, which improves the mechanical properties of the weld metal (Murugan and Gunaraj, 2005). They presented the effect of controllable process variables like voltage, wire feed rate, welding speed, and nozzle to plate distance on weld bead geometry in graphical form. In addition, they have observed that weld bead quality can be maintained by selecting the right process variables. Another researcher proposed optimum weld pool geometry in Pulsed Current Tungsten Inert Gas Welding (PCTIG) of titanium alloy using a mathematical model of Box-behnken design, and observed that weld bead size can be related to pulse current parameters using mathematical equations (Balasubramaniam et al., 2016). Sensitivity analysis was also used in this study. Using multiple curvilinear

regression analysis, Karaoglu and Secgin (2008) investigated how parameters like welding current, voltage, and welding speed can be fine-tuned to achieve optimal weld bead geometry where penetration is more resistant to changes in voltage and speed. This approach was also used to determine the influence of different weld bead parameters on weld bead volume. The findings show that sensitivity analysis can help to regulate weld bead volume and improve weld quality (Gunaraj and Murugan, 2000). For a specific region of HAZ, comparative research was conducted to forecast and analyse the bead on the plate and the bead on the joint weld plate. Results revealed that the HAZ of bead on a plate is greater than that of a bead on joint, but the effect of welding parameters are the same in both cases (Gunaraj and Murugan, 1999). Another study combined a microstructural analysis with an oval-shaped heat source model to predict HAZ width, transient temperature distribution, and weld pool on mild steel plate. It was discovered that the predicted and actual thermal fields are reasonably similar. Furthermore, microstructure analysis reveals that the fusion zone has higher grain growth and finer equiaxed grains than the HAZ (Yadav et al., 2017).

In addition, a few researchers evaluated the weld bead parameters affected by various welding process variables, but their findings were insufficient to produce satisfactory results. As a result, it was critical to create a manufacturing process that produces desirable weld quality therefore Gunaraj and Murugan, (1999); Singh et al., (2016) used a technique to examine the weld bead geometry affected by polarity. This is done by predicting critical dimensions using straight and reverse polarity.

By performing welding using recycled slag, they have studied the effects of welding parameters (such as arc voltage, wire feed rate, welding speed, and contact tube to

plate distance) on the bead geometry and shape relationships of mild steel bead on plate. For this, linear regression analysis was used to develop empirical models to relate welding parameters (wire feed rate, arc voltage, travel speed, and nozzle to tip distance) with responses (such as bead width, bead height, bead penetration, weld penetration shape factor, and weld reinforcement form factor). These models are then checked for adequacy and significance of coefficients using 'F' test and 't' test, respectively. The adequacy test revealed that the newly designed slag proves beneficial in presaging the weld bead quality.

6.2 Elements of Weld Bead Geometry

Weld bead geometry and shape relationships are significant as these dimensions and ratios elaborate the load bearing capacity of the weld metal. This includes bead width (w), depth of penetration/ bead penetration (p), Height of reinforcement/ bead height (h), weld penetration shape factor (WPSF) and weld reinforcement form factor (WRFF). Figure 6.1 depicts various terms used in weld bead geometry.

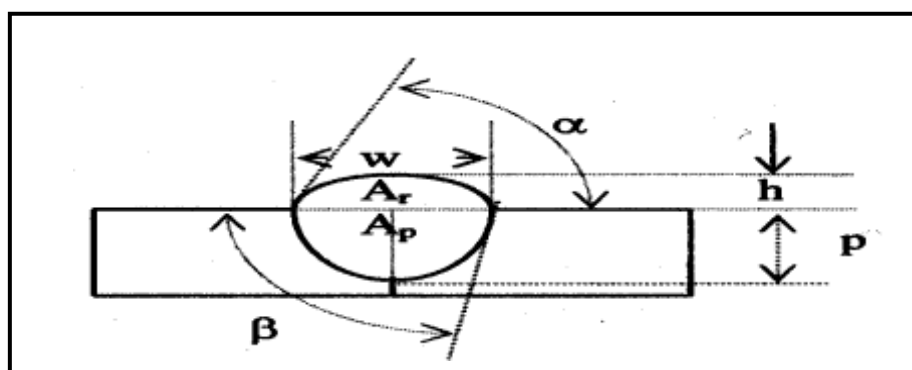


Figure-6.1: Weld bead geometry

As mentioned in Figure 6.1, various terms used in bead geometry and shape relationships are as follows:

w = Weld bead width

p = Weld bead penetration

h = Weld bead height

α = Angle of convexity

β = Angle of entry

WPSF (w/p) = Weld penetration shape factor

WRFF (w/h) = Weld reinforcement form factor

A_p = Area of penetration

A_r = Area of reinforcement

$A_t = A_p + A_r$ = Total bead area

% Dilution = $(A_p / A_t) \times 100$ = Percent dilution

$$H = \frac{\eta VI}{S} \cos \Phi \text{ J/mm}$$

Where H = Heat input per unit length, J/mm

η = Heat transfer efficiency

V = Arc voltage, volts

I = Welding current, amps

S = Welding speed, mm/sec

$\cos \Phi$ = Power factor

6.2.1 Bead Width

Bead width is the most important physical characteristic of the weldment. It is defined as the maximum width of the fused area of the base plate. The bead width of a welded junction is useful in determining the strength and quality of the welded structure (Chaudhary, 2021). Higher bead width is desired in submerged arc welding when hard facing applications are preferred to cover the entire region with the minimum number of passes. Sharapov (1972) proposed a relation between welding parameters and dimensionless pool width. This aids in the calculation of the bead width of the butt weld during submerged arc welding. Cary (1979); Mc Glone (1982) discovered that arc voltage varies proportionally with arc length, which results in increasing the bead width. Other parameters such as polarity, in addition to process variables like welding current, arc voltage, and electrode diameter, have a significant impact on the weld bead width. According to Yang et al. (1992), when negative electrode polarity is applied, bead width decreases. This may be caused by an increase in heat input as the welding current increases. According to Gunaraj and Murugan (1999), when the electrode stick out increases, the diameter of the HAZ decreases. Furthermore, increasing electrode extension aids in melting wire by giving more energy, resulting in a slower melting of the base metal and a narrower bead width. Ghosh et al. (2007) discovered that when the arc voltage is increased, the welding current increases, making the weld bead broader and flatter; yet, as the travel speed increases, the bead width decreases.

6.2.2 Bead Height

Bead height is defined as the distance from the top of the weld bead to the base plate surface. It is mainly influenced by the wire feed rate and electrode polarity (Gunaraj and Murugan, 1999). Furthermore, the reinforcement increases as the voltage, electrode diameter, and welding speed increases. Rathi (2021) found that electrode diameter, wire feed rate, the interaction of electrode diameter and wire feed rate, and the interaction of arc voltage and flux combination all results in improving reinforcement. On the other hand, Chaudhary (2021) observed that when voltage and welding speed increase, reinforcement diminishes. They also found that Furthermore, when the wire feed rate increases as the current thus resulting in a higher deposition of filler metal.

6.2.3 Bead Penetration

Weld bead penetration is defined as the maximum distance between the top surface of the base plate and depth to which the fusion takes place. It is widely known that penetration is highly influenced by the welding parameters. Chaudhary et al. (2021) supported this observation and concluded that depth of penetration varies with the change in process parameters. They have observed that penetration varies directly with the wire feed rate and arc voltage. This may be due to increase in overall heat input into the weld metal, thus increases the depth of penetration. On the contrary, Caddell (1967); Gunaraj and Murugan (1999) reported that penetration varies inversely with the arc voltage. For a given set of welding current and voltage, increase in travel speed results in decreased penetration; weld reinforcement and heat input per unit length of weld Chandel et al. (1987). Ghosh et al. (2007) found that, with the increase in arc voltage, weld bead width become wider and flatter thus resulting in

decrease in penetration. Rathi et al. (2020) concluded that electrode diameter and wire feed rate has predominant effect on depth of penetration and negligible effect on arc voltage. They found that the penetration can be maintained by the welding current but remains unaffected by travel speed and welding voltage. Moreover, they have concluded that hardness of weldment is mainly affected by voltage. Murugan and Gunaraj (2005) observed that, travel speed varies directly with depth of penetration and reinforcement. Similarly, penetration exhibits same behaviour with increase in wire feed rate whereas it shows the reverse behaviour with increasing voltage, travel speed and contact tip to work distance. Polarity plays a crucial role in affecting the depth of penetration. It was found that penetration is higher in direct current electrode positive (DCEP) polarity whereas it decreases in direct current electrode negative (DCEN) polarity. This is because welding current is higher in DCEP, thus produces higher heat input which gives rise to higher penetration (Sharma et al., 2009).

Chandel et al. (1987) considered the effect of electrode extension and polarity and hence developed the following model:

$$P \text{ (for DCEP)} = \frac{(L)^{0.99} (A)^{0.41} (I)^{1.19} (S)^{0.209}}{(V)^{1.08} (D)^{0.84}} \frac{1}{76}$$

Where,

P = Penetration, mm

I = Welding current, amperes

V = Arc voltage, volts

S = Travel speed, mm/min

D = Electrode diameter, mm

L = Electrode extension, mm

A = Included angle, degrees

From this model, they concluded that with increase in welding current, electrode extension and groove angle the penetration increases whereas with increase in electrode diameter and arc voltage the depth of penetration decreases.

Flux viscosity has a predominant effect on bead penetration where fluxes with high viscosity results in restraining the weld bead and concentrating the heat transfer to a narrow region of the base metal, thus providing higher depth of penetration for the weld metal prepared using manganese silicate and calcium silicate fluxes suggested by (Olson et al., 1993; Yang et al., 1992).

Robinson (1983) found that, as the polarity changes from DCEP to DCEN there occurs changes in the amount of heat developed at the electrode and work piece and hence the weld bead geometry and mechanical properties of the weld. DCEN polarity creates high melting rates whereas DCEP produces low melting rates. Electrode melting rates behave linearly with increase in welding current (Renwick and Patchett, 1976). On the other hand, Nadkarni (1988) observed that DCEN generates a stable arc with small weld bead width, which aids in better control of weld bead profile. It gives shallow penetration due to high metal deposition rate over wide area. Therefore, it was concluded that alternating current (AC) produces deeper penetration than that obtained by DCEN, apart from polarity various mechanical properties such as yield strength, UTS and hardness varies with its highest value in DCEP as compared to DCEN (Kanjilal, 2006).

Attempts have been made by the researcher to propose relation between weld bead geometry with the flux used in SAW. Flux consists of various ingredients such as CaCO_3 , SiO_2 , MnO_2 , and Al_2O_3 . Any change in these ingredients leads to the change in weld bead output parameters. Palm (1972) observed that, due to addition of MnO in the flux there is an increase in weld bead penetration. It was observed that different ingredients can cause deeper, shallow or medium penetration. For example, addition of CaCO_3 , K_2CO_3 and CaF_2 can cause shallow penetration, whereas addition of MgO , SiO_2 , MnO_3 and Al_2O_3 can cause medium penetration. On the other hand, addition of MgCO_3 can produce deeper penetration (Hezlett, 1957). Due to addition of CaO to the $\text{MnO-SiO}_2\text{-CaO}$ flux system the weld penetration increased.

Penetration can also be related to the welding parameters such as welding current, flux particle size, slag basicity etc. Wanka (1980) and Feldstein (1980) observed that as the welding current varies it causes changes in penetration. Particle size is the most important feature used for selecting the flux. Finer the flux deeper the flux cavity thus producing better weld bead geometry. Srinath (1975) found that it is possible to produce deeper penetration with the use of fine grained flux. Similarly, increase in particle size of the flux results in deeper penetration (Visvanath, 1982). In addition, weld bead width varies directly with the particle size.

6.2.4 Weld Penetration Shape Factor

The ratio of bead width to penetration is known as WPSF. Polarity helps in predicting the behaviour of WPSF. Renwick and Patchett (1976) discovered that when DCEP polarity is used instead of DCEN polarity, WPSF increases. This is owing to the fact that DCEN polarity produces higher reinforcement. According to Singh et al. (2016),

WPSF increases with increasing open circuit voltage and decreases with increasing wire feed rate. They also discovered that WPSF has a lower value in DCEP polarity than DCEN polarity. Furthermore, WPSF increases as the open circuit voltage increases. According to Ferrera and Olson (1975), WPSF reduces when the basicity index rises, although there are other process parameters that have a greater impact on WPSF. These factors include welding current, arc voltage, and electrode diameter (Demyantserich, 1974). Whereas welding speed has negligible influence on WPSF. Mandatov (1969) observed that WPSF increases with the increase in arc voltage. As the value of WPSF rises it can lead to an increase in the chances of centreline solidification cracking, as observed by Bailey (1977).

6.2.5 Weld reinforcement form Factor

Weld reinforcement form factor is defined as the ratio of bead width to reinforcement. As the value of WRFF increases, it results in a smoother weld surface. Houldcroft (1989) reported that when the value of WRFF lies between 2 and 7 it results in yielding improved mechanical properties. Due to the varying properties of the molten metal pool, the value of WRFF varies. Singh et al. (2016) observed that the voltage varies directly with WRFF. Also, DCEP has a predominant effect on WRFF.

6.2.6 Dilution

Dilution is defined as the change in chemical composition of a deposited filler material produced by adding base material to the deposited weld bead, and it is responsible for both the mechanical and metallurgical qualities of the welded specimen. The degree of dilution is determined by the chemical composition difference between the weld and the base metal, as well as the welding process and

technique used. The degree of dilution can have a big impact on strength, ductility, weld fracture resistance, corrosion resistance, heat treatment, and other qualities (Shukla and Pandey, 2012). The parent metal has melted in with the filler wire and has diluted it and this dilution may be expressed as (Davies, 1996):

$$\% \text{ Dilution} = \frac{\text{Area of weld bead penetration}}{\text{Total weld bead area}} * 100$$

Dilution was found to be the maximum in the case of single run welds on thin sections with square edge preparation, whereas it is the minimum for multi-pass welds with normal edge preparation. Dilution is significant for dissimilar weld metals and in the welding of clad material (Lancaster, 1999). Clearly, there is always significant dilution in any root run. The dilution increases with the amount of weaving. When different metals are welded together, the resultant weld will be diluted by each parent metal, and a successful weld must be free of major defects, including the chance of cracking. Furthermore, the physical and mechanical properties, as well as corrosion resistance, must be as close to those of the parent metal as possible. Since all of the criteria are not always met, the welding wire with the best qualities for the case must be chosen. Dilution is especially important in hard surfacing and welding with electrodes that are not of the same composition as the base metal (Singh, 2007).

6.3 Plan of Investigation

1. Identifying the important welding parameters and determining their upper and lower limits
2. Developing the design matrix

3. Conducting the experiments as per design matrix using recycled slag
4. Recording the response parameters
5. Developing the empirical models
6. Evaluating the Coefficients of the Polynomials
7. Evaluating the significance of coefficients and obtaining the final model
8. Analysing the adequacy of empirical models

6.3.1 Identifying the important welding parameters and determining their upper and lower limits

Wire feed rate (W), arc voltage (V), travel speed (S) and contact tube to plate distance (N) were identified as four independently controllable parameters to carry out experimentation and develop the empirical models. For determining their working range, trial runs were carried out by varying one parameter and keeping the others constant. The two levels selected provided the weld beads with acceptable profiles and were free from visual defects. Parameters were coded as (+1) and (-1) or simply (+1) and (-1) corresponding to high and low levels. Table 6.1 shows the welding parameters with their upper and lower limit.

Table-6.1: Welding parameters with their upper and lower limit

Parameters	Units	Symbol	Low (-1)	High (+1)
Arc Voltage	Volts	V	25	40
Wire Feed Rate	cm/min	W	97	156
Travel speed	cm/min	S	32	40
Contact tube to plate distance	mm	N	18	23

6.3.2 Developing the Design Matrix

Design matrix was developed for two-level half factorial design where the rows correspond to different trials and column to the level of the parameters. The design matrix for bead geometry and shape relationships was mentioned in Table 3.7 in Chapter 3. Table 3.8 of Chapter 3 shows design matrix after confounding.

6.3.3 Conducting the Experiments as Per Design Matrix using Recycled Slag

As per design matrix, bead on mild steel plate having dimensions as 12 mm X 70 mm X 160 mm were deposited using recycled slag with 3.15 mm EH14 wire. A constant potential transformer-rectifier type of power source was used with current capacity of 800 amperes and open circuit voltage range from 12-48 volts. In order to avoid systematic error, experiments were conducted randomly with three replicates in each run. Eight sets of weld beads prepared on specimens were shown in Fig. 6.2.



Figure-6.2: Eight sets of bead geometry welded specimen

6.3.4 Recording of the Response Parameters

Once the experiments were conducted, the welded specimens were removed from the middle (approximately 20 mm in length) of mild steel plates. The cutting was performed using a power hacksaw, and then the specimen surface was smoothed using a grinding machine. After grinding, they were polished by the metallurgical polishing methods, followed by etching with a 2% nital solution (98% alcohol + 2% nitric acid). The weld bead profiles were measured using an optical profile projector. With the help of a profile projector, weld bead width, weld bead height, and weld bead penetration were calculated. WPSF and WRFF being a ratio of w/p and w/h respectively, it can be directly calculated from the other response parameters. Figure 6.3 shows the specimen removed for observing responses. The observed values of weld bead geometry and shape relationships were shown in Table 6.2. Table 6.3 shows observed mean values of weld bead geometry and shape relationships. Table 6.4 represents predicted and actual values of weld bead geometry and shape relationships.

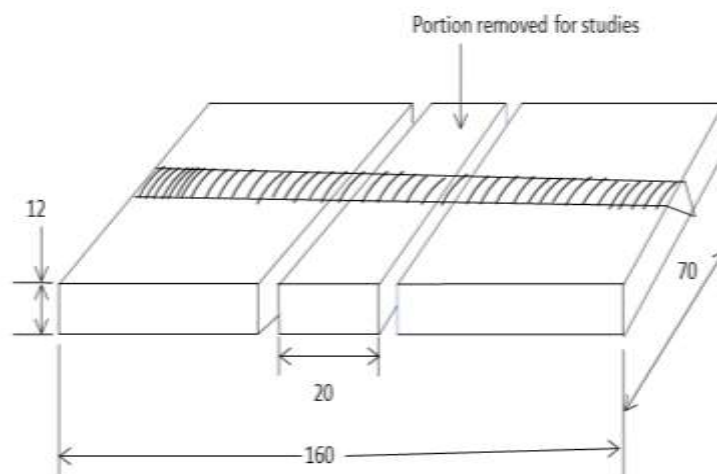


Figure-6.3: Specimen removed for observing responses

Table-6.2: Observed values of weld bead geometry and shape relationships

Trial No.	Bead width (mm)		Bead Height (mm)		Bead penetration (mm)		WPSF		WRFF	
	1	2	1	2	1	2	1	2	1	2
1.	14	14	2.16	1.90	2.6	3	5.34	5	6.98	6.80
2.	14	12	2.04	1.96	1.9	1.7	7.28	7.64	5.95	7.05
3.	17	17	2.49	2.50	4.9	4.2	3.23	4.04	7.10	6.50
4.	19	20	2	2	4.9	5	3.80	3.90	9.50	10
5.	14	12	2.72	3	2.1	2.3	5.70	5.65	4.78	4.54
6.	13.4	14.8	2.12	2.11	2.4	2.5	5.36	5.64	7.06	6.30
7.	17	16	2.46	2.53	4.5	4.5	3.60	3.60	6.44	6.60
8.	18	18	2.40	2.40	3.5	3.5	5.13	5.14	7.80	7.50

Table-6.3: Observed mean values of weld bead geometry and shape relationships

Trial No.	Bead width (mm)	Bead Height (mm)	Bead penetration (mm)	WPSF	WRFF
1.	14	2.03	2.8	5.0	6.89
2.	13	2	1.7	7.64	6.5
3.	17	2.5	4.2	4.04	6.8
4.	19.5	2	5.0	3.9	9.75
5.	13	2.86	2.3	5.65	4.54
6.	14.1	2.11	2.5	5.64	6.68
7.	16.5	2.53	4.5	3.60	6.52
8.	18	2.4	3.5	5.14	7.5

Table-6.4: Predicted and actual values of weld bead geometry and shape relationships

Trial no.	Bead Width		Bead Height		Bead Penetration		WPSF		WRFF	
	Predicted	Actual	Predicted	Actual	Predicted	Actual	Predicted	Actual	Predicted	Actual
1.	13.6	14	2.11	2.03	2.9	2.8	5	5	6.59	6.89
2.	13.8	13	2.03	2	1.9	1.7	7.09	7.64	6.88	6.5
3.	17	17	2.49	2.5	4.1	4.2	4.27	4.04	6.90	6.8
4.	18.8	19.5	1.87	2	4.6	5	4.20	3.9	9.50	9.75
5.	12.3	13	2.73	2.86	1.9	2.3	5.95	5.65	4.29	4.54
6.	14.1	14.1	2.10	2.11	2.4	2.5	5.80	5.64	6.83	6.68
7.	17.3	16.5	2.56	2.53	4.7	4.5	3.05	3.6	6.90	6.52
8.	17.6	18	2.48	2.4	3.6	3.5	5.14	5.14	7.20	7.5

6.3.5 Developing the Empirical Models

The response function can be expressed as:

$$Y = f(V, W, S, N) \dots\dots\dots 6.1$$

Where,

Y - Response parameter i.e. bead geometry and shape relationships (bead width, bead height, bead penetration, WPSF, WRFF).

V - Arc Voltage,

W- Wire feed rate,

S - Travel speed,

N - Contact tube to plate distance

Assuming linear relationship, the possible two factor interactions are taken into consideration, therefore the above expression rewritten as:

$$Y = b_0 + b_1V + b_2W + b_3S + b_4N + b_{12}VW + b_{13}VS + b_{14}VN + b_{23}WS + b_{24}WN + b_{34}SN \dots\dots\dots 6.2$$

After confounding the given empirical model can be expressed as:

$$Y = b_0 + b_1V + b_2W + b_3S + b_4N + b_5(VW + SN) + b_6(VS + WN) + b_7(VN + WS) \dots\dots\dots 6.3$$

A Design matrix for calculating coefficients after confounding was mentioned in Table 3.8 of Chapter 3.

6.3.6 Evaluating the Coefficients of the Polynomials

The significance of each coefficient was tested using ‘t’ test. Here the value of ‘t’ from the standard table is 2.3 for confidence level 95% and degree of freedom is 8.

Table 6.5 shows coefficients of the model and their significance.

Table-6.5: Coefficients of the model and their significance

Parameter	Coefficient	b ₀	b ₁ (V)	b ₂ (W)	b ₃ (S)	b ₄ (N)	b ₅ (VW)	b ₆ (VS)	b ₇ (WS)
Bead Width	value	15.63	0.51	2.11	-0.23	-0.38	0.48	-0.26	0.13
	‘t’ value	55.22	1.80	7.45	0.81	1.34	1.69	0.91	0.45
	significant	Yes	No	Yes	No	No	No	No	No
Bead Height	value	2.30	-0.17	0.05	-0.17	0.13	0.01	-0.06	-0.04
	‘t’ value	60.52	4.47	1.31	4.47	3.42	0.26	1.57	1.05
	significant	Yes	Yes	No	Yes	Yes	No	No	No
Bead Penetration	value	3.31	-0.13	0.98	-0.11	-0.38	0.08	-0.18	-0.06
	‘t’ value	28.29	1.11	8.37	0.94	3.24	0.68	1.53	0.51
	significant	Yes	No	Yes	No	Yes	No	No	No
WPSF	value	5.07	0.50	-0.90	-0.06	0.54	-0.15	0.26	-0.12
	‘t’ value	30.91	3.04	5.48	0.36	3.29	0.91	1.58	0.73
	significant	Yes	Yes	Yes	No	Yes	No	No	No
WRFF	value	6.89	0.71	0.74	0.58	-0.56	0.27	-0.04	0.07
	‘t’ value	49.56	5.10	5.32	4.17	4.02	1.94	0.28	0.50
	significant	Yes	Yes	Yes	Yes	Yes	No	No	No

6.3.7 Evaluating the Significance of Coefficients and Obtaining the Final Model

The design matrix developed was used to determine the coefficients of model, substituting the values of these coefficients in equation 3.3 as mentioned in Chapter 3, we obtain final developed model. Table 6.6 illustrates final developed models for weld bead geometry and shape relationships.

Table-6.6: Final developed models for weld bead geometry and shape relationships

S. No.	Responses	Developed Model
1.	Bead Width	$w = 15.63 + 2.11 W$
2.	Bead Height	$h = 2.30 - 0.17 V - 0.17 S + 0.13 N$
3.	Bead Penetration	$p = 3.31 + 0.98 W - 0.38 N$
4.	WPSF	$WPSF = 5.07 + 0.50 V - 0.90 W + 0.54 N$
5.	WRFF	$WRFF = 6.89 + 0.71 V + 0.74 W + 0.58 S - 0.56 N$

6.3.8 Checking the Adequacy of Empirical Models

The adequacy of the model was determined by ANOVA technique. According to this technique, the F- ratio of the model was compared with the F-ratio from the standard table. The F-ratio from the table for 95% confidence level and 8 degree of freedom is 4.12. When calculated value of F-ratio of model is less than tabulated value for a desired level of confidence then the model is adequate. It was observed that the models developed are adequate within 95% level of confidence. Table 6.7 elaborates model adequacy test for weld bead geometry and shape relationships.

Table-6.7: Model adequacy test for weld bead geometry and shape relationships

Responses	Degree of freedom S_y^2 S_{ad}^2		Variance of optimization S_y^2	Standard deviation of coefficient S_{bj}	Variance of adequacy S_{ad}^2	F-ratio Model F_m	F ratio from table F_t	Whether model significant or not $F_m < F_t$
Bead width	8	3	0.645	0.283	1.993	3.08	4.12	Yes
Bead Height	8	3	0.012	0.038	0.028	2.33	4.12	Yes
Bead penetration	8	3	0.110	0.117	0.406	3.69	4.12	Yes
WPSF	8	3	0.215	0.164	0.661	3.07	4.12	Yes
WRFF	8	3	0.156	0.139	0.507	3.25	4.12	Yes

6.4 Results and Discussions

Experimentation was carried out by using half factorial design to analyse the effects of independent variables such as wire feed rate, arc voltage, travel speed, and contact tube to plate distance on the responses, for instance bead width, bead height, bead penetration, WPSF, and WRFF are shown in Table 6.2.

A linear regression model was suggested to check the adequacy of the model, and for this variance of optimization parameter (S_y^2), variance of adequacy (S_{ad}^2), and standard deviation of coefficient (S_{bj}) were calculated in order to find F value where tabulated F value is 4.12 for the degree of freedom and the confidence interval of 8 and 95 %, respectively. According to this model, if the calculated F-value is less than the tabulated F-value, then the model is significant. It was observed in Tables 6.3 and 6.5 that 't' and 'F' values for given responses were adequate and within the range of defined parameters. Using this model, the final equations are obtained in actual

factors, which are used to forecast the output. These equations are given in Table 6.4. Based on the diagnostics of model adequacy, a scatter plot diagram was plotted in order to test the goodness of fit or model. Figure 6.4 to 6.8 shows a scatter diagram where actual values on the X axis and predicted values on the Y axis are presented. The points closer to the fitted line indicate a good fit model with a narrow confidence interval.

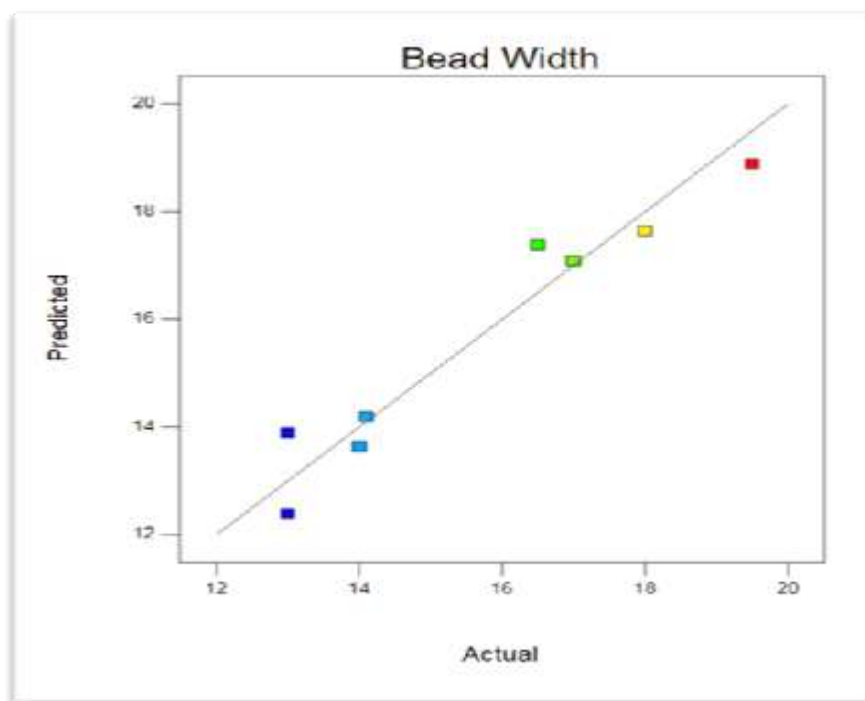


Figure-6.4: Scatter diagram between predicted and actual values of bead width

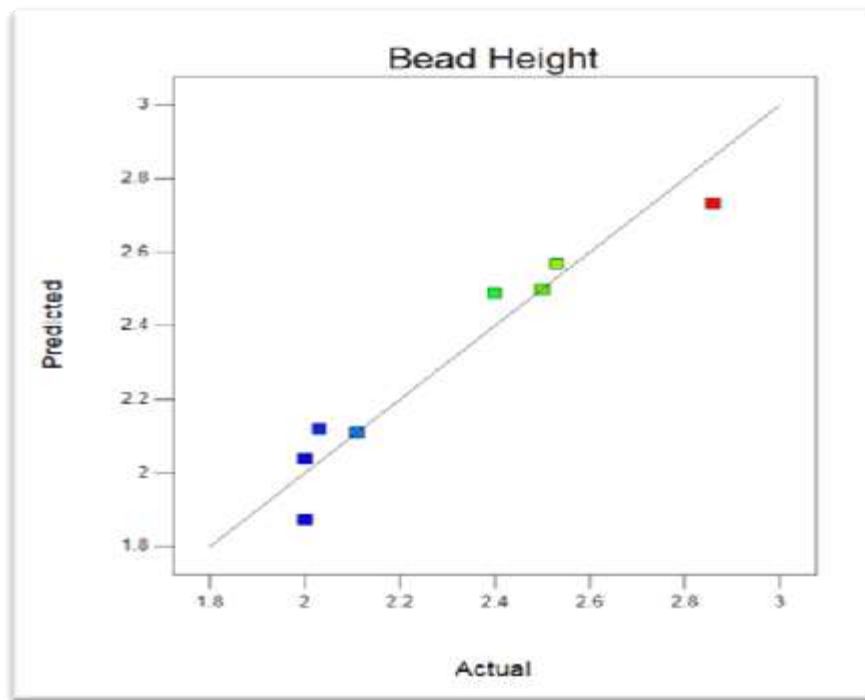


Figure-6.5: Scatter diagram between predicted and actual values of bead height

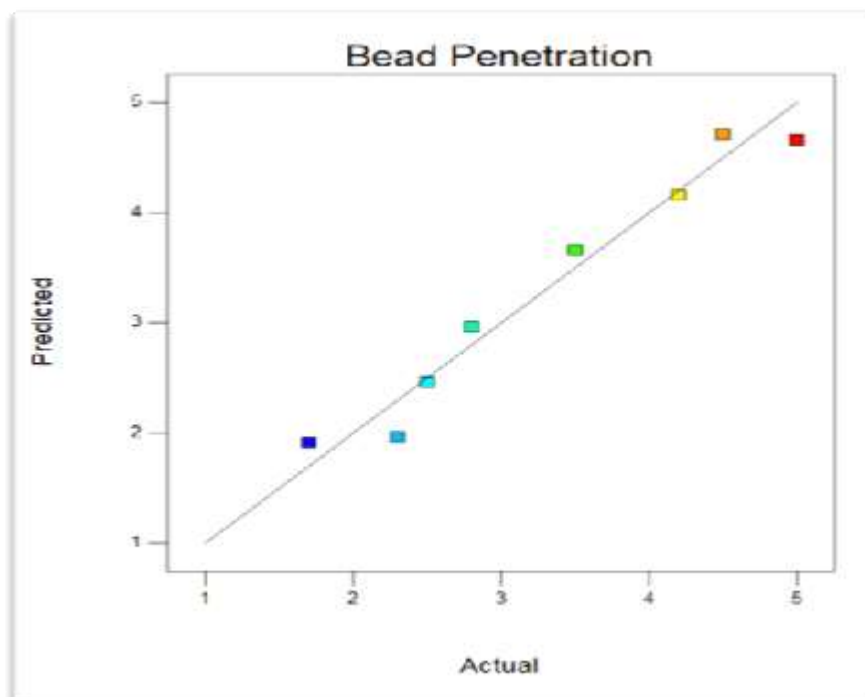


Figure-6.6: Scatter diagram between predicted and actual values of bead penetration

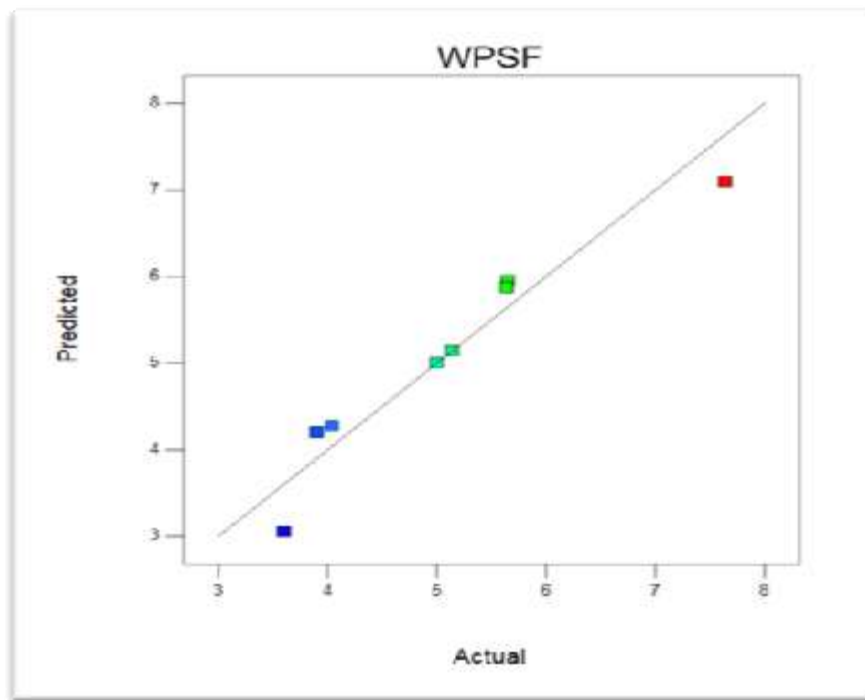


Figure-6.7: Scatter diagram between predicted and actual values of WPSF

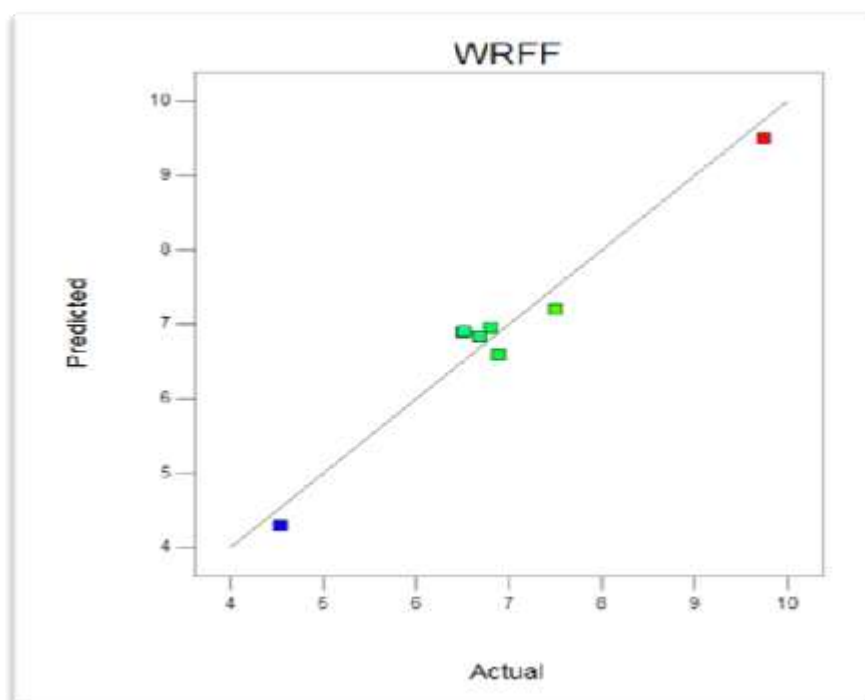


Figure-6.8: Scatter diagram between predicted and actual values of WRFF

6.4.1 Effect of Welding Parameters on Bead Width

The developed model for weld bead width is $w = 15.63 + 2.11W$ and Figure 6.10 shows how wire feed rate affects weld bead width. The developed model and Figure 6.9 clearly show that as the wire feed rate increases from 97 to 156 cm/min, the bead width increases from 13.5 to 17.7 mm. It was observed that the bead width varies directly with the increasing wire feed rate, this can be related to the fact that increasing wire feed rate leads to an increase in welding current, which increases the heat input. Higher the heat input, higher will be the melting rate of base metal, and therefore, the molten weld pool expands and leads to increase in bead width.

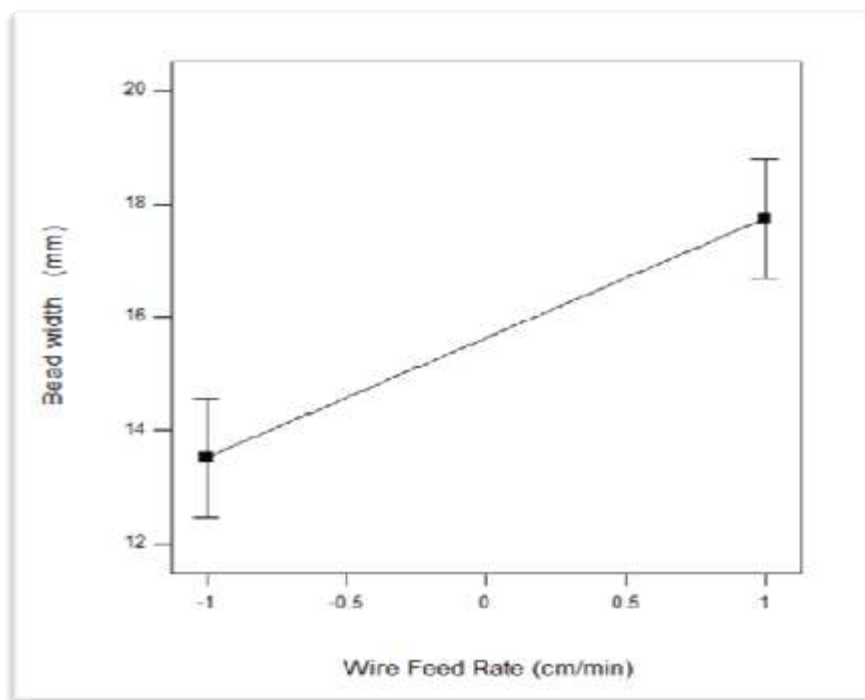


Figure-6.9: Effect of wire feed rate on bead width

6.4.2 Effect of Welding Parameters on Bead Height

The developed model for weld bead height is $h = 2.30 - 0.17V - 0.17S + 0.13N$, and Figures 6.10, 6.11, and 6.12 represent the effects of arc voltage, travel speed, and contact tube to plate distance on weld bead height, respectively. As mentioned in the developed model, it is clearly mentioned in Figure 6.10 that bead height decreases from 2.48 to 2.12 mm with an increase in arc voltage from 25 to 40 volts. The decreasing trend of bead height with arc voltage is due to the fact that as the arc voltage increases, the arc length increases, which leads to an increase in the spread of the arc. As a result, the arc strikes a larger surface area and therefore a decrease in weld bead height. Figure 6.11 shows that bead height decreases from 2.47 to 2.13 mm with an increase in travel speed from 32 to 40 cm/min. This decreasing trend is attributed to the fact that with the melting rate of filler wire is constant, with an increase in travel speed; the same amount of molten metal is spread over a longer length, which tends to reduce the bead height. In Figure 6.12, it was observed that weld bead height increased from 2.34 to 2.61 mm with an increase in contact tube to plate distance from 18 to 23 mm. The increasing trend of bead height with contact tube to plate distance occurs is mainly due to the fact that an increase in contact tube to plate distance results in an increase in height due to more spread of arc above the weld surface. This arc spread reduces to a minimum as the contact tube to plate distance decreases and therefore bead height increases.

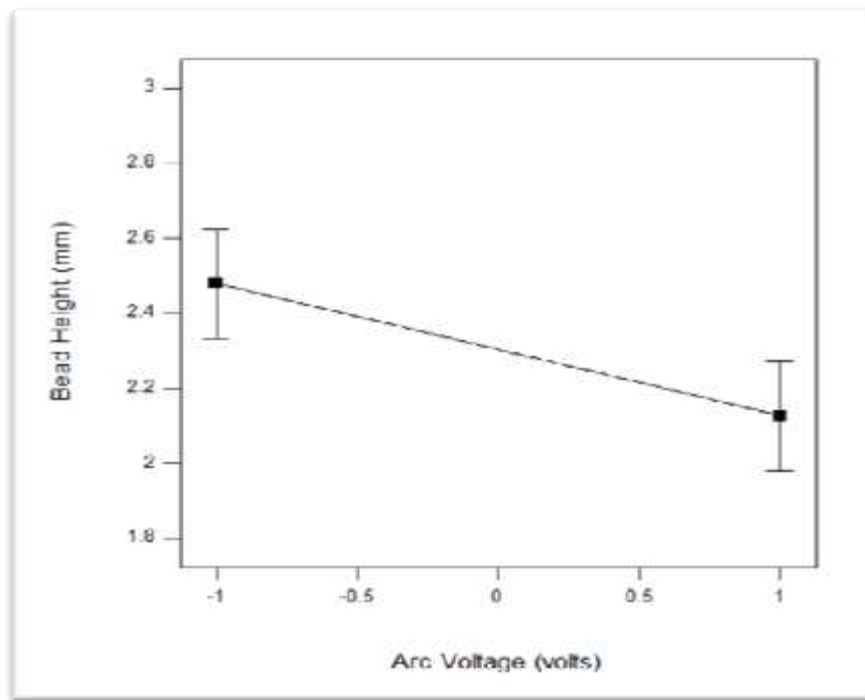


Figure-6.10: Effect of arc voltage on bead height

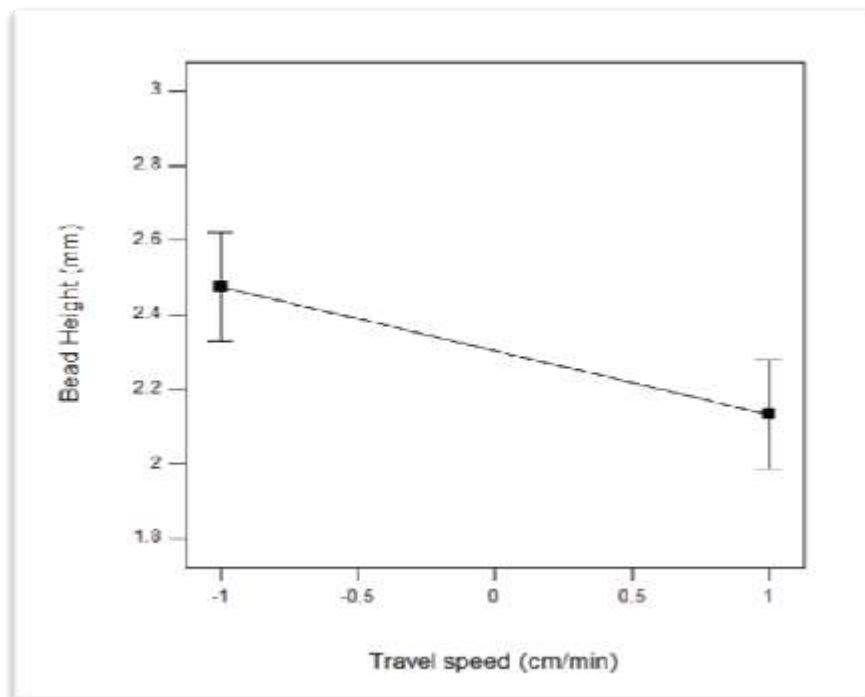


Figure-6.11: Effect of travel speed on bead height

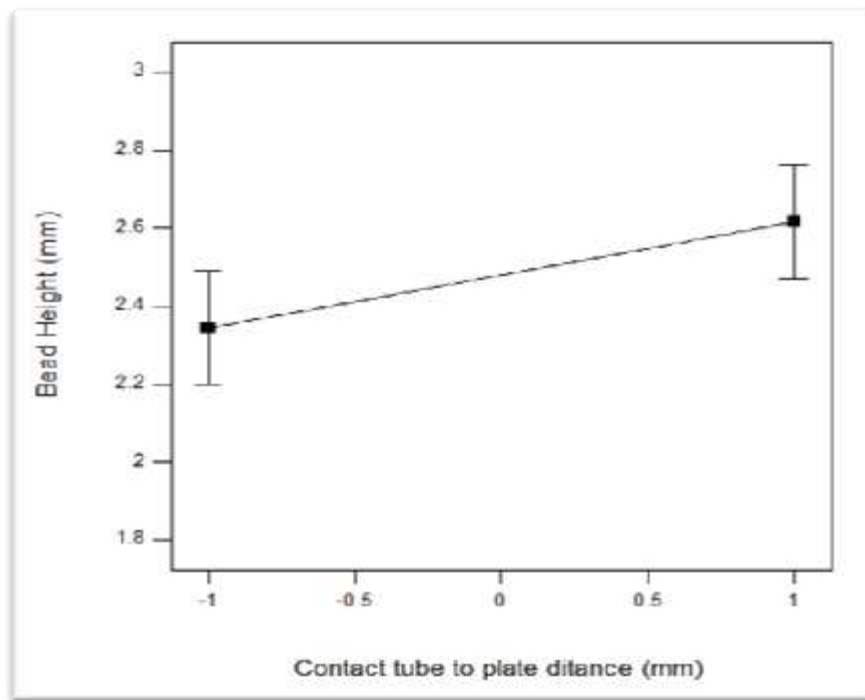


Figure-6.12: Effect of contact tube to plate distance on bead height

6.4.3 Effect of Welding Parameters on Bead Penetration

The developed model for weld bead penetration is $p = 3.31 + 0.98W - 0.38N$ and Figures 6.13 and 6.14 show the effects of wire feed rate and contact tube to plate distance on bead penetration. In Figure 6.13, it was observed that bead penetration increased from 2.3 to 4.3 mm with an increase in wire feed rate from 97 to 156 cm/min. This is due to the fact that the increase in wire feed rate causes an increase in welding current, which increases the heat input. As a result, there is an increase in metal deposition on the base metal, causing an increase in weld bead penetration. In Figure 6.14, the decreasing trend of bead penetration from 3.8 to 3 mm with increasing contact tube to plate distance from 18 to 23 mm was attributed to the fact with rising value of contact tube to plate distance, there is more resistance created and the amperage drops due to this there will be porosity and spatter thus results in shallow penetration.

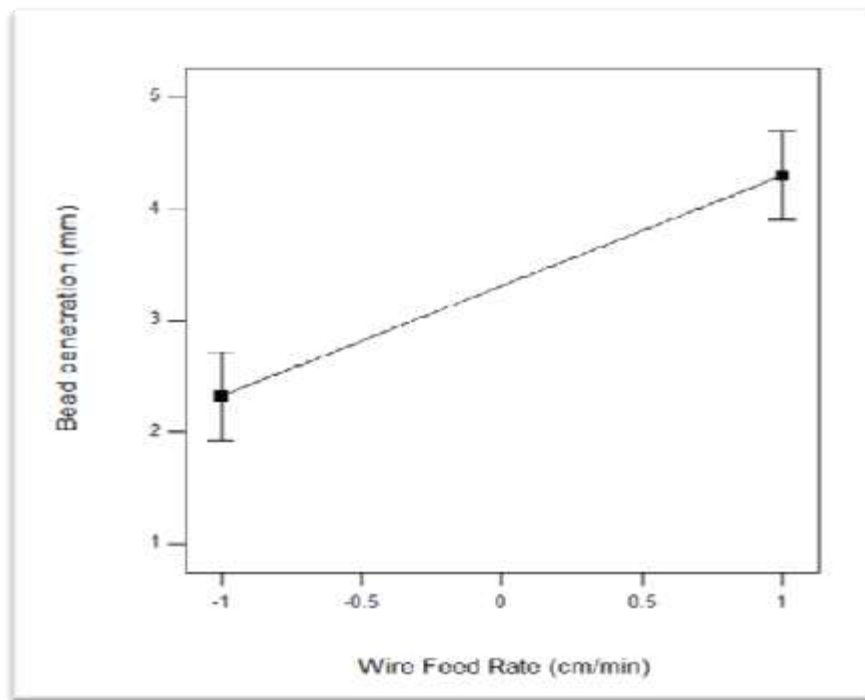


Figure-6.13: Effect of wire feed rate on bead penetration

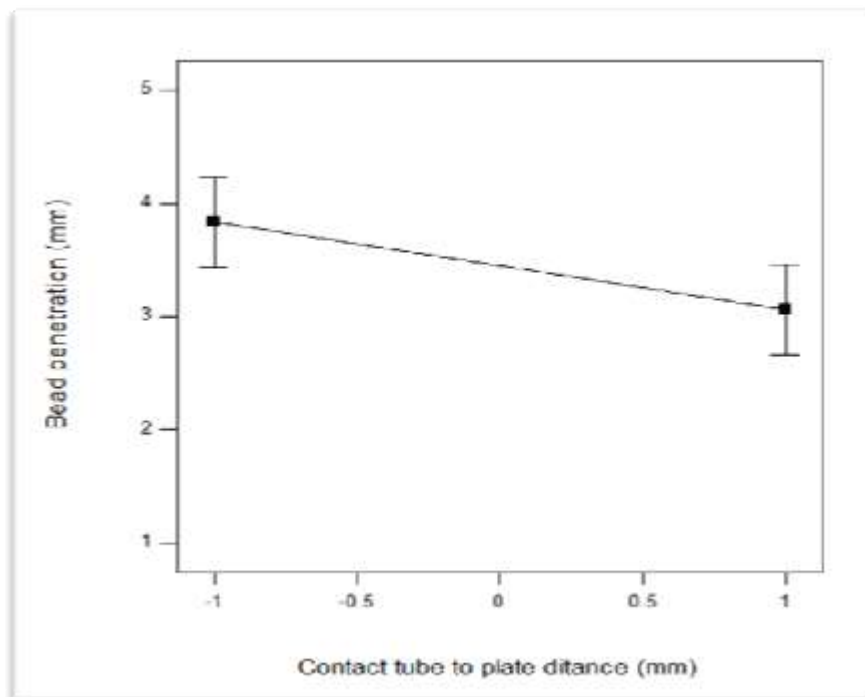


Figure-6.14: Effect of Contact tube to plate distance on bead penetration

6.4.4 Effect of Welding Parameters on Weld Penetration Shape Factor

The empirical model developed for weld penetration shape factor $WPSF = 5.07 + 0.50 V - 0.90 W + 0.54 N$. From this model and Figure 6.15, clearly indicates that weld penetration shape factor changes from 3.98 to 4.99 with an arc voltage varying from 25 to 40 volts. With the increase in arc voltage, there is an increase in bead width, and as this bead width increases, weld penetration shape factor also increases. Figure 6.16 shows that weld penetration shape factor reduces from 5.98 to 4.17 with wire feed rate varying from 97 to 156 cm/min. This decreasing trend is attributed to the fact that when there is a rise in wire feed rate, it causes welding current to increase. As a result, penetration increases, leading to a decrease in weld penetration shape factor (weld penetration shape factor is the ratio of bead width to bead penetration, i.e., w/p). As mentioned in Figure 6.17, there is an increase in weld penetration shape factor from 4.53 to 5.61 with an increase in contact tube to plate distance from 18 to 23 mm. As explained earlier, it was observed that penetration increases with the decrease in contact tube to plate distance and weld penetration shape factor increases with the decrease in penetration. Therefore, weld penetration shape factor varies directly with the contact tube to plate distance.

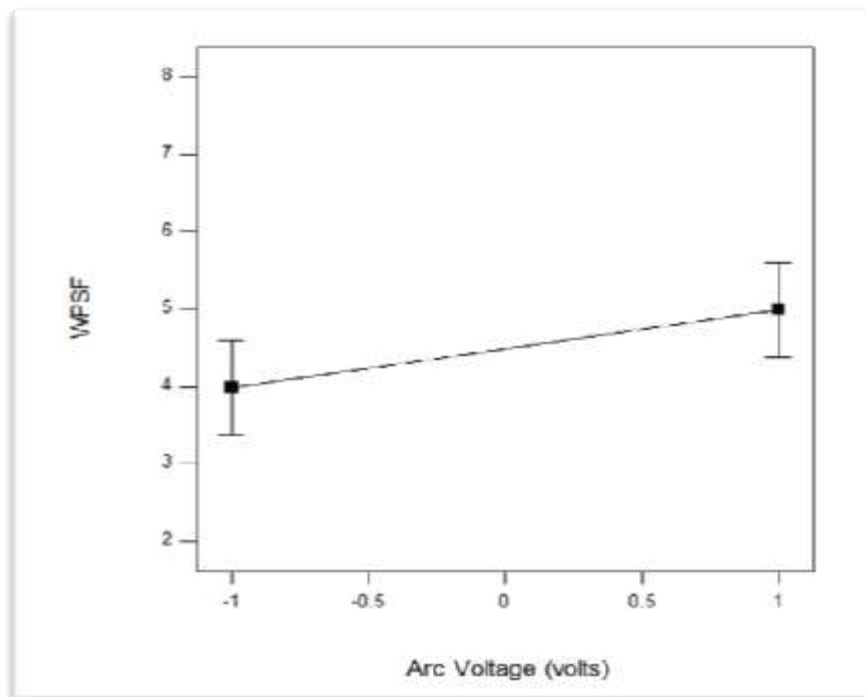


Figure-6.15: Effect of arc voltage on WPSF

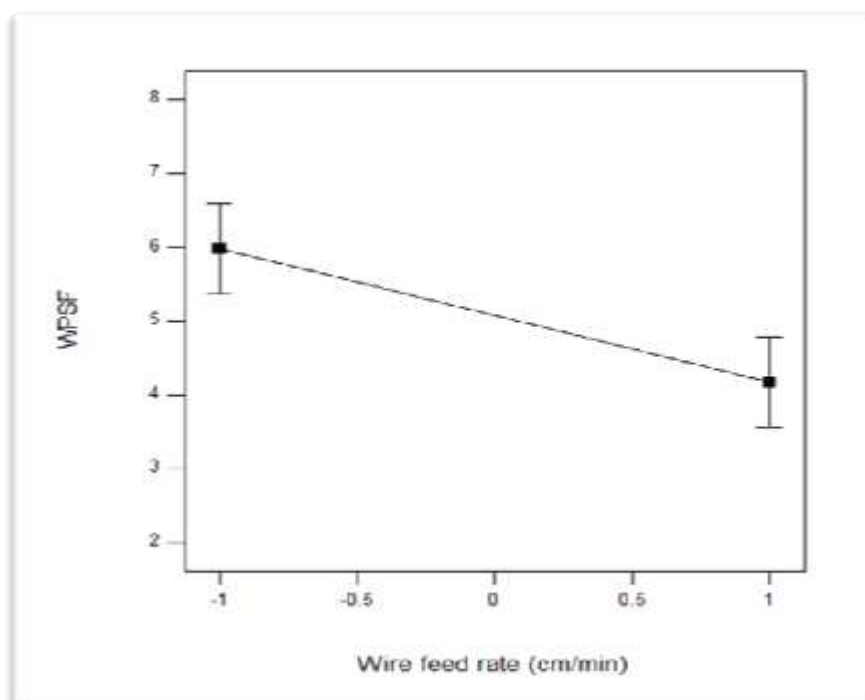


Figure-6.16: Effect of wire feed rate on WPSF

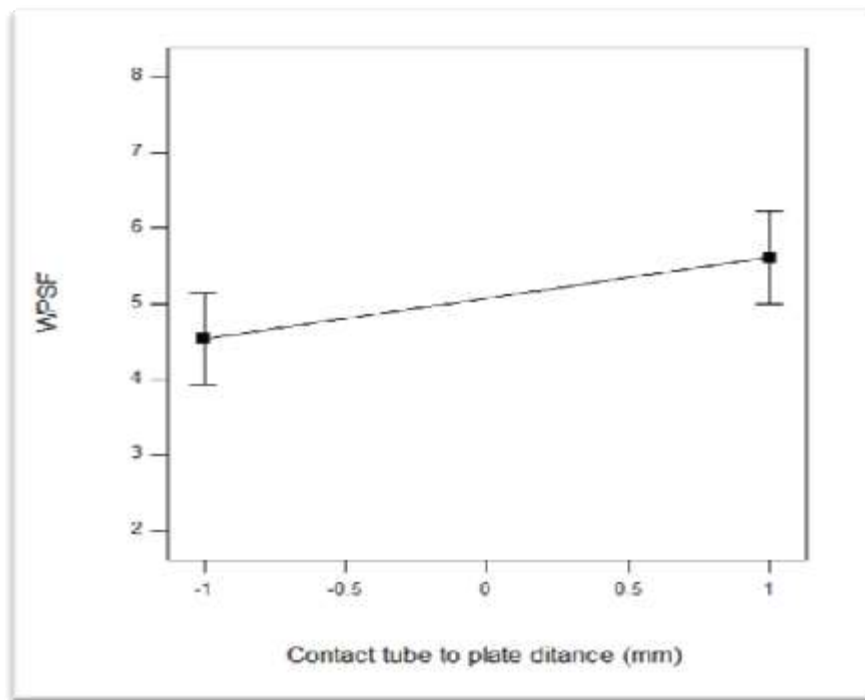


Figure-6.17: Effect of contact tube to plate distance on WPSF

6.4.5 Effect of Welding Parameters on Weld Reinforcement form Factor

The developed model for weld reinforcement form factor is $WRFF = 6.89 + 0.71 V + 0.74 W + 0.58 S - 0.56 N$. Figures 6.18 to 6.21 indicates the effect of welding parameters on weld reinforcement form factor. It is clearly evident from Figure 6.18 that as weld reinforcement form factor increases from 6.18 to 7.60, there is an increase in arc voltage from 25 to 40 volts. Figure 6.19 shows that increasing the wire feed rate from 97 to 156 cm/min increases the weld reinforcement form factor from 6.15 to 7.64. This is due to the fact that as wire feed rate increases, it causes an increase in bead width, which is directly proportional to weld reinforcement form factor as w/h . Figure 6.20 shows that weld reinforcement form factor increases from 6.31 to 7.48 with travel speed varying from 32 to 40 cm/min. This is because bead height is inversely proportional to the travel speed, which leads to increase in weld

reinforcement form factor. Figure 6.21 shows that weld reinforcement form factor decreases from 6.75 to 5.62 with the increase in contact tube to plate distance from 18 to 23 mm. As mentioned above, bead height varies directly with the contact tube to plate distance, and therefore it leads to a decrease in weld reinforcement form factor.

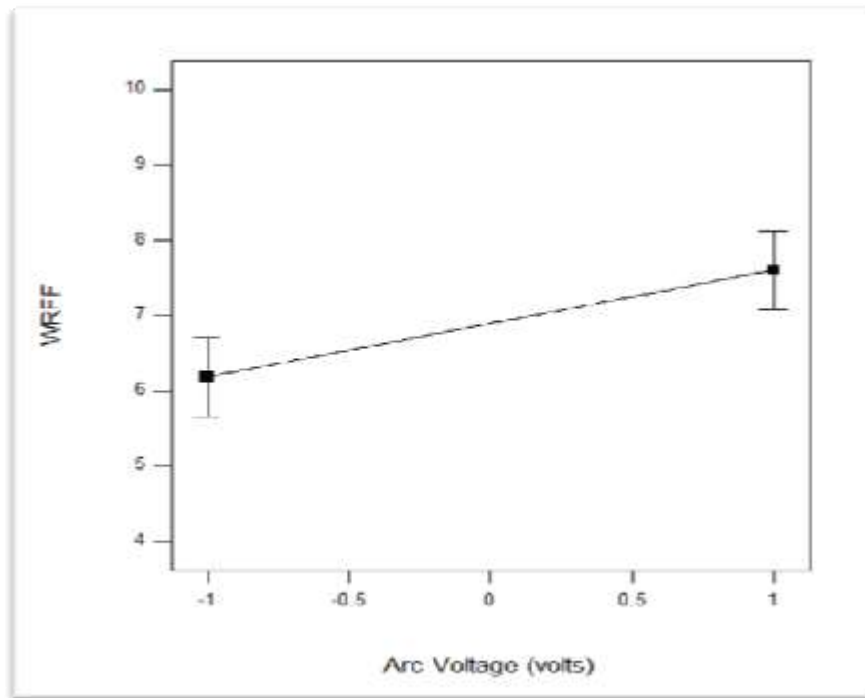


Figure-6.18: Effect of arc voltage on WRFF

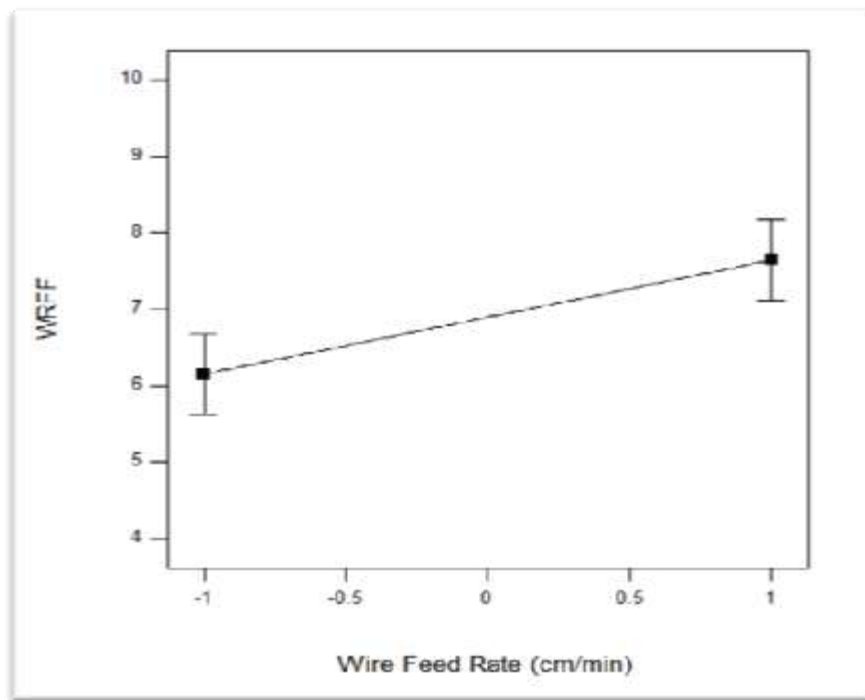


Figure-6.19: Effect of wire feed rate on WRFF

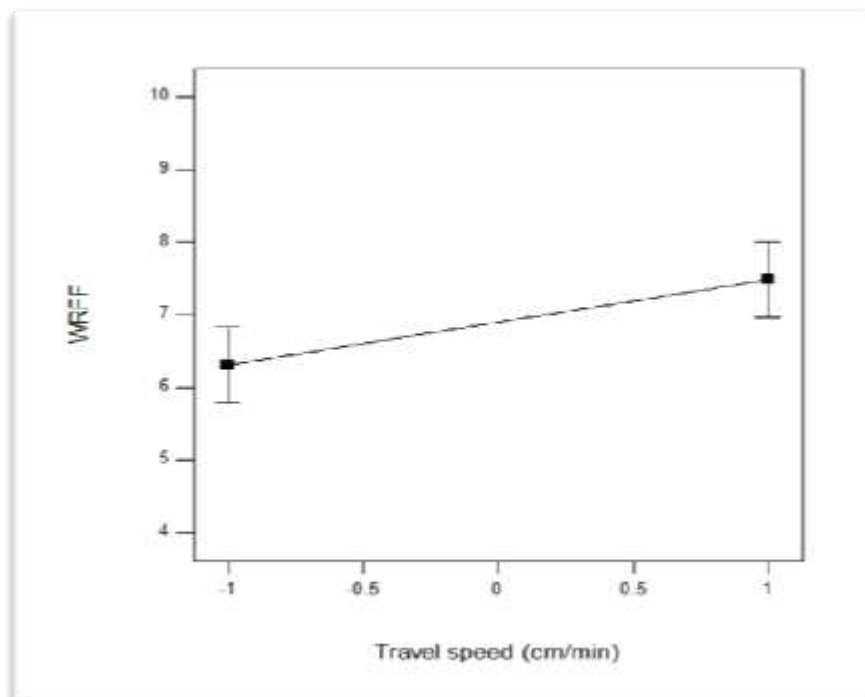


Figure-6.20: Effect of travel speed on WRFF

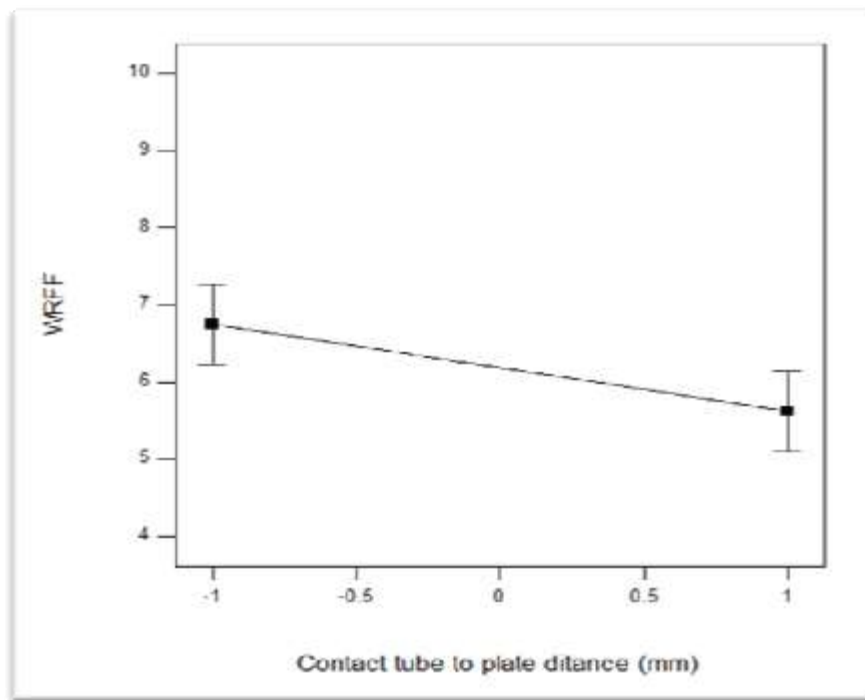


Figure-6.21: Effect of Contact tube to plate distance on WRFF

6.5 Summary

1. Two level half factorial Technique can be suitably applied for conducting the experiments and further ANOVA applied for analysing the effect of welding parameters on weld bead geometry and shape relationship.
2. Predicted values were found to be in fair agreement with actual values of bead width, bead height, and bead penetration, weld penetration shape factor, and weld reinforcement form factor.
3. Recycled slag proves reliable for obtaining suitable weld bead geometry
4. Empirical models can be easily employed and effective in acquiring desirable weld bead characteristics.

5. Responses such as bead width, bead penetration and weld reinforcement form factor increased with the increase in wire feed rate.
6. Bead height is inversely proportional to the travel speed whereas weld reinforcement form factor is directly proportional to the travel speed.
7. Bead height, weld penetration shape factor increased with an increase in contact tube to plate distance whereas bead penetration and weld reinforcement form factor decreased with an increase in contact tube to plate distance.

METALLURGICAL STUDIES

7.1 Introduction

Welding is a significant metallurgical process that involves melting and solidification, surface phenomena, and gas metal and slag-metal reactions, among other things. These processes occur at a faster rate during welding in comparison with metal fabrication, casting, or heat treatment. A greater understanding of weldments is essential for this purpose. The size, form, and pattern of distribution of micro-constituents and inclusions determine the weldment's properties. Better mechanical properties arise from finer and more evenly distributed inclusions (Stuck et al., 1972; Jenney and Brien, 2001).

7.2 Microstructure of Mild Steel

Mild steel is an iron and carbon alloy with iron content as 98 percent, carbon content ranging from 0.05 to 0.30 percent, manganese content ranging from 0.4 to 0.7 percent, silicon content ranging from 0.1 to 0.5 percent, and traces of other elements such as sulphur, phosphorus, chromium, cobalt, molybdenum, nickel etc. The Fe-C equilibrium diagram makes it simple to explain the microstructural changes that occur in mild steel. The iron phase diagram is depicted in Figure 7.1.

As shown in Figure 7.1, iron exists in various of allotropic forms. Various allotropes of iron are as follows:

a) **Alpha Ferrite:** A solid carbon-iron solution. At 0°C, its pure iron with a BCC crystal structure. Carbon has a maximum solubility in iron of 0.02 percent at 723°C. At 0°C, the solubility drops to 0.008 percent. The carbon atoms are properly positioned in the crystal interstices (Jenney and Brien, 2001).

b) **Austenite:** An austenite is a solid carbon-iron solution. It has an FCC crystal structure and high carbon solubility as compared to ferrite. Solubility increases to a maximum of 2% carbon in solid solution on the other hand ferrite dissolves only 0.025% (Jenney and Brien, 2001). At 723°C, the solubility drops to 0.8%. The carbon atoms are dissolved interstitially. The hardening of steel lies in between austenite and ferrite with different solubility .

c) **Cementite:** Cementite is an intermetallic compound composed of 6.67% carbon and 93.33% iron. Cementite, iron carbides present in pearlite or as massive carbides in high carbon steels (Jenney and Brien, 2001). Each unit cell of cementite has twelve iron and four carbon atoms. It has an orthorhombic crystal structure, which makes it a hard and brittle compound. When the carbon solubility limit in ferrite is increased, cementite (Fe_3C) is formed at the bottom. As shown in Figure 7.1, Fe_3C has a gamma phase between 727 and 1150°C. Cementite is very hard and brittle; its presence improves the strength of steel.

d) **Delta Ferrite:** Delta ferrite has BCC crystal structure with a solid carbon-iron mixture. The maximum solubility of C in Fe is 0.09 percent at 1493°C. When austenite transforms into ferrite and cementite, it reaches the eutectoid point, which is shown in Figure 7.1. This eutectoid reaction can be represented by the symbol.

When the solid austenite phase cools, it transforms into iron and cementite. Steel is differentiated according to the carbon percentage in it. Hypo eutectoid steel is mild steel that has a maximum carbon percentage of 0.3%. Figure 7.2 depicts the phase changes that occur in mild steel when it cools from a higher temperature to room temperature.

At approximately 875°C, at point c, the microstructure will be fully comprised of the gamma phase, as depicted schematically in Figure 7.2. Both of these phases will coexist in the given microstructure while cooling at point d, around 775 °C, which is the alpha-gamma phase zone. The majority of the tiny alpha particles will form along the original gamma grain boundaries. Cooling from point d to e, just above the eutectoid point but still in the alpha-gamma zone, will result in an increased fraction of the alpha phase and a microstructure similar to that seen in Figure 7.2.

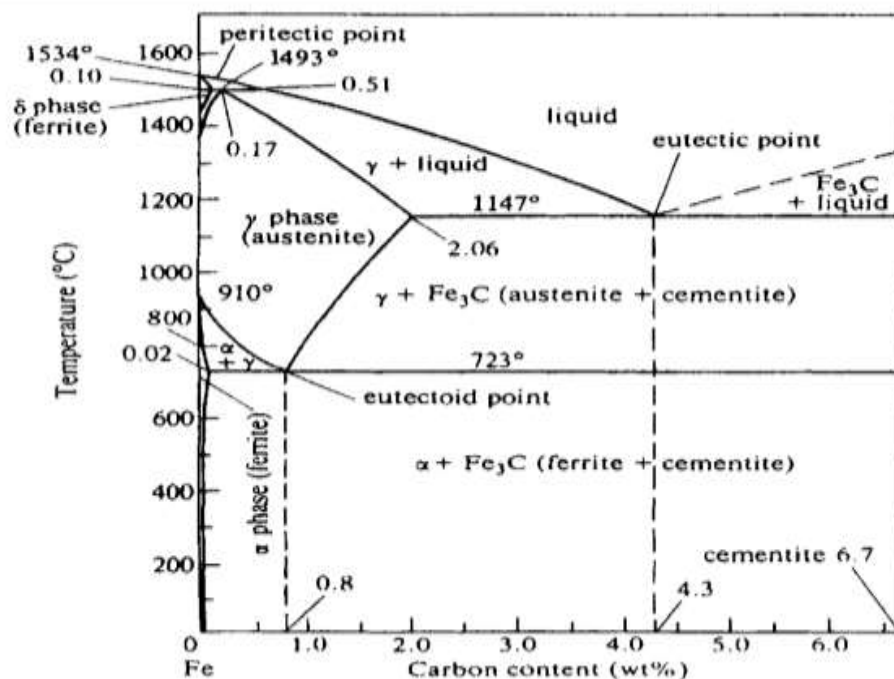


Figure-7.1: Iron Carbon phase diagram (Lancaster, 1998)

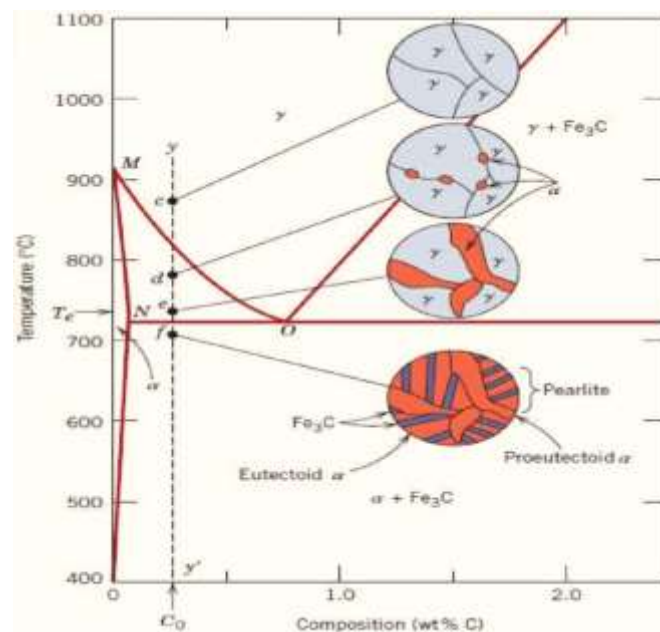


Figure-7.2: Microstructural changes during cooling of mild steel (Haidemenopoulos, 2018)

As the temperature is reduced to slightly below the eutectoid, to point f, all of the gamma phase that was at temperature T_e (and had the eutectoid composition) will be converted to pearlite via the eutectoid reaction. At crossing the eutectoid temperature, there will be little change in the alpha phase that existed at point e—it will generally be present as a continuous matrix phase encircling the isolated pearlite colonies. The microstructure at point f will be depicted in Figure 7.2 as the relevant schematic diagram. As a result, the ferrite phase will be present in both the pearlite and the alpha and gamma phase regions as the pearlite cools. The ferrite found in pearlite is known as eutectoid ferrite, whereas the ferrite formed above is known as pro-eutectoid (meaning pre-or before eutectoid) ferrite. Joarder et al. (1991) observed that varying cooling rate in weld metal results in wide range of microstructure such as periodic pearlite, grain boundary ferrite with pearlite and side plate boundary with cementite.

Figure 7.3 shows Optical micrograph of (a) Base metal; (b) grain refined HAZ; (c) grain coarsened HAZ; (d) weld metal.

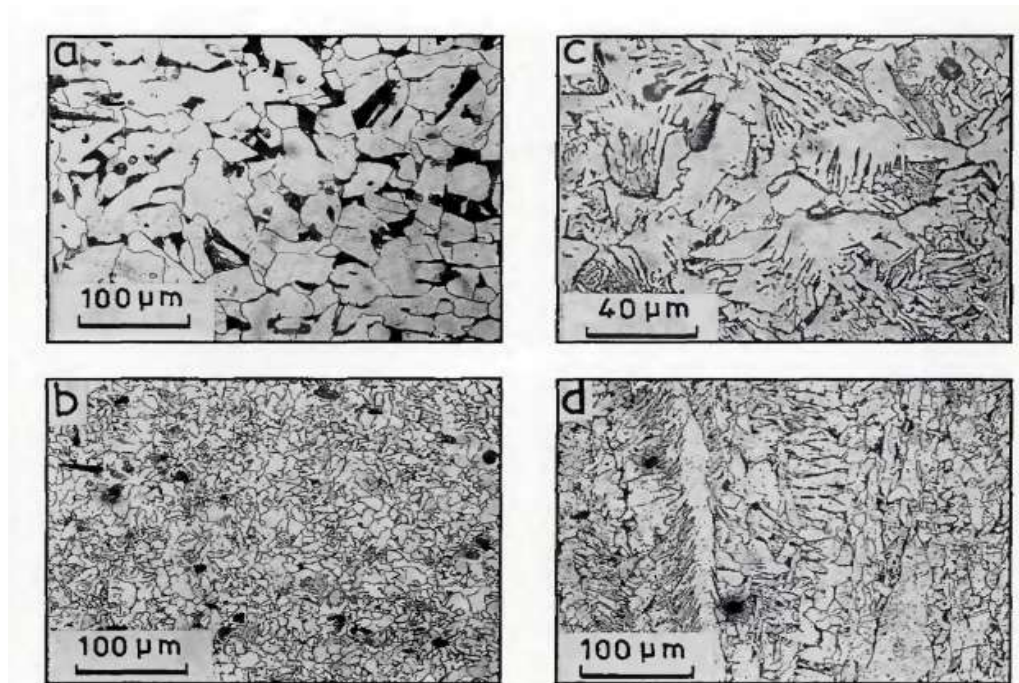


Figure-7.3: Optical micrograph of (a) Base metal; (b) grain refined HAZ; (c) grain coarsened HAZ; (d) weld metal (Joarder et al., 1991)

Pearlite is a single grain composed of alternate strips of ferrite and cementite. The distance between the plates and their thickness are determined by the rate at which the different materials cool down; fast cooling results in thin plates that are close together, whereas slow cooling results in a much coarser structure with less toughness. A fully pearlite structure forms at 0.76 percent carbon. Addition of more carbon content will result in the formation of cementite at the grain boundaries, which reduces toughness and increase the hardness of the steel.

Martensite is formed when steel is rapidly cooled from austenite and the face-centered cubic structure changes to pearlite. As a result, a deformed structure with fine needles is formed. There is no partial transformation associated with martensite; it either

exists or not. However, martensite will form only in regions that cool quickly; in a thicker section, it will only exist upto a particular depth, and it forms in small pockets if the shape is complex. The martensite hardness is primarily determined by its carbon percentage; its generally very high unless the carbon level is extremely low.

7.3 Weld Pool Solidification

The majority of what we know about weld pool solidification comes from freezing castings, ingots, and single crystals at lower temperature gradients and slower growth rates. As a result, significant parameters are used in defining microstructures in casting, like growth rate (R), temperature gradient (G), cooling rate, and alloy composition. These parameters also influence the formation of microstructures in welds. However, the physical reactions that happens because of the interaction of the heat source and the metal during welding include melting, heat and fluid flow, vaporisation, gas dissolution, solidification, subsequent solid-state transformation, and stresses. These processes and their interactions have a significant impact on weld pool solidification and microstructure. When the molten pool is moved through the material, the growth rate and temperature gradient changes significantly the weld pool. The growth rate increases as the weld centreline approaches, while the temperature gradient decreases. The growth rate is slowest at the fusion line, where the temperature gradient is steepest. As a result, the microstructure that forms varies significantly from the edge to the centreline of the weld. Weld pool solidification happens frequently and spontaneously in welds due to epitaxial growth on partially melted grains. Because weld metal solidification occurs spontaneously by epitaxial growth of partially melted grains in the base metal, the weld zone grain structure is

mostly governed by the base metal grain structure and the welding conditions. Crystallographic effects influence grain growth by promoting growth along specific crystallographic directions. As a result, among the randomly oriented grains in a polycrystalline specimen, those grains with one of their easy growth crystallographic axes roughly aligned with the heat-flow direction will grow at the cost of their neighbouring least favourable oriented grains. This is referred to as "competitive growth." This will induce a coarse grain structure in the absence of further nucleation. Low values of $G/(R)^{1/2}$ indicate as higher chances of constitutional super cooling thus promoting the dendritic mode of solidification. Whereas steep temperature gradients in the liquid and slow growth rates favour cellular growth (Kou, 2003). Figure 7.4 shows effect of temperature gradient, grain growth rate and cooling rate on solidification.

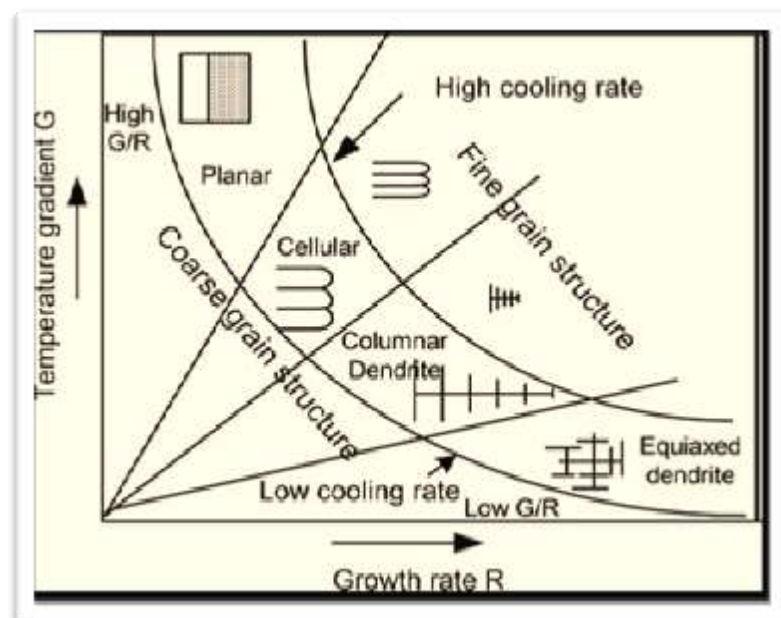


Figure-7.4: Effect of temperature gradient, grain growth rate and cooling rate on solidification (Kou, 2003)

7.4 Welding Zones

The heat affected zone (HAZ) is defined as the zone between the interface of the deposited weld metal and the base metal far enough that any phase change occurs.

The heat affected zone (HAZ) is the area of a base material, either metal or thermoplastic, where the microstructure and characteristics have been altered by welding or heat-intensive cutting processes. With the help of etching and hardness profiles microstructure can be observed in weldments (Jenney and Brien, 2001)

Figure 7.5 shows different subzones of a fusion zone. The transition from the weld interface to the termination of the sensitising temperature in the base metal is caused by welding heat and followed by re-cooling. The extent and magnitude of property change are mainly determined by the base material, the weld filler metal, and the amount and concentration of heat input by the welding process. HAZ is a part of the weld since it affects the service life of the weld. In many welds, HAZ is the most crucial part. For instance, if you welded hardened steel, HAZ might harden to an unfavourable level. If one examines the macrostructure of the weld zone closely, three separate zones can be identified.

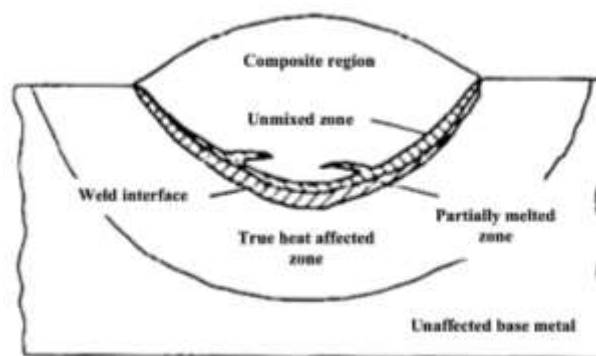


Figure-7.5: Different subzones of a fusion zone (Sinha, 2003)

7.4.1 Composite Zone

In this zone, base metal is melted by filler metal which is in a superheated state. After melting, it completely mix with the filler metal and forms an alloy having composition intermediate between the base metal and that of filler metal.

7.4.2 Unimixed Zone

This zone forms a laminar flow molten boundary layer outside the composite region. The composition of the metal in this region is identical to that of base metal apart from few changes which occurs due to diffusion.

7.4.3 Partially Melted Zone

A weld metal zone develops as the weld metal solidifies from its molten state. This is a mixture of parent metal, electrode metal, and filler metal; the ratio depends on the welding technique and the thickness of the joint plate. The weld metal zone is a cast metal with a specific composition of a mixture that has been cooled; its microstructure indicates the rate of cooling in the weld. A martensitic structure in the weld suggests a relatively high cooling rate depending on the chemical composition; fine pearlite and coarse pearlite reveal a comparatively low cooling rate. The first metal solidifies epitaxial upon the solid grains of the base metal from the molten weld pool. The weld solidifies into a cellular or dendritic growth pattern depending on the composition and solidification rate. Both modes cause alloying element segregation, and as a result, the weld metal is less homogeneous on the micro level than the base metal and thus

cannot be expected to have the same properties as the wrought parent metal unless the filler metal and the parent metal have similar characteristics.

7.4.4 True Heat Affected Zone

It is comprised of parent metal that is heated to very high temperatures without melting for a long period of time to cause grain growth and mechanical and microstructural features to develop by welding heat. The HAZ is subjected to a complicated thermal cycle that involves temperatures ranging from the melting range of the steel to significantly lower temperatures. HAZ is often made up of a range of microstructures. These structures can range from very narrow regions of hard martensitic to coarse pearlitic structures. As a result, the HAZ is the weakest zone in the weld. The HAZ in SAW is divided into three subzones.

7.4.5 Unaffected Base Metal

The base metal is the part of the workpiece that has not been metallurgically altered. Despite being metallurgically identical, the unaffected parent metal as well as the entire weld joint is likely to have considerable residual transverse and longitudinal shrinkage stresses, depending on the degree of constraint applied to the weld.

7.5 Experimental Procedure

The beads-on-plate were deposited using pure slag, fresh flux, and recycled slag in combination with EH 14 wire. The chemical composition of the base plate and filler wire was discussed in Chapter 3 (Table 3.1). After removing the slag from the weld bead, specimens were taken from the centre of the plate and processed using standard

metallurgical processes for micro-hardness surveys and metallurgical investigations of the weld metal. The specimens were etched using a 2% nital solution. Micrographs of the weld metal were taken at 100X magnification for metallurgical research.

A micro-hardness study was performed on a cross section of weld beads deposited with pure slag, fresh flux, and recycled slag, in that order. The micro-hardness of a weld bead was measured at intervals of 0.5 mm along a downward vertical line beginning from the top of the bead and ending 1 mm from the top of the bead

7.6 Results and Discussions

7.6.1 Microstructure Investigations

Figures 7.6 to 7.11 shows the micrographs of base metal; weld metal prepared using pure slag, recycled slag, and fresh flux. Here, Figure 7.6 depicts the base metal's microstructure, which shows a normal ferrite-pearlite structure in mild steel with 0.197 percent carbon. Figure 7.6 clearly shows that the base metal is made up of ferrite and pearlite structures. The microstructure of weld metal deposited with pure slag is shown in Figure 7.7. According to the findings, there is a formation of columnar grains with grain boundary ferrite and polygonal ferrite. The microstructure appears to fit (a) chemical analysis, which indicates low percentages of carbon, manganese and silicon; (b) low tensile and yield strength; and (c) low hardness values. The low carbon content of 0.108 % can be related to the substantially low volume fraction of grain boundary ferrite and polygonal ferrite.

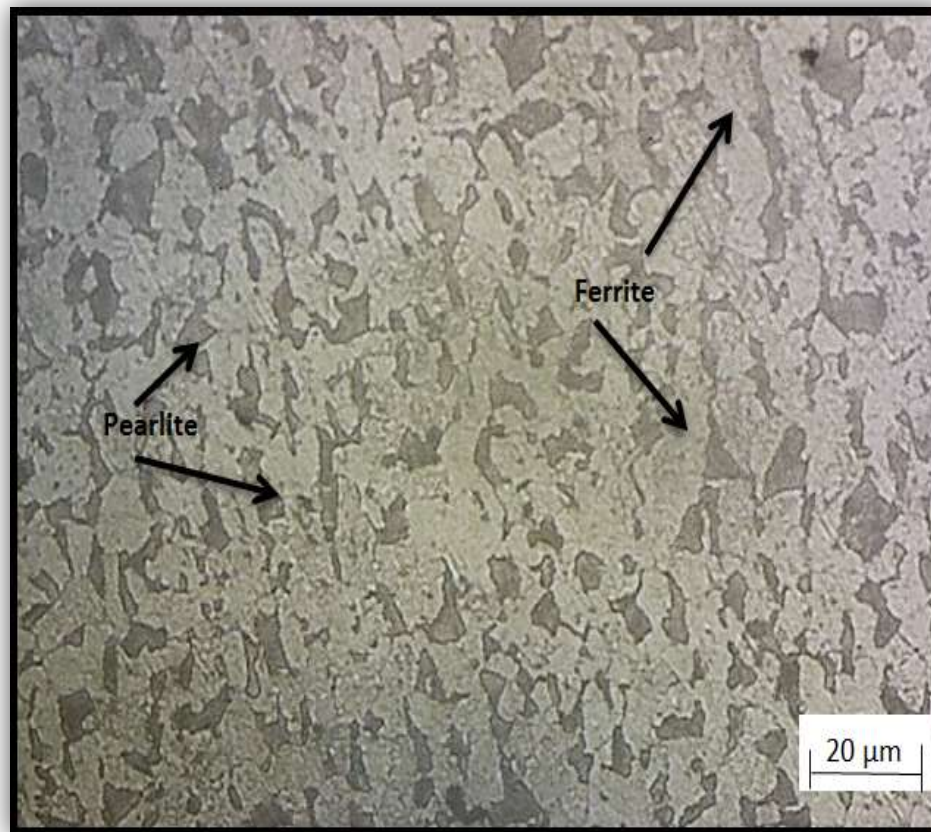


Figure-7.6: Microstructure of base metal

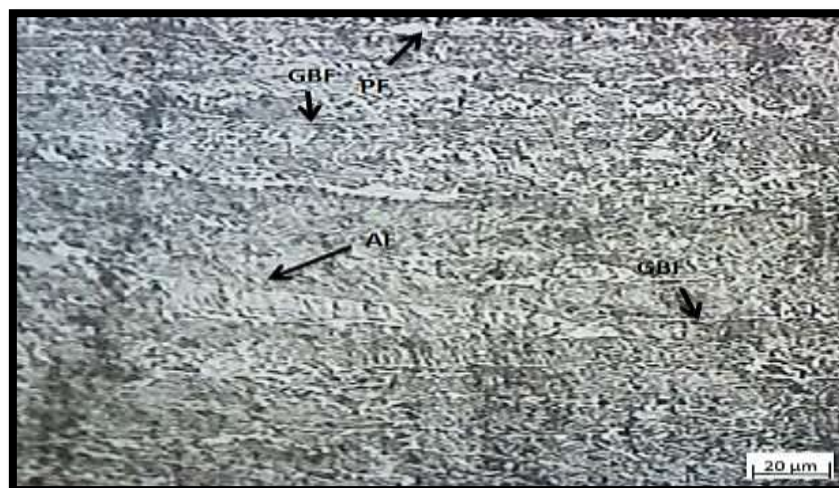


Figure-7.7: Microstructure of weld metal deposited with pure slag

(AF-acicular ferrite, GBF-grain boundary ferrite, PF-polygonal ferrite)

Figure 7.8 depicts the microstructure of weld metal prepared using recycled slag. The grain boundary ferrite, as well as the crystallite size within columnar grains, is observed to be reduced. Also, at the expense of grain boundary ferrite, the amount of acicular ferrite is enhanced. The increase in carbon content (0.089 %) and manganese content (1.101 %) of the weld metal can be attributed to the growing tendency of acicular ferrite. The findings are consistent with those of Gunaraj et al. (2002) and Kanjilal et al. (2005). Furthermore, it was discovered that weld metal prepared using recycled slag had higher tensile and yield strength, owing to increase in carbon and manganese concentration in the weld metal.



Figure-7.8: Microstructure of weld metal deposited with recycled slag

(AF-acicular ferrite, GBF-grain boundary ferrite, PF-polygonal ferrite)

The microstructure of a weld deposited with fresh flux and EH 14 filler wire is shown in Figure 7.9. As a result of the findings, it was established that the microstructure produced by recycled slag is comparable to that produced by virgin flux. The

microstructure at the fusion boundary of a weld formed with pure slag and recycled slag, respectively, as mentioned in Figures 7.10 and 7.11.

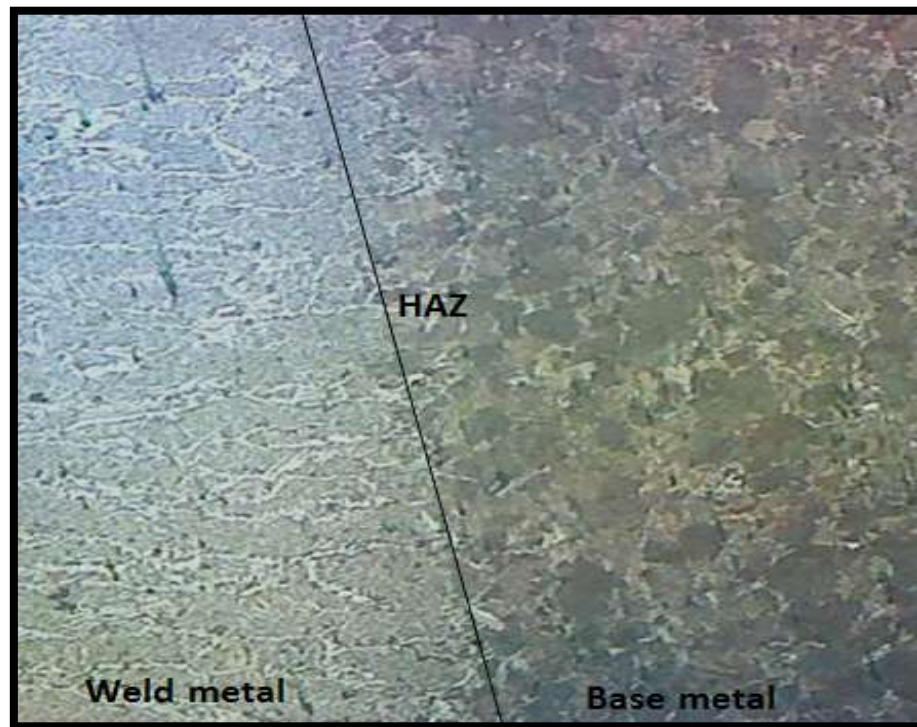


Figure-7.9: Microstructure of weld metal deposited with fresh flux

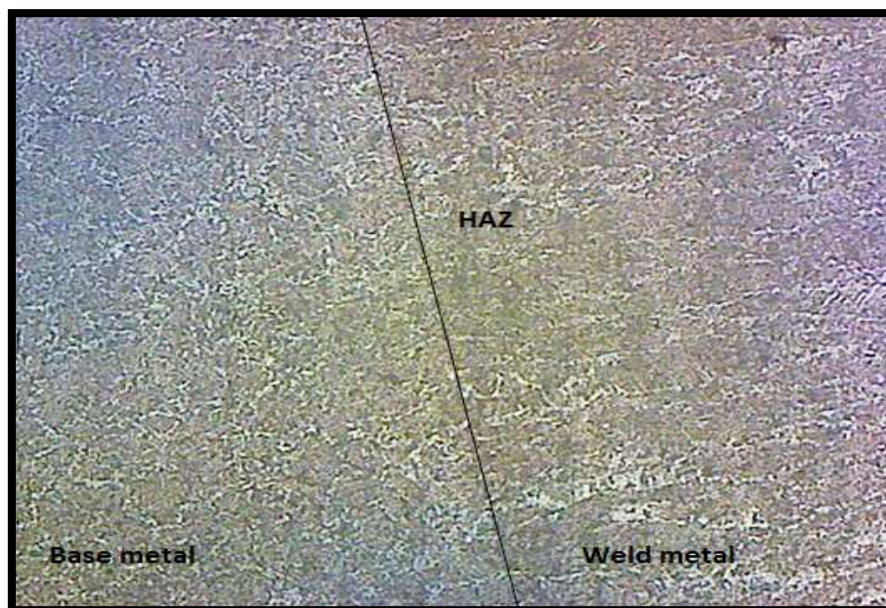


Figure-7.10: Microstructure at the fusion boundary of weld deposited with pure slag

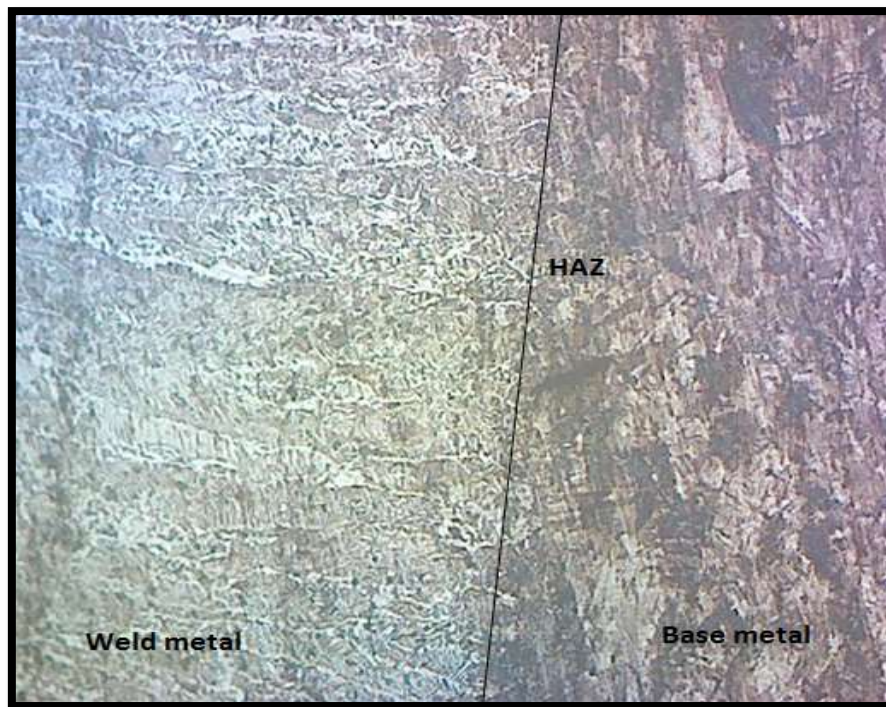


Figure-7.11: Microstructure at the fusion boundary of weld deposited with recycled slag

7.6.2 Micro-Hardness Survey

Hardness is a crucial aspect in defining the properties of a metal and alloy, and the results of such measurements are frequently used to decide whether to accept or reject a weldment. The extent of the HAZ is evaluated by measuring the micro-hardness across this zone, which is diffusion controlled and thermally dependent (Davis, 1994). As a result, micro-hardness analysis in various zones is essential, as the relationship between microstructure and micro-hardness helps in the confirmation of results. This study also provides an idea of the soundness and mechanical properties of the weldments that can be expected from welds produced under different sets of welding parameters. To investigate the phase presence responsible for hardness variation, extensive micro-hardness tests of the weld zone were performed.

Figure 7.12 compares the micro-hardness surveys performed on weld beads deposited with pure slag, fresh flux, and recycled slag. It shows that the hardness obtained with recycled slag is greater than that obtained from pure crushed slag and is comparable to that obtained with fresh flux. Increased carbon and manganese percentages in the weld metal prepared by fresh flux and recycled slag resulted in higher hardness, consistent with the findings of Surian et al. (1992).

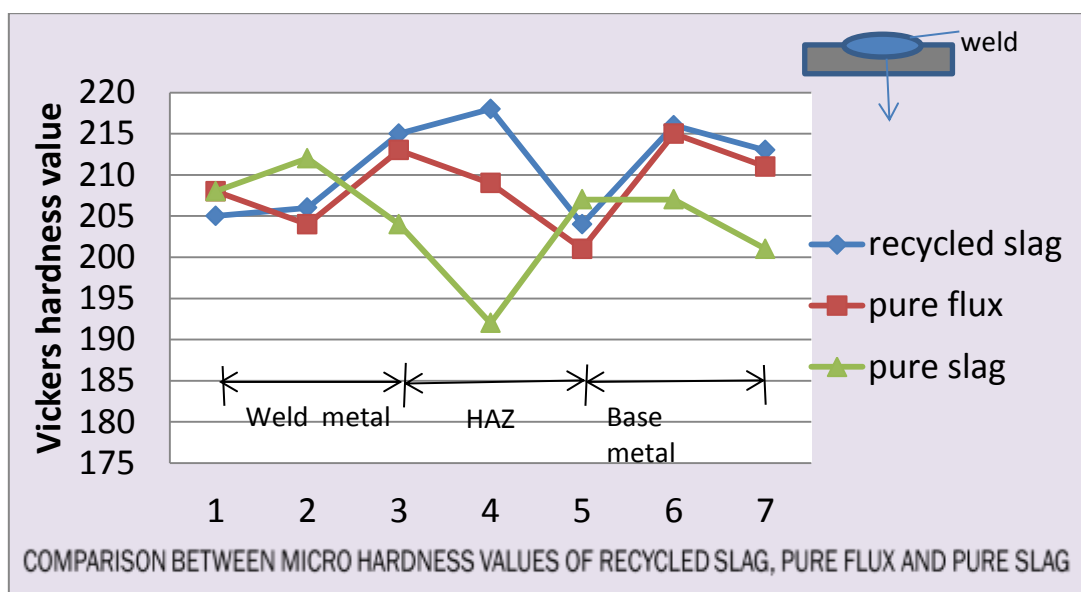


Figure-7.12: Micro-hardness survey across the weld bead

7.7 Summary

1. The weld zone is covered in granulated flux, which causes it to cool slowly in SAW.
2. The microstructure produced by pure slag in a mild steel specimen suggests a ferrite pearlite structure with approximately 0.108 percent carbon. It has side plates and columnar grains with polygonal ferrite. This structure is in good agreement with the results of (i) chemical analysis, which shows low

percentage of carbon, manganese and silicon; (ii) low tensile and yield strength; (iii) low micro hardness.

3. Micrographs obtained using recycled slag show a reduction in columnar grain width with a rise in acicular ferrite. The increase in acicular ferrite can be attributed to the increase in the percentage of carbon (0.089%) and manganese (1.101%) in the weld metal. This microstructure is in good agreement with the results of higher tensile strength (427 N/mm^2) and yield strength (366 N/mm^2) of the weld metal.
4. Welded specimens prepared using recycled slag, have micrographs that demonstrate an increase in acicular ferrite and a decrease in columnar grain width. It was observed that the microstructure obtained with recycled slag is comparable with the microstructure achieved using fresh flux.
5. Recycled slag has a micro-hardness that is comparable to fresh flux and significantly superior to pure slag. It was found that higher concentrations of C, Mn and Si in the weld metal prepared using fresh flux and recycled slag results in increasing the hardness of the weld metal.

COST ANALYSIS

8.1 Introduction

The term "cost analysis" is defined as the study of the expenditures incurred during the production of goods and services. It demonstrates how various expenditures are estimated together with their associated benefits prior to implementation. Additionally, it elaborates various levels of operation where it is cost-effective. In the present scenario, it is important to evaluate the overall cost of manufacturing the product in order to analyse the cost effectiveness of the process. This cost is comprised of labour cost, material cost, and overhead charges. To prove that recycling of slag is economically beneficial, it is necessary to perform a cost analysis (Garg and Singh, 2016). The recycling process includes various costs such as the cost of collecting slag from industry, the cost of crushing and milling the slag, and the cost of sintering. To assess whether recycling of slag is cost-effective, the price of an equivalent 50 kg of flux purchased at market price was compared to recycled slag. Once it is established that recycled slag is economically effective and can produce high-quality welds, it can be acquired commercially in large quantities instead of fresh flux.

8.2 Type of Cost

The process of recycling slag involves a variety of costs, including labour costs, material costs of additives and binders, processing costs, and overhead expenses.

Simple mathematical calculations were performed by considering the market value of various additives and binders added together with the processing cost. These different types of costs are explained below.

8.2.1 Material Cost

The cost of the material required to produce a product or to provide a service is referred to as the material cost. If the material cost is estimated properly, it may be determined whether or not the purchase of material is worthwhile or not. It is important to ensure that the material chosen is of high quality. In this case, the material is waste slag that has been recycled later. This slag has been dumped as a waste by various industries performing submerged arc welding. The only cost incurred is the transportation of slag from industry to the laboratory. This cost is variable, increasing in direct proportion to the distance between the source and the laboratory. This slag was collected from Cheema boilers in Kurali, Punjab. The total material cost was determined by adding the transportation cost of slag to the cost of additives and binders used to recycle slag. These costs of additives were calculated by multiplying their cost (market price) with the quantity used.

8.2.2 Processing Cost

It is the total cost of the various processes required to perform the recycling of slag. These processes involve crushing, milling, and baking the recycled slag to the specified temperature. Here, crushing and milling were carried out in a ball mill having 25 kg capacity. This agglomerated mass of slag was then baked at 850 °C in a stir-casting furnace. All these processes involved in recycling slag were then

calculated by evaluating the power consumed in each process multiplied by commercial rate of electricity.

8.2.3 Overhead Cost

Overhead costs consist of all indirect costs of manufacturing a product that are not covered by the material and labour costs. It is essential to consider both direct and indirect costs when estimating the suitable price of the product. Overhead expenditures associated with a particular industry include industry overhead, general and administrative overhead and advertising expenses. Allocating overhead costs is essential to determine the overall cost of manufacturing a product and hence establishing a profitable market price for the product. Indirect materials, maintenance and repair, administrative personnel, taxes, supervisory and rent were considered overhead costs for a product. To ensure that the costs of all job orders are distributed fairly, they must be properly allocated within the specified overhead costs. The methods of distribution are as follows:

1. Percentage of direct labour cost
2. Percentage of prime cost
3. Direct labour cost.

Out of these methods, it was found that a percentage of prime cost is commonly used in many industries; therefore it was selected to perform the cost analysis of the recycling of slag.

8.3 Results and Discussions

Flux plays an important role in SAW process. This flux is converted into slag, and recycling this slag involves a certain cost. Cost analysis was conducted by evaluating the cost involved in recycling slag to act as a fresh flux (Singh, 2007; Mahto and Kumar, 2010). Finally, the cost involved in recycling the slag per 50 kg was compared with the price of same amount of fresh flux. The cost of slag prepared by recycling the slag was initiated by adding material costs, which includes the cost of procuring the slag, the cost of additives and binders, all fixed and variable costs, and processing costs. In addition, 10% overhead costs and a 10% profit have been considered while performing cost analysis. This cost was then compared with the price of an equal amount of fresh flux. This cost analysis concludes that the slag prepared by recycling of slag is cheaper by 33% as compare to fresh flux. This is due to the fact that slag is normally thrown away as a waste and does not involve any cost whereas fresh flux involves certain purchase cost. Also, labour cost and overhead expense incurred in recycling of slag were very less. Table 8.1 shows cost analysis of recycled slag and fresh flux per 50 kg.

Table-8.1: Cost analysis of recycled slag and fresh flux per 50 kg

S. No.	Cost Head	Material	Process	Cost (INR)
Material Cost				
1.	Pure slag	Slag	Slag collected includes transportation cost	300
2.	Additives	Mn, Al, Potassium titanate, CaCO_3	Purchase cost of additives including processing and transportation cost	1858
3.	Binder	Potassium silicate solution	Purchase cost	150

S. No.	Cost Head	Material	Process	Cost (INR)
<u>Processing Cost</u>				
4.	Crushing and Milling		Slag crushed and rotated in ball mill	300
5.	Sintering		Slag mixture heated without liquefaction	300
6.	Labour cost		Cost of labour	150
7.	Subtotal			3058
<u>Overhead Cost</u>				
8.	Overhead cost@10%			3364
9.	Profit@10%			3364
10.	Cost of reclaimed slag per 50 kg			3670
11.	Market price of fresh flux per 50 kg			5500
12.	Saving			1830
13.	% Saving			33%

8.4 Summary

1. Slag plays a major role as a raw material for developing recycled slag.
2. Slag is proved economical by 33%.

CONCLUSIONS AND FUTURE SCOPE

9.1 Introduction

The main purpose of this research is to define a technology for recycling slag in submerged arc welding. The abstract conclusions obtained from the work done on various aspects are reproduced again to develop a comprehensive idea of practicability and employment of my research work. The conclusions including different aspects of the whole research work are as follows:

9.2 Conclusions from Chapter 4 - Recycling of Slag and Weldability

1. Slag recycling proved reliable as the yielding characteristics were found to be equivalent to the flux in the same submerged arc welding process.
2. It was concluded that 87.5% slag when mixed with 5.5% of calcium carbonate and Al powder along with 7% potassium titanate and Mn powder in addition to potassium silicate solution to wet the mixture was suitable composition to be used as recycled slag.
3. Weld metal chemistry for recycled slag was found to be satisfactory as per ASME SFA 5.17.
4. The results of the tensile test and impact test lie within the acceptable range of ASME SFA 5.17.
5. Dye penetrant test was also performed on the specimen and revealed a defect-free surface for reclaimed slag welded specimen.

6. Radiographic test results were comparable to those of fresh flux when observed for recycled slag whereas in case of pure slag, the welded specimen does not pass the radiographic test.
7. Slag detachability and arc stability were both adequate as per the requirement. Both showed an explicit characteristic when observed for recycled slag.
8. Weld beads with an acceptable appearance were observed.

9.3 Conclusions from Chapter 5 - Element Transfer Behaviour

1. Carbon content is directly proportional to the arc voltage, whereas it is inversely proportional to the wire feed rate. Both welding speed and contact tube to plate distance have insignificant effect on it.
2. Manganese content is directly proportional to the arc voltage, whereas it is inversely proportional to the wire feed rate.
3. Silicon content is inversely related to the wire feed rate but remains the same with varying arc voltage, welding speed, and contact tube to plate distance.
4. Sulphur content decreased with an increase in wire feed rate but remains the same with varying arc voltage, welding speed, and contact tube to plate distance.
5. Phosphorus content increased with an increase in arc voltage and decreased with the increase in wire feed rate but remained almost constant in the case of contact tube to plate distance and welding speed.
6. It was concluded that the contact tube to plate distance has an insignificant effect on weld metal chemistry.

9.4 Conclusions from Chapter 6 - Weld Bead Geometry and Shape Relationships

1. Two level half factorial Technique can be suitably applied for conducting the experiments and further ANOVA applied for analysing the effect of welding parameters on weld bead geometry and shape relationship.
2. Predicted values were found to be in fair agreement with actual values of bead width, bead height, and bead penetration, weld penetration shape factor, and weld reinforcement form factor.
3. Recycled slag proves reliable for obtaining suitable weld bead geometry
4. Empirical models can be easily employed and effective in acquiring desirable weld bead characteristics.
5. Responses such as bead width, bead penetration and weld reinforcement form factor increased with the increase in wire feed rate.
6. Bead height is inversely proportional to the travel speed whereas weld reinforcement form factor is directly proportional to the travel speed.
7. Bead height, weld penetration shape factor increased with an increase in contact tube to plate distance whereas bead penetration and weld reinforcement form factor decreased with an increase in contact tube to plate distance.

9.5 Conclusions from Chapter 7 - Metallurgical Studies

1. The weld zone is covered in granulated flux, which causes it to cool slowly in SAW.

2. The microstructure produced by pure slag in a mild steel specimen suggests a ferrite pearlite structure with approximately 0.108 percent carbon. It has side plates and columnar grains with polygonal ferrite.
3. Micrographs obtained using recycled slag show a reduction in columnar grain width with a rise in acicular ferrite.
4. Welded specimens prepared using recycled slag, have micrographs that demonstrate an increase in acicular ferrite and a decrease in columnar grain width.
5. Recycled slag has a micro-hardness that is comparable to fresh flux and significantly superior to pure slag.

9.6 Conclusions from Chapter 8 - Cost Analysis

1. Slag plays a major role as a raw material for creating recycled slag.
2. Slag is proved economical by 33%.

9.7 Scope for Future Work

There is a scope in every field of research for further improvement. The following are the areas that can still be explored in the context of the present research:

1. Slag can be recycled by using other different percentages of additives and other alloying elements.
2. Recycled slag can be used with different grades of filler wire.
3. Recycled slag can be used for multi-wire submerged arc welding.

REFERENCES

1. Arya, H.K., Singh, K. and Saxena, R.K., 2018. Effect of weld cooling rates on mechanical and metallurgical properties of submerged arc welded pressure vessel steel. *Journal of Pressure Vessel Technology*. 140, pp. 1-7.
2. ASME Sec.-II Part C, 2010. Specifications for carbon steel electrodes and fluxes for submerged arc welding. Boiler and pressure vessel codes: pp. 393-409.
3. Bahrami, H. and Kolahan, F., 2010. Mathematical modelling and optimization of weld bead geometry in cladding by flux cored arc welding. *11th Iranian Conference on Manufacturing Engineering, 19-21 October, Society of Manufacturing Engineering of Iran*.
4. Bailey, N., 1977. Solidification cracking of ferritic steels during submerged arc welding. *The Welding Institute Report, Cambridge*. pp. 1-26.
5. Bailey, N., 1991. Submerged arc welding ferritic steels with alloyed metal powder. *Welding Journal*. 70(8), pp. 187s-197s.
6. Balasubramanian, M., 2016. Prediction of optimum weld pool geometry of PCTIG welded titanium alloy using statistical design. *Engineering Science and Technology, an International Journal*. 19, pp. 15-21.
7. Bang, K.S., Park, C., Jung, H.C. and Lee, J.B., 2009. Effects of flux composition on the element transfer and mechanical properties of weld metal in submerged arc welding. *Metals and Materials International*. 15(3), pp. 471-477.

8. Basu, B. and Raman, R., 2002. Microstructural variations in a high strength structural steel weld under iso heat input conditions. *Welding Journal*. 81(11), pp. 239s-248s.
9. Beck, H.P. and Jackson, A.R., 1996. Recycling of SAW slag proves reliable and repeatable. *Welding Journal*. 75(66), pp. 51-54.
10. Belton, G.R., Moore, T.J. and Tanking, E.S., 1963. Slag metal reactions in submerged arc welding. *Welding Journal*. 68(3), pp. 289-290.
11. Biswas, A., Bhaumik, S., Majumdar, G., Datta, S. and Mahapatra, S.S., 2011. Bead geometry optimization of Submerged Arc Weld: Exploration of Weighted Principal Component Analysis (WPCA). *2nd International Conference on Mechanical, Industrial and Manufacturing Technologies, Singapore* 26-28 February.
12. Brien, A.O., 2004. *Welding Handbook*. Vol. II. 9th edition. Miami: American Welding Society.
13. Butler, C.A. and Jackson, C.E., 1967. Submerged arc welding characteristics of CaO-TiO₂-SiO₂ system. *Welding Journal*. 46(10), pp. 445s-448s.
14. Caddell, R.M., 1967. The influence of physical properties on penetration in arc welding. *Transactions of the ASME*. May, pp. 328-331.
15. Calik, A., 2009. Effect of cooling rate on hardness and microstructure of AISI 1020, AISI 1040 and AISI 1060 Steels. *International Journal of Physical Sciences*. 4(9), pp. 514-518.
16. Cary, H.B., 1979. *Modern Welding Technology*. USA: Prentice-Hall.

17. Chai, C.S. and Eagar, T.W., 1980. The effect of submerged arc welding parameters on weld metal chemistry. *Welding Journal*. 59(3), pp. 93s-98s.
18. Chai, C.S. and Eagar, T.W., 1981. Slag metal reactions in binary CaF_2 metal oxide welding fluxes. *Welding Research Supplement*. pp. 229-232.
19. Chandel, R.S., Bala, S.R. and Malik, L., 1987. Effect of submerged arc process variables. *Welding and Metal Fabrication*. 55(6), pp. 302-304.
20. Chandel, R.S., Seow, H.P. and Cheong, F.L., 1998. Using metal powders in submerged arc welding efficiently. *Welding Journal*. 77(4), pp. 65-68.
21. Chandgude, S.B. and Asabe, S.S., 2014. Investigation of recycled slag in submerged arc welding for pressure vessels. *5th International and 26th All India Manufacturing Technology, Design and Research Conference*, December 12th-14th, IIT Guwahati.
22. Chaudhary, C.S., Kashish, and Khanna, P., 2021. Effect of welding parameters on the weld bead profile of submerged arc welded low carbon steel plates. *IOP Conference Series: Materials Science and Engineering*. pp. 1-11.
23. Cho, D.W., Kiran, D.V. and NA, S.J., 2015. Analysis of the flux consumption and metal transfer for tandem submerged arc welding process under isoheat input conditions. *Welding Journal*. 94, 396s-401s.
24. Cotsee, T., 2020. Phase chemistry of submerged arc welding (SAW) fluoride based slags. *Journal of Materials Research and Technology*. 9(5), pp. 9766-9776.

25. Das, B., Prakash, S., Reddy, P.S.R. and Misra, V.N., 2007. An overview of utilization of slag and sludge from steel industries. *Resources, Conservation and Recycling*. 50, pp. 40-57.
26. Datta, G.L. and Nagesh, D.S., 2002. Prediction of weld bead geometry and penetration in shielded metal arc welding using artificial neural network. *Journal of Material Processing Technology*. 23(2), pp. 303-312.
27. Datta, I. and Paresh, M., 1989. Filler metal flux basicity determination using optical basicity index. *Welding Research Supplement*. 68(10), pp. 68s-73s.
28. Datta, S. and Mahapatra, S.S., 2010. Multi-objective optimization of submerged arc welding process. *The Journal of Engineering Research*. 7(1), pp. 42-52.
29. Datta, S., Bandyopadhyay, A. and Pal P.K., 2008. Modelling and optimization of features of bead geometry including percentage dilution in submerged arc welding consuming mixture of fresh flux and fused slag. *International Journal of Advanced Manufacturing Technology*. 36, pp. 1080-1090.
30. Datta, S., Bandyopadhyay, A. and Pal, P.K., 2008. Solving multi-criteria optimization problem in submerged arc welding consuming a mixture of fresh flux and fused slag. *International Journal of Advanced Manufacturing Technology*. 35(9-10), pp. 935-942.
31. Davies, A.C., 1996. *Welding*. 10th edition. Cambridge: Cambridge University Press.
32. Davies, J.R., 1994. Aluminium and Aluminium alloys. *ASM speciality Handbook*. 376-419. ASM International, Materials Park, Ohio.

-
33. Davies, M.L.E. and Bailey, N., 1982. Properties of submerged arc fluxes- A fundamental study. *Metal Construction*. pp.207-209.
 34. Davis, M.L.E. and Bailey, N., 1991. Evidence from inclusion chemistry of element transfer during submerged arc welding. *Welding Research Supplement*. pp. 57s-67s.
 35. Davis, M.L.E., 1980. How submerged arc flux composition influences element transfer. *International Conference on Weld Pool Chemistry and Metallurgy*, Cambridge, England: The British Welding Institute.
 36. Debarata, P., Mandal, N.R. and Das, S., 2014. Heat source modelling and analysis of submerged arc welding. *Welding Journal*. 93, pp. 183s – 192s.
 37. Demyantsevich, V.P., 1974. Dependence of penetration on automatic submerged arc welding conditions. *Welding Production*. (7), pp. 36-38.
 38. Dhas, J.E.R. and Kumanan, S., 2011. Optimization of parameters of submerged arc welds using non-conventional techniques. *Applied Soft Computing*. 11, pp. 5198–5204.
 39. Dippenaar, R., 2005. Industrial uses of slag (the use and reuse of iron and steel making slags). *Iron and Steelmaking*. 32(1), pp. 35-46.
 40. Dowling, J.M., Corbett, J.M. and Kerr H.W., 1986. Inclusion phases and the nucleation of acicular ferrite in submerged arc welds in high strength low alloy steels. *Metallurgical Transactions A*. Vol 17 A, pp. 1611-1623.
 41. Eroglu, M, Aksoy, M. and Orhan, N., 1999. Effect of coarse initial grain size on microstructure and mechanical properties of weld metal and HAZ of low carbon steel. *Material Science and Engineering: A*. 269(1-2), pp. 59-66.

-
42. Esfahani, S. and Barati, M., 2016. Effect of slag composition on the crystallization of synthetic $\text{CaO-SiO}_2\text{-Al}_2\text{O}_3\text{-MgO}$ slags: Part I- Crystallization behaviour. *Journal of Non-Crystalline Solids*. 436, pp. 35-43.
 43. Ferrera, K.P. and Olson, D.L., 1975. Performance of the $\text{MnO-SiO}_2\text{-CaO}$ system as a welding flux. *Welding Journal*. 54(7), pp. 211s-215s.
 44. Fisher, L.V. and Barron, A.R., 2019. The recycling and reuse of steelmaking slags – A review. *Resources, Conservation and Recycling*. 146, pp. 244-255.
 45. Garg, J. and Singh K., 2012. Reuse of slag in stainless steel cladding and its effect on chemistry of cladding. *Journal of Environmental Research and Development*. Vol. 6 No. 3A, pp.674-680.
 46. Garg, J. and Singh, K., 2010. Recycling of submerged arc welding slag for economy & environment. *National Conference on Advancements and Futuristic Trends in Mechanical and Materials Engineering*. February 19-20.
 47. Garg, J. and Singh, K., 2016. Slag recycling in submerged arc welding and its effects on the quality of stainless steel claddings. *Materials and Design*. 108, pp. 689-698.
 48. Ghosh, A., Chattopadhyaya, S. and Sarkar, P.K., 2007. Effects of input parameters on weld bead geometry of SAW process. *Proceedings of International Conference on Mechanical Engineering (ICME07-AM-50)*, Dhaka, Bangladesh. pp. 1-6.
 49. Ghosh, A., Chattopadhyaya, S. and Sarkar, P.K., 2011. Critical analysis of confounded parameters of SAW process. *Procedia Engineering*. 10, pp. 2786–2790.

-
50. Gott, G., Gericke, A., Henkel, K.M. and Uhrlandt, D., 2016. Optical and spectroscopic study of a submerged arc welding cavern. *Welding Journal*. 95, pp. 491-499.
 51. Gunaraj, V and Murugan, N., 2000. Prediction and optimization of weld bead volume for the submerged arc process-part-2. *Welding Research Supplement*. 79(11), pp. 331–338.
 52. Gunaraj, V. and Murugan, N., 2000. Prediction and optimization of weld bead volume for the submerged arc process-Part-1. *Welding Research Supplement*. 79(10), pp. 286–294.
 53. Gunaraj, V., Murugan, N., 1999. Prediction and comparison of the area of the heat-affected zone for the bead-on-plate and bead-on-joint in submerged arc welding of pipes. *Journal of Material Processing Technology*. 95, pp. 246-261.
 54. Guo, J., Bao, Y. and Wang, M., 2018. Steel slag in China: Treatment, recycling and management. *Waste Management*. 78, pp. 318-330.
 55. Gupta, S.R. and Arora N., 1991. Influence of flux basicity on weld bead geometry and heat affected zone in submerged arc welding. *Indian Welding Journal*. 24 (7), pp. 127-133.
 56. Haidemenopoulos, G.N., 2018. *Physical Metallurgy principles and Design*, 1st Edition, CRC press, Taylor and Francis group, LLC, Boca Raton.
 57. Hatch, G.G. and Chipman, J., 1949. Sulphur Equilibria between Iron blast furnace slags and metal. *The journal of the minerals, Metals and Materials Society*. 1, pp. 274-284.

-
58. Hezlett, T.H., 1957. Coating ingredients influences on surface tension arc stability and bead shape. *Welding Journal*. 38(1), pp. 18s-22s.
 59. Honavar, D.S., 2006. Cost effective productivity in welded fabrication. *Technology Trends*. September pp. 13–6.
 60. Houldcroft, P.T., 1989. *Submerged arc welding*. 2nd edition. Cambridge: Woodhead Publishing Ltd.
 61. <https://www.twi-global.com>
 62. Indacochea, J.E., Blander, M., Christensen, N. and Olson, D.L., 1985. Chemical reactions during submerged arc welding with FeO-MnO-SiO₂ fluxes. *Metallurgical Transactions*. 16 (B), pp. 237-245.
 63. Jeffus, L., 2004. *Welding: Principles and applications*. 5th edition. Chennai, India: Chennai Micro Print Pvt. Ltd.
 64. Jenny, C.L. and Brien, A.O., 2001. *Welding Handbook*. Vol. I. 9th edition. Miami: American Welding Society.
 65. Jindal, S., Chibber, R. and Mehta, N.P., 2013. Investigation on flux design for submerged arc welding of high strength low alloy steel. *Proc IMechE Part B: Journal of Engineering Manufacture*. 227(3), pp. 383-395.
 66. Jindal, S., Chibber, R. and Mehta, N.P., 2014. Prediction of element transfer due to flux and optimisation of chemical composition and mechanical properties in high-strength low-alloy steel. *Proceedings of the Institution of Mechanical Engineers, Part B: Journal of Engineering Manufacture*. 229(5), pp. 785-801.

-
67. Joarder, A., Saha, S.C. and Ghose, A.K., 1991. Study of submerged arc weld metal and heat affected zone microstructures of a plain carbon steel. *Welding Journal*. 70(6), pp. 141s-147s.
 68. Kalpakjian, S., Schmid, R.S., 2006. *Manufacturing Engineering and Technology*. Pearson Education Inc.
 69. Kanjilal, P., Majumdar, S.K. and Pal, T.K., 2005. Prediction of acicular ferrite from flux ingredients in submerged arc weld metal of carbon-manganese steel. *ISIJ International*. 45(6), pp. 876-885.
 70. Kanjilal, P., Pal, T.K. and Majumdar, S.K., 2006. Combined effect of flux and welding parameters on chemical composition and mechanical properties of submerged arc weld metal. *Journal of Materials Processing Technology*. 171, pp. 223–231.
 71. Kanjilal, P., Pal, T.K. and Majumdar, S.K., 2007. Prediction of element transfer in submerged arc welding. *Welding Research Journal*. 86, pp. 135-14.
 72. Karadeniz, E., Ozsarac, U. and Yildiz, C., 2007. The effect of process parameters on penetration in gas metal arc welding processes. *Materials and Design*. 28, pp. 649–656.
 73. Karaoglu, S. and Secgin, A., 2008. Sensitivity analysis of submerged arc welding process parameters. *Journal of Materials Processing Technology*. 202, pp. 500–507.
 74. Kiran, D.V., Basu, B. and De, A., 2012. Influence of process variables on weld bead quality in two wire tandem submerged arc welding of HSLA steel. *Journal of Material Processing Technology*. 212(10), pp. 2041-2050.

75. Kolhe, K.P. and Datta, C.K., 2008. Prediction of microstructure and mechanical properties of multi pass SAW. *Journal of Material Processing Technology*. 197, pp. 241-249.
76. Kou, S., 2003. *Welding Metallurgy*. 2nd Edition. New York. John Wiley.
77. Kozyrev, N.A., Kryukov, R.E., Kozyreva, O.E., Lipatova, U.I. and Filonov, A.V., 2016. Production of welding fluxes using waste slag formed in silicomanganese smelting. *IOP Conference Series: Materials Science and Engineering*. 125, pp. 1-6.
78. Kumar, A., Maheshwari, S. and Sharma, S.K., 2015. Fuzzy logic optimization of weld properties for SAW using silica based agglomerated flux. 3rd *International Conference on Recent trends in computing (ICRTC-2015)*. *Procedia Computer Science*. 57, pp. 1140-1148.
79. Kumar, A., Maheshwari, S. and Sharma, S.K., 2015. Optimization of Vickers hardness and impact strength of silica based fluxes for submerged arc welding by Taguchi method. *4th International Conference on Materials Processing and Characterization Materials Today: Proceedings*. 2, pp. 1092 – 1101.
80. Kumar, A., Singh, H. and Maheshwari, S., 2012. Modelling and analysis by response surface methodology of hardness for submerged arc welded joints using developed agglomerated fluxes. *Indian Journal of Engineering and Materials Sciences*. 19(6), pp. 379-385.
81. Kumar, K.M., Gopal Krishna, P.V. and Kishore, K., 2020. Study of metallurgical and mechanical Properties in submerged arc welding with

- different composition of fluxes – A review. *Materials Today: Proceedings*. 22, pp. 2300-2305.
82. Kumar, V., Mohan, N. and Khamba, J.S., 2009. Development of cost effective agglomerated fluxes from waste flux dust for submerged arc welding. *Proceedings of the World Congress on Engineering, July 1-3*. Vol. 1.
83. Kumar, V., Mohan, N. and Khamba, J.S., 2010. Development of agglomerated acidic flux for submerged arc welding. *Estonian Journal of Engineering*. 16(2), pp. 135-141.
84. Kumar, R. and Singh, R., 2007. Effects of Process Variables on HAZ in Submerged Arc Welds of Structural Steel Pipes. *Manufacturing Technology Today*. 6(4), pp. 23-30.
85. Lan, L., Qiu, C., Zhao, D., Gao, X. and Du, L., 2012. Analysis of microstructural variation and mechanical behaviour in submerged arc welded joint of high strength low carbon bainitic steel. *Material Science and Engineering: A*. 558, pp. 592–601.
86. Lancaster, J.F., 1998. *Metallurgy of Welding*. 4th edition. London: Allen and Unwin Ltd.
87. Lau, T., Weatherly, G.C. and Mc Lean A., 1986. Gas/metal/slag reactions in submerged arc welding using CaO-Al₂O₃ based fluxes. *Welding Research Supplement*. pp. 31-38.
88. Lee, C.S., Chandel, R.S. and Seow, H.P., 2000. Effect of welding parameters on the size of heat affected zone of submerged arc welding. *Materials and Manufacturing Processes*. 15(5), pp. 649-666.

-
89. Li, K., Wu, Z., Zhu, Y. and Liu, C., 2017. Metal transfer in submerged arc welding. *Journal of Materials Processing Technology*. 244, pp. 314–319.
 90. Lin, L., Bao, Y.P., Wang, M. and Zhou, H.M., 2014. Influence of Al_2O_3 modification on phosphorus enrichment in P bearing steelmaking slag. *Ironmaking and Steelmaking*. 41(3), pp. 193-198.
 91. Lincoln electric company, 1994. The procedure handbook of arc welding.
 92. Livshits, L.G. and Shiryaev, A.I., 1960. A new ceramic flux for hard facing. *Welding Production*, January. pp. 28-29.
 93. Mahto, D. and Kumar, A., 2010. Novel method of productivity improvement and waste reduction through recycling of submerged arc welding slag. *Jordan Journal of Mechanical and Industrial Engineering*. 4, pp. 451-466.
 94. Mandatov, N.M., 1969. Shape relationships for under water welding. *Welding Production*. 16(3), pp. 18-23.
 95. Mc Glone, J.C., 1982. Weld bead geometry prediction- A review. *Metal Construction*. 14(7), pp. 378-384.
 96. Mendez, P.F., Gott, G. and Guest, S., 2015. High speed video of metal transfer in submerged arc welding. *Welding Journal*. 94(10), pp. 326s-333s.
 97. Mercado, A.M.P., Lopez-Hirata, V.M. and Munoz, M.L.S., 2005. Influence of the chemical composition of flux on the microstructure and tensile properties of submerged arc welds. *Journal of Materials Processing Technology*. 169, pp. 346–351.
 98. Metals handbook 1983. *Welding, Brazing and Soldering*, ASM. Vol 6(9).

-
99. Min, D.J. and Tsukihashi, F., 2017. Recent advances in understanding physical properties of metallurgical slags. *Metals and Materials International*. 23(1), pp. 1-19.
 100. Mitra, U., and Eagar, T.W., 1984. Slag metal reactions during welding part I. Evaluation and reassessment of existing theories. *Metallurgical Transactions*. 22(B), pp. 65-71.
 101. Mohan, N. and Pandey, S., 2005. Modelling for element transfer in submerged arc welding. *Proceedings of International Conference on Mechanical Engineering in Knowledge Age*, December 12-14, Delhi College of Engineering, Delhi. pp. 454-459.
 102. Mohandas, T. and Reddy, G.M., 2001. Solidification cracking studies on steels. *Indian Welding Journal*. 34(3), pp. 13-19.
 103. Moi S. C., Bandyopadhyay A. and Pal P. K., 2001. Submerged arc welding with a mixture of fresh flux and fused slag. *Proceedings of National Seminar on Advances in Material and Processing, IIT, Roorkee, India*.
 104. Montgomery, D.C., 2013. *Design and analysis of experiments*. 8th edition. New York: John Willey and Sons.
 105. Moradpour, M.A., Hashemi, S.H. and Khalili, K., 2015. Multi-objective optimization of welding parameters in submerged arc welding of API X65 steel plates. *Journal of Iron and Steel Research International*. 22(9), pp. 870-878.

-
106. Morete, G.F., Paranhos, D.R. and Franca De Holanda, J.N., 2007. Utilization of welding slag in ceramic materials for civil construction. *Welding International*. 21(8), pp. 584-588.
 107. Murugan, N. and Gunaraj, V., 2005. Prediction and control of weld bead geometry and shape relationships in submerged arc welding of pipes. *Journal of Materials Processing Technology*. 168, pp. 478-487.
 108. Murugan, N. and Parmar, R.S., 1997. Effect of welding conditions on microstructure properties of type 316L stainless steel submerged arc cladding. *Welding Journal*. 210s-220s.
 109. Myers, R.H., 1990. *Response surface methodology in statistical and analysis of industrial experiments*. New York: Marcel Dekkar.
 110. Nadkarni, S.V., 1988. *Modern Arc Welding Technology*. 1st edition. New Delhi, India: IBH publications.
 111. North, T.H., Bell, H.B., Nowicki, A. and Craig, I., 1978. Slag/Metal reaction, oxygen and toughness in submerged arc welding. *Welding Research Supplement*. pp.63-75.
 112. Olson, D.L., Liu, S., Frost, R.H, Edwards, G.R. and Fleming, D.A., 1993. Nature and Behaviour of fluxes used for Welding. *ASM Handbook*. Vol. 6 (10), pp. 55–63.
 113. Pal, P.K., Bandyopadhyay A. and Bala, A.K., 2001. Some aspect on submerged arc welding with mixture of fresh flux and fused slag. *International Conference*. Dhaka, Bangladesh.

-
114. Palm, J.H., 1972. How fluxes determine the metallurgical properties of submerged arc welds. *Welding Journal*. 51(7), pp. 358s-365s.
115. Pandey S., Bharti N.D., Arulmani R. and Gupta S.R., 1994. Effect of submerged arc welding parameters and fluxes on element transfer behaviour and weld-metal chemistry. *Journal of Materials Processing Technology*. 40, pp. 195-211.
116. Pandey, S. and Narender, M., 2003. Investigation into flux consumption in submerged arc welding. *International Conference on CAD, CAM, Robotic and Autonomous Factories. IIT, Delhi*.
117. Pandey, S. and Narender, M., 2003. Welding current in submerged arc welding. *Indian Welding Journal*. 36(1), pp. 16-22.
118. Pandey, S., 2004. Welding current and melting rate in submerged arc welding- A new approach. *Australasian Welding Journal*. 49(2), pp. 34-42.
119. Paniagua-Mercado, A.M. and Lopez-Hirata, V.M., 2011. Chemical and Physical properties of fluxes for SAW of low carbon steels. *Arc Welding*. pp. 281-298.
120. Paniagua-Mercado, A.M., Lopez-Hirata, V.M., Dorantes-Rosales, H.J., Diaz, P.E. and Valdez E.D., 2009. Effect of TiO₂ containing fluxes on the mechanical properties and microstructure in submerged arc weld steels. *Material Characterization*. 60, pp. 36-39.
121. Parmar, R.S., 1997. *Welding Process and Technology*, third edition, Khanna Publication.

-
122. Patchett, B.M. and Milner, D.R., 1972. Slag-metal reactions in the electro slag process. *Welding Journal*. 51(10), pp. 491s-505s.
 123. Patnaik, A., Biswas, S. and Mahapatra, S.S., 2007. An evolutionary approach to parameter optimisation of submerged arc welding in the hard-facing process. *International Journal of Manufacturing Research*. 2(4), pp. 462-483.
 124. Peng, Y., Chen, W. and Xu, Z., 2001. Study of high toughness ferrite wire for submerged arc welding of pipeline steel. *Materials Characterization*. 47, pp. 67-73.
 125. Penkov, O.M., 1993. Methods of developing fluxes for automatic closed-arc welding aluminium and its alloys. *Welding International*. 7(1), pp. 63-64.
 126. Potapov, N.N., 1978. A quantitative evaluation of basicity of fluxes. *Welding Production*. 25(9), pp. 4-8.
 127. Prasad, K. and Dwivedi, D.K., 2008. Some investigations on microstructure and mechanical properties of submerged arc welded HSLA steel joints. *International Journal of Advanced Manufacturing Technology*. 36, pp. 475–483.
 128. Rao, S.S., 2001. *Engineering optimization: Theory and Practice*. New Delhi: New Age Publishers.
 129. Rathi, A.K., 2021. To study the effect of submerged arc welding on bead geometry and hardness for mild steel (IS-2062A) using fractional factorial design. *Materials Today: Proceedings*. 34(Part 2), pp. 525-530.

-
130. Reddy, K.S., 2013. Optimization & prediction of welding parameters and bead geometry in submerged arc welding. *International Journal of Applied Engineering Research and Development*. 3(3), pp. 1-6.
 131. Renwick, B.G. and Patchett, B. M., 1976. Operating characteristics of the submerged arc process. *Welding Journal*. 55(3), pp. 69-76.
 132. Robinson, M.H., 1983. Observation on electrode melting rates during submerged arc welding. *Welding Journal*. 62(11), pp. 503s-509s.
 133. Ross, P.J., 1996. *Taguchi techniques for quality engineering*. New York: McGraw Hill.
 134. Sahni, V., Singh, K. and Pandey, S., 2009. Waste to wealth: reuse of slag as a flux in submerged arc welding. *Asian Journal of Chemistry*. 21(10), pp. 72-75.
 135. Sailender, M., Suresh, R., Reddy, G.C. and Venkatesh, S., 2019. Prediction and comparison of the dilution and heat affected zone in submerged arc welding (SAW) of low carbon alloy steel joints. *Measurement*. 150.
 136. Saini, S. and Singh, K., 2020. Some feasibility studies for recycling of steel slag as a useful flux for submerged arc welding. *Journal of Advanced Manufacturing Systems*. 19(02), pp. 277-289.
 137. Sarfo, P., Das, A., Wyss, G. and Young, C., 2017. Recovery of metal values from copper slag and reuse of residual secondary slag. *Waste Management*. 70, pp. 272-281.
 138. Schwemmer, D.D., Olson, D.L. and Williamson, D.L., 1979. The relationship of weld penetration to the welding flux. *Welding Journal*. 58(5), pp. 153s-159s.

-
139. Sharapov, Yu. V., 1972. Width calculation for automatic submerged arc butt welds. *Welding Production*. No.3: pp. 45-47.
140. Sharma, A., Chaudhary, A.K., Arora, N. and Mishra, B.K., 2009. Estimation of heat source model parameters for twin-wire submerged arc welding. *Journal of Advanced Manufacturing Technology*. 45, pp. 1096-1103.
141. Sharma, L. and Chibber, R., 2018. Design and development of submerged arc welding fluxes using $\text{TiO}_2\text{-SiO}_2\text{-CaO}$ and $\text{SiO}_2\text{-CaO-Al}_2\text{O}_3$ flux system. *Proceedings of the Institution of Mechanical Engineers, Part E: Journal of Process Mechanical Engineering*. 233(4), pp. 739-762.
142. Sharma, L. and Chibber, R., 2019. Investigating the physiochemical and thermo-physical properties of submerged arc welding fluxes designed using $\text{TiO}_2\text{-SiO}_2\text{-MgO}$ and $\text{SiO}_2\text{-MgO-Al}_2\text{O}_3$ flux systems for linepipe steels. *Ceramics International*. 45(2) part A, pp. 1569-1587.
143. Sharma, L. and Chibber, R., 2020. Study of weld bead chemical, micro-hardness and microstructural analysis using submerged arc welding fluxes for linepipe steel applications. *Ceramics International*. Vol. 46(15), pp. 24615-24623.
144. Shen, H. and Forssberg, E., 2003. An overview of recovery of metals from slags. *Waste Management*. 23, pp. 933-949.
145. Shen, S., Oguocha, I.N.A. and Yannacopoulos, S., 2012. Effect of heat input on weld bead geometry of submerged arc welded ASTM A709 Grade 50 steel joints. *Journal of Materials Processing Technology*. 212, pp. 286– 294.

146. Shukla, D.K. and Pandey, S., 2012. Dilution control by advanced submerged arc welding. *Advanced Materials Research*. Vol 488-489, pp. 1737-1741.
147. Singh, A. and Singh, R.P., 2020. A review of effect of welding parameters on the mechanical properties of weld in submerged arc welding process. *Materials Today: Proceedings*. 26(2) part 2, pp. 1714-1717.
148. Singh, B., Khan, Z.A., Siddiquee, A.N. and Maheshwari, S., 2018. Experimental study on effect of flux composition on element transfer during submerged arc welding. *Sadhana*. 43(26), pp. 1-12.
149. Singh, H., Kumara, J. and Maheshwari, S., 2013. XRD and DTA analysis of developed agglomerated fluxes for submerged arc welding. *Journal of Metallurgy*. pp. 7-15.
150. Singh, J., Singh, K. and Garg, J., 2011. Reuse of slag as flux in submerged arc welding & its effect on chemical composition, bead geometry & microstructure of the weld metal. *International Journal of Surface Engineering & Materials Technology*. 1, pp. 24-27.
151. Singh, K. and Pandey, S., 2009. Recycling of slag to act as a flux in submerged arc welding. *Resources, Conservation and Recycling*. 53, pp. 552–558.
152. Singh, K. and Singh, J. and Mani, R.A., 2006. Recycling of submerged arc welding slag. *Australasian Welding Journal*, 51, 2nd quarter, pp. 34-38.
153. Singh, K. and Singh, J., 2010. Influence of slag flux mixture on mechanical properties of welds in submerged arc welding. *National Conference on*

-
- Advancements and Futuristic Trends in Mechanical Engineering*. February 19-20.
154. Singh, K. and Pandey, S., 2009. Recycled slag consumption in submerged arc welding and its effect on microstructure of weld metal. *Indian Welding Journal*. 42(4), pp. 46-51.
155. Singh, K., 2007. Some studies in Recycling of submerged arc welding slag as a flux. *Ph.D. Thesis*, IIT Delhi.
156. Singh, R.P., Garg, R.K. and Shukla, D.K., 2016. Mathematical modelling of effect of polarity on weld bead geometry in submerged arc welding. *Journal of Manufacturing Processes*. 21, pp. 4–22.
157. Singh, R.P., Singh, C. and Verma, A.K., 2020. Effect of quenching and annealing on the hardness of submerged arc welded mild steel plates. *Materials today: proceedings*. 26(2), pp. 1822-1826.
158. Singh, S., Panwar, V., Singh, M. and Singh, T., 2014. Effect of welding parameter of flux consumption in submerged arc welding. *Frontiers in Materials Research and Applications*. pp. 93-96.
159. Sinha, A.K., 2003. *Physical Metallurgy Hand Book*. 3.105-3.114, Mc Graw Hill.
160. Sirin, K., Sirin, S.Y. and Kaluc, E., 2016. Influence of the inter-pass temperature on $t_{8/5}$ and the mechanical properties of submerged arc welded pipe. *Journal of Materials Processing Technology*. 238, pp. 152–159.

161. Solokha, A.M, Yushchenko, K.A. and Galinich, V.I., 1979. A flux for the automatic welding of cold resistant steel containing nitrogen. *Automatic Welding*. 32(8), pp. 31-36.
162. Srinath, H., 1975. Some aspects of submerged arc welding process. *Indian Welding Journal*. 8(9), pp. 67-74.
163. Srivastav, B.K., Tewari, S.P., Prakash, J., 2010. A review on effect of arc welding parameters on mechanical behaviour of ferrous metals/alloys. *International Journal of Engineering Science and Technology*. 2(5), pp. 1425-1432.
164. Srivyas, P.D., Thappa, S. and Singh, B., 2014. Study of various challenges in submerged arc welding – A Review. *International Conference on Newest Drifts in Mechanical Engineering*. pp. 595-600.
165. Surian, E. and Boniszewski, T., 1992. Effect of manganese and type of current on properties and microstructure of all-weld- metal deposit with E7016 electrode. *Welding Journal*. 72(9), pp. 348s-360s.
166. Tanaka, J., Kitada, T., Naganawa, Y. and Kunisada, Y., 1980. Element transfer behaviour during submerged arc welding. *International Conference on Weld Pool Chemistry and Metallurgy*, Cambridge, U.K: The Welding Institute, pp. 279-288.
167. Thirunavukkarasu, K., Kavimani, V., Gopal, P.M. and Das, D., 2021. Recovery and Recycling silica flux in submerged arc welding – Acceptable properties and economical correlation. *Silicon*. 13, pp. 2337-2346.

168. Tiwari, M.K., Bajpai, S. and Dewangan, U.M., 2016. Steel slag utilization-overview in Indian perspective. *International journal of Advanced Research*. 4(8), pp. 2232-2246.
169. Tulani, S.S., Boniszewski, T. and Eatan, N.F., 1972. Carbonate fluxes for submerged arc welding of mild steel. *Welding and Metal Fabrication*. 40(7), pp. 248-250.
170. Turkdogan, T.E., 1996. *Fundamentals of steelmaking*. The Institute of Materials, London, England.
171. Tusek, J., 1996. Submerged arc welding with multiple electrodes achieves high production rates. *Welding Journal*. 75(8), pp. 41-44.
172. Verma, J. and Taiwade, R.V., 2017. Effect of welding processes and conditions on the microstructure, mechanical properties and corrosion resistance of duplex stainless steel weldments – A review. *Journal of Manufacturing Processes*. 25, 134-152.
173. Visvanath, P.S., 1982. Submerged arc welding fluxes. *Indian Welding Journal*. 15 (1), pp. 27-30.
174. Visvanath, P.S., 1983. Hydrogen control in submerged arc welding fluxes. *National Welding Seminar*. pp. 13.8-31.1.
175. Wang, J., Huang, Y., Xiao, J., Feng, J., Tian, C.Y. and Wang, J., 2014. Metal transfer with force analysis in consumable and non-consumable indirect arc welding process. *Welding Journal*. 93, pp. 431s-438s.

-
176. Wang, X., Geysen, D., Gerven, T.V., Jones, P.T., Blanpain, B. and Guo, M., 2017. Characterization of landfilled stainless steel slags in view of metal recovery. *Frontiers of Chemical Science and Engineering*. 11(3), pp. 353-362.
177. Wang, X., Han, F., Liu, X., Qu, S. and Zou, Z., 2008. Microstructure and wear properties of the Fe-Ti-V-Mo-C hardfacing alloy. *Wear*. 265, pp. 583-589.
178. Wang, Z. and Sohn, I., 2019. A review on reclamation and reutilization of ironmaking and steelmaking slags. *Journal of Sustainable Metallurgy*. 5, pp. 127-140.
179. Wanka, R., 1980. The influence of physical properties of fluxes on submerged arc welding. *Weld pool chemistry and metallurgy. International Conference*. Cambridge, England: The Welding Institute report, pp. 93-95.
180. Weisman, C., 1976. *Welding Handbook*. Vol. 1. 7th edition. Miami: American Welding Society.
181. Weman, K., 2003. *Welding Processes Handbook*. Cambridge, England: Woodhead publishing Ltd.
182. Wilson, E.M., 1996. SAW of 1% Titanium, 18% Nickel-Co-Mo marging steel. *British Welding Journal*. 13(2), pp. 67-74.
183. Wittstock, G.G., 1976. Selecting submerged arc fluxes for carbon and low alloy steels. *Welding Journal*. 97(9), pp. 733-741.
184. Wittung, L., 1980. Some physical and chemical properties of welding slag and their influence on slag detachability. *Weld Pool Chemistry and Metallurgy, International Conference, Cambridge, England: The Welding Institute*. pp. 93-95.

185. Yadav, A., Ghosh, A. and Kumar, A., 2017. Experimental and Numerical Study of Thermal Field and Weld Bead Characteristics in Submerged Arc Welded Plate. *Journal of Material Processing Technology*. 248, pp. 262-274.
186. Yang, L.J., Bibby, M.J., Chandel, R.S., 1999. Linear regression equations for modelling the submerged-arc welding process. *Journal of Material Processing and Technology*. 39, pp. 33–42.
187. Yang, L.J., Chandel, R.S. and Bibby M.J., 1992. The effects of process variables on the bead width of submerged-arc weld deposits. *Journal of Materials Processing Technology*. 29(1–3), pp. 133–144.
188. Zhang, Z.D., 2010. Activating flux tungsten inert gas welding of Mg alloys. *Welding and Joining of Mg alloys*. pp. 253-273.

CURRICULUM VITAE

Name – Deepanjali Nimker

Born - 17.04.1985

Education

- (i) B. Tech in Mechanical and Automation from Indira Gandhi Institute of Technology (Affiliated to Guru Gobind Singh Indraprastha University, Delhi)
- (ii) M. Tech in Production Engineering from Delhi Technological University
- (iii) Ph.D. Thesis submitted to the Department of Mechanical Engineering, Delhi Technological University

Publications

S. No.	Title of the paper	Publication Type	Name of the Journal/ Conference (Indexing & Impact factor)	Authors	Year of publication
1.	Cost Analysis and Waste Reduction of Reclaimed Slag over Fresh Flux in Submerged Arc Welding	UGC Approved Journal (International)	International Journal for Research in Applied Science and Engineering Technology (IJRASET) Vol 5, Issue IX, pp: 759-762. ISSN: 2321-9653 SJIF- 7.429	Deepanjali Nimker & Reeta Wattal	2017
2.	Recycling of submerged arc welding slag for Sustainability	ESCI Indexed Journal (International)	Production and Manufacturing Research (Taylor and Francis) Vol 8, Issue 1, pp: 182-195. ISSN: 2169-3277 Impact factor- 2.09	Deepanjali Nimker & Reeta Wattal	2020

S. No.	Title of the paper	Publication Type	Name of the Journal/ Conference (Indexing & Impact factor)	Authors	Year of publication
3.	Weld bead geometry and shape relationship in submerged arc welding using recycled slag	SCOPUS Indexed Journal (International)	International Journal of Mechanical and Production Engineering Research and Development (IJMPERD) (Trans Stellar) Vol 10, Issue 3, pp: 597-610. ISSN: 2249-8001 SJR Impact factor- 0.202	Deepanjali Nimker & Reeta Wattal	2020
4.	Metallurgical studies on recycled slag in submerged arc welding	International Conference (presented)	International Conference on Advances in Mechanical, Civil and Construction Engineering (ICAMCCE), 23 rd August 2020, New Delhi, India	Deepanjali Nimker & Reeta Wattal	2020
5.	Zero waste concept: Recycling of slag to use as flux in submerged arc welding	International Conference (presented)	1 st International Conference on Energy, Materials Sciences and Mechanical Engineering (EMSME) – 2020, (30 th October – 1 st November 2020), NIT Delhi, India Proceedings published in Lecture Notes in Mechanical Engineering (Springer Link)	Deepanjali Nimker & Reeta Wattal	2020

S. No.	Title of the paper	Publication Type	Name of the Journal/ Conference (Indexing & Impact factor)	Authors	Year of publication
6.	Prediction of element transfer using recycled slag in submerged arc welding	International Journal	International Journal of Mechanical and Production Engineering Research and Development (Trans Stellar) Vol 11, Issue 2, April 2021, Page no: 417- 426 ISSN: 2249-8001 SJR Impact factor -0.202	Deepanjali Nimker & Reeta Wattal	2021